PREDICTION OF CONCENTRATION PROFILES OF A PARTICLE - LADEN SLURRY FLOW IN HORIZONTAL AND VERTICAL PIPES

By

KARTHIK RAMISETTY

Bachelor of Technology in Mechanical Engineering

Jawaharlal Nehru Technological University

Hyderabad, Andhra Pradesh

2008

Submitted to the Faculty of the
Graduate College of the
Oklahoma State University
in partial fulfillment of
the requirements for
the Degree of
MASTER OF SCIENCE
December, 2010

PREDICTION OF CONCENTRATION PROFILES OF

A PARTICLE - LADEN SLURRY FLOW IN

HORIZONTAL AND VERTICAL PIPES

Thesis Approved:

Dr. Frank W. Chambers

Thesis Adviser

Dr. Andrew S. Arena

Dr. David G. Lilley

Dr. Mark E. Payton

Dean of the Graduate College

ACKNOWLEDGEMENTS

I would like to thank my advisor Dr. Frank W. Chambers for giving me an opportunity to work for him. My interactions with him always made things easy on me as he provided valuable information and ideas that helped me in a number of ways. Besides my advisor, I would also like to thank my graduate committee, Dr. Andrew S. Arena and Dr. David G. Lilley, for considering this work worthy enough to be associated with.

I would like to thank my friend and colleague Abhishek for his invaluable time and immense cooperation. I must thank my friends Arka, Butto, Bongu, Curry, Idly, and Kodi for being my energy and happiness. I thank Ashish, Vamsi, and Vineet for giving me good company and support throughout my masters.

Finally, I would like to dedicate this thesis to my loving parents Nageswara Rao and Vijaya Lakshmi, my brother Nani, and my loving friend Swetu.

NOMENCLATURE

C:	Initial Efflux concentration by volume
D:	Diameter of pipe, (m)
d_p:	Particle size, (μm)
k:	Turbulent kinetic energy, (m^2/s^2)
L_s:	Characteristic length scale, (m)
l:	Length of pipe, (m)
p':	Pressure fluctuation, (Kpa)
Re_D:	Pipe Reynolds number
St:	Stokes number
T':	Temperature fluctuation, (K)
U_{cl}:	Center line velocity, (m/s)
V_s:	Characteristic velocity scale, (m/s)
v':	Velocity fluctuation in Y-direction, (m/s)

w': Velocity fluctuation in Z-direction, (m/s)

$\alpha_{k:}$ Volume fraction of k^{th} phase

ε: Turbulent dissipation, (m^2/s^3)

ε_{xy}: Shear strain, (1/s)

μ: Dynamic viscosity, (Pa-s)

μ_m: Dynamic viscosity of a slurry, (Pa-s)

μ_t: Turbulent viscosity, (Pa-s)

ρ: Density of fluid, (Kg/m^3)

ρ_m: Density of slurry, (Kg/m^3)

τ_{ij}: Reynolds stress tensor, (N/m^2)

φ: Density of dispersed phase, (Kg/m^3)

ABBREVIATIONS

ADP:	2-Amino-4, 6-dimethyle Pyrimidine
APCI:	Atmospheric Pressure Chemical Ionization
CFD:	Computational Fluid Dynamics
DART:	Direct Analysis in Real Time
DNS:	Direct Numerical Simulation
ESI:	Electron Spray Ionization
LES:	Large Eddy Simulation
MS:	Mass Spectroscopy
NIR:	Near Infra-red
RANS:	Reynolds-Averaged Navier-Stokes
TOFMS:	Time of Flight Mass Spectrometry
VOF:	Volume of Fluid

TABLE OF CONTENTS

LIST OF TABLES

LIST OF FIGURES

Figure Page

CHAPTER I

INTRODUCTION

1.1 Background:

Agricultural chemical is a generic name for fertilizers, nutrients, and various chemical products used in agriculture. Pesticides intended for preventing, destroying, repelling or mitigating any pest are agricultural chemicals. Agricultural chemicals are used to control organisms that are considered harmful. For example, they are used to promote or inhibit the growth of field crops. In the 1940's manufacturers began to produce large amounts of agricultural chemicals and their use became widespread. An agricultural chemical is a mixture of substances. Often they are produced as a combination of solids and liquids. Technically speaking, it is a slurry. A slurry is defined as a thick suspension of solids in liquid. The flow of this thick suspension is called a slurry flow.

Flows may be categorized into two types, single-phase flows and multi-phase flows. When the flow has only one phase, it is called a single-phase flow. The flow of water through a pipe is the most common type of single-phase flow we see in our daily lives. It is easy to characterize a single-phase flow. Complexity arises when the flow is multi-phase. Multi-phase flows are defined as those with simultaneous movement of two or more different phases, where the phase refers to the state of matter (solid, liquid, or gas). Liquid-gas flow, gas-solid flow, and solid-liquid flow are examples of multi-phase flows. Solid-liquid flow is also called slurry flow. Slurry flow is a very complex process to understand, design, and analyze. During the transportation of slurries, liquid is referred to as the continuous phase, and solid is referred to as the disperse phase.

In batch processing reactors, real time measurement of the slurry concentration is a challenging task. The reactions and mixing with an impeller are highly turbulent and it is difficult to measure the concentrations in the reactor. A schematic of the batch reactor and recirculation loop system is shown in Figure 1.1.

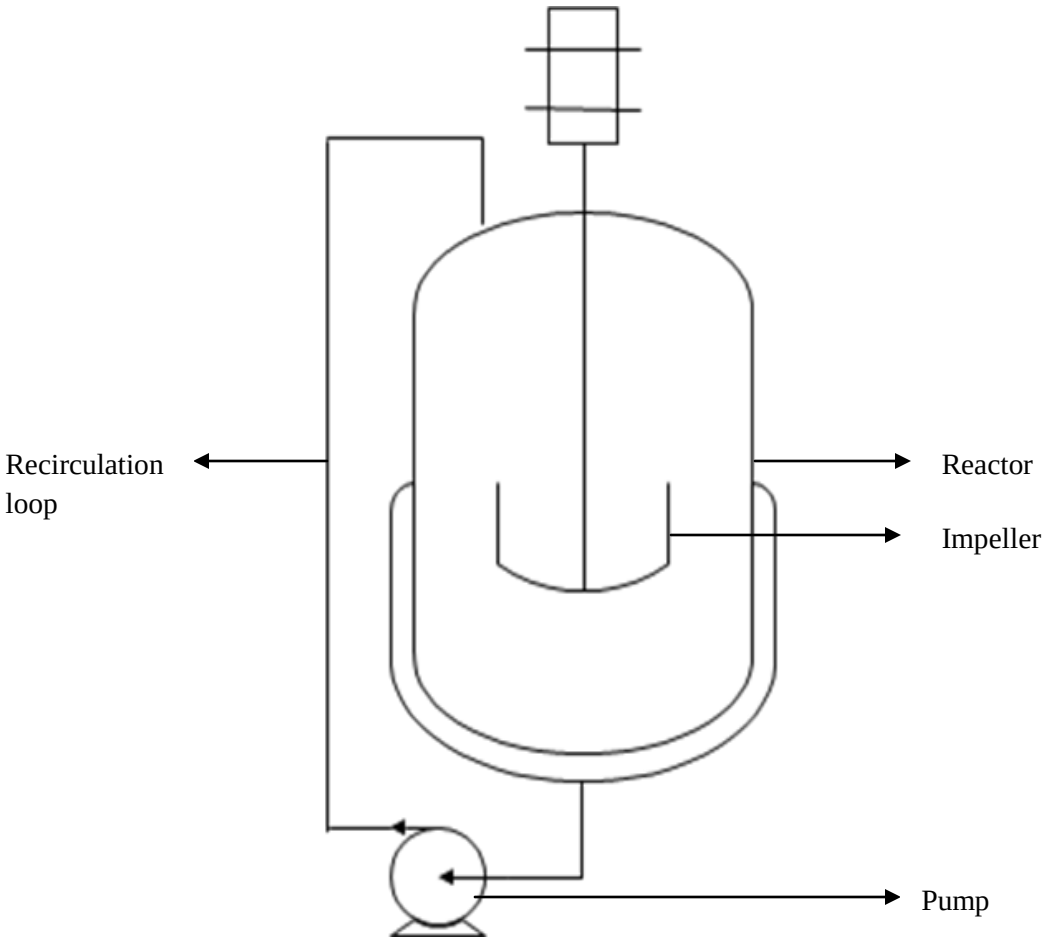

Figure 1.1: Schematic of the batch reactor and recirculation loop slurry system

Measurements in the recirculation loop are less difficult than measurements in the reactor itself because we know the direction of the flow and the turbulent intensity is less compared to the turbulent intensity in the reactor. In the recirculation loop measurements are performed at the fully-developed region. The fully-developed region is the location beyond which the velocity and turbulent intensity profiles do not change in the flow direction.

Monitoring the chemical composition of the flowing slurry is very important in chemical and pharmaceutical industries because it can be used to produce the product

more efficiently with better quality. Near Infrared Spectroscopy and Mass Spectroscopy help chemists to determine the elemental composition of the slurry. To perform Mass Spectroscopy any sample withdrawn from the recirculation loop must be representative of the slurry in the reactor. A proposed sampling pipe located at the fully-developed region of the recirculation loop is show in Figure 1.2.

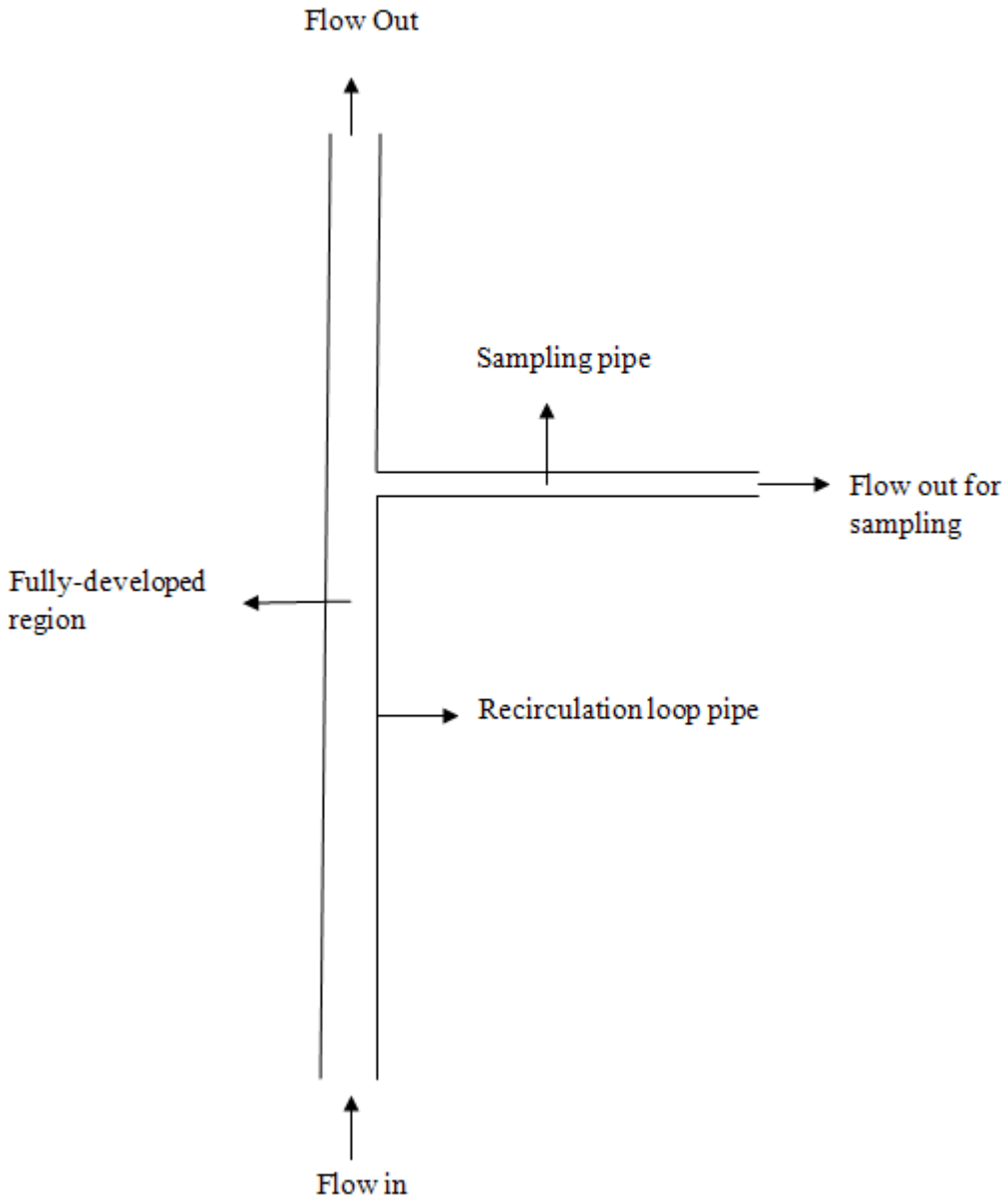

Figure 1.2: Schematic of the sampling pipe located in the fully-developed region of recirculation loop

A first step that can be performed to gain some knowledge about the sample being withdrawn is determining the concentration profiles in the sampling pipe and comparing with concentration profiles in the fully developed region of the recirculation loop. The sampling pipe is located in the fully developed region of the recirculation loop for performing off-line sampling. Often an isokinetic sampling probe is used to measure the concentration profiles in particle laden flows. An isokinetic sampling probe is used to collect the sample from the process stream in such a way that sample entering the probe has a velocity equal to the slurry passing around the probe. In the next step, off-line density measurements are performed on the collected samples to determine the concentration of the solid particles. Therefore, performing isokinetic sampling causes unwanted delays.

Performing off-line sampling using a small diameter pipe to collect samples and presenting it to the mass spectroscope is the new sampling technique that researchers are trying to develop. Off-line sampling is done by taking a sample directly from the recirculation loop with a small diameter pipe located in the fully-developed region. To perform off-line sampling, it is of prime importance to check whether the sample flowing in the off-line sampling pipe represents the sample in the recirculation loop. It is also important to find the location in the recirculation loop to perform off-line sampling. Problems pertaining to off-line sampling are particle motion and flow rates. Low flow rates may cause the particles to deposit in the sampling pipe. Particle dynamics is another factor to be considered while performing off-line sampling. The particulate flow with bigger particles is highly inertial and will lag changes in the fluid flow. These variables are discussed in greater detail in the literature review section.

1.2 Objective:

The objective of the present study is divided into two sections.

(i) First objective is to use CFD to predict the concentration profiles of the slurry in both horizontal and vertical pipes. The concentration profiles in both the pipes will be compared to find a good location to perform Near Infrared Spectroscopy and to withdraw representative samples from the recirculation loop for Mass-Spectroscopic analysis.

(ii) Second objective is to predict the concentration profiles of the slurry in the sampling pipe located in the fully-developed region of the recirculation loop. The concentration profiles will be predicted computationally by varying particle size and initial solid concentration.

CHAPTER II

REVIEW OF LITERATURE

This section deals with the research work done on slurry flows and mass spectroscopy. Slurry flow and mass spectroscopy are completely different fields. Research work on slurry flows is reviewed first and then followed by a brief introduction to mass spectroscopy. The major part of this literature review is concentrated on slurry flow. A brief introduction to slurry flows is presented followed by a discussion of the important parameters pertaining to slurry flows.

2.1 Slurry Flows

As mentioned before, slurry flow is a complicated process. The complexity arises because of the interaction between the different phases and particles, and sometimes due to the turbulent nature of the flow. In slurry flows, the liquid phase is referred to as the primary phase and the solid phase is referred to as the secondary phase.

Doron and Barnea (1996) presented different flow patterns that are observed in horizontal liquid-solid pipeline transportation. The four most common flow patterns are – "homogeneous suspension flow", "heterogeneous suspension flow", "flow with a moving bed", and "flow with a stationary bed." In homogeneous suspension flow all the solid particles are distributed uniformly across the pipe cross-section. This happens at very high mixture velocities and it is considered not practical. In heterogeneous flow the solid particles are distributed almost uniformly across the pipe cross-section but with a higher percentage of the particles transported at the lower part of the pipe cross-section. It is considered the most popular flow for all applications. As the velocity decreases the solid particles start to accumulate at the bottom of the pipe and they form a packed bed layer, which moves with the flow. With further reduction in the velocity the packed bed layer moving with the flow stops and forms a stationary bed. Operating at this velocity causes plugging or blockage. Visual observations are the key in finding these flow patterns. These flow patterns affect the magnitude of pressure drop, pipe erosion, and other performance characteristics. Figure

2.1 shows the schematic views of flow patterns and concentration distributions in a direction perpendicular to the pipe axis.

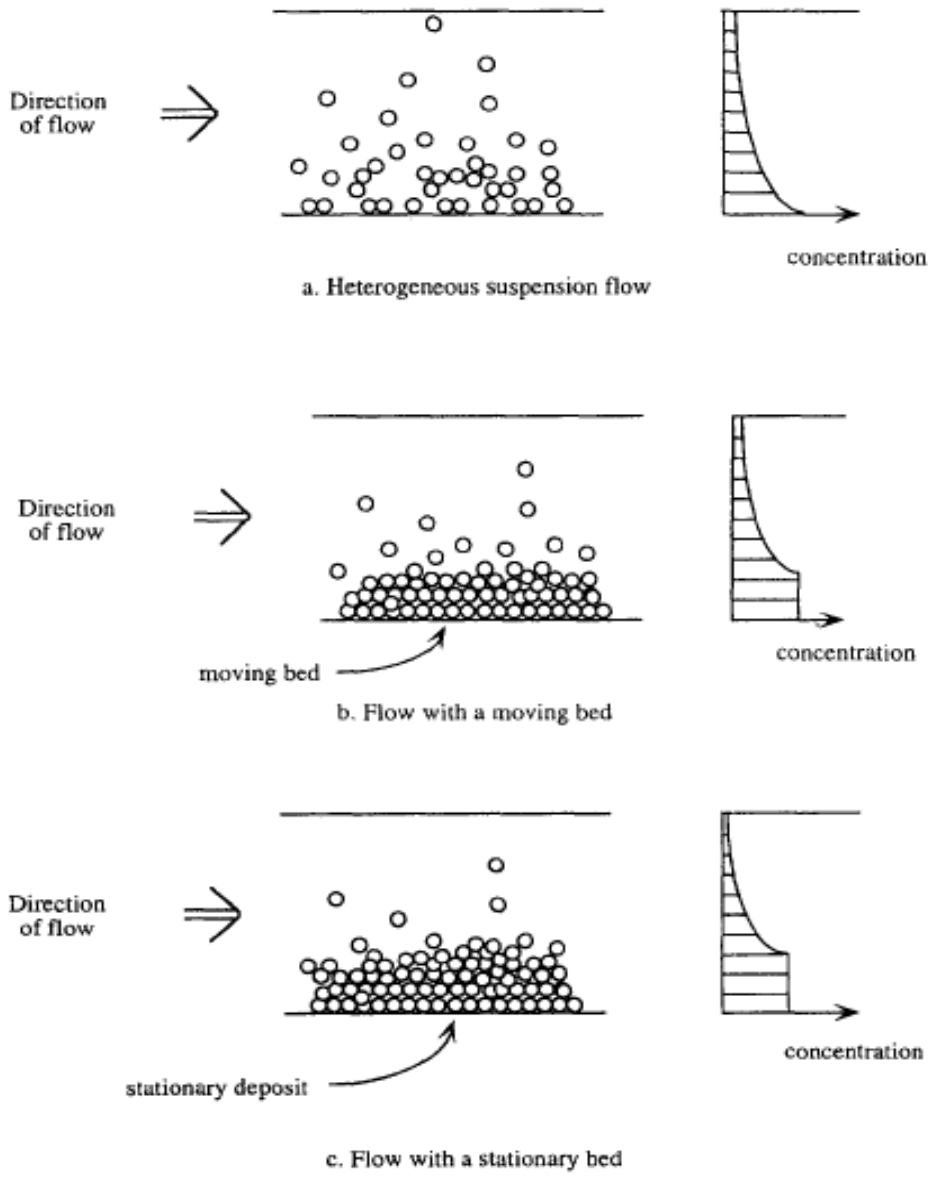

Figure 2.1: Schematic views of flow patterns and concentration distributions in a direction perpendicular to the pipe axis (Doron and Barnea 1996)

One of the key parameters in slurry flows is deposition velocity. Deposition velocity is the flow velocity at which deposition of particles begins. Deposition velocity represents the slowest velocity at which slurry pipelines can operate and it depends on various parameters including particle size, particle density, solid concentration, and pipe diameter. Slurry transportation should be operated at a velocity greater than the deposition velocity to avoid problems. Pressure drop, concentrations of solids, and turbulence in the flow are the key parameters that affect the overall performance of the slurry transport system along with deposition velocity. According to Kaushal et al. (2002) almost 60 correlations have been proposed on predicting deposition velocity. One of the important correlations on deposition velocity was given by Durand (1963) considering the diameter of the pipe (D), density of solid (ρ_s), density of liquid (ρ_l), and Froude number (F_L). The correlation is given as:

$$V_D = F_L\left[2gD\left(\frac{\rho_s - \rho_l}{\rho_l}\right)\right]^{1/2} \tag{2.1}$$

This correlation does not consider the particle diameter (d) and initial solids concentration (C_v). Wasp et al. (1970) modified Durand's correlation and derived a deposition velocity equation for lower concentrations which is given as:

$$V_D = 1.87\left(\frac{d}{D}\right)^{1/6}\sqrt{2gD\left(\frac{\rho_s}{\rho_l} - 1\right)} \tag{2.2}$$

The above correlation describes the behavior of 1% dilute suspension. Later Wasp et al. (1977) derived a correlation describing the behavior of higher concentration slurries (up to 40%). It is given as:

$$V_D = 4.0\left(\frac{d}{D}\right)^{1/6}(C_v)^{1/5}\sqrt{2gD\left(\frac{\rho_s}{\rho_l} - 1\right)} \tag{2.3}$$

The above three correlations are the most important correlations for deposition velocity.

Kaushal et al. (2002) performed experiments to determine the deposition velocity and the parameters that affect it. They performed experiments in a big recirculation loop slurry system and found that at high velocities all the particles are uniformly distributed and with the decrease in velocity the particles start to settle at the bottom of the pipe forming a stationary bed. Through a visualization technique they calculated the deposition velocity and concluded that particle size, solid concentration, particle density, and pipe diameter all affect it.

Fadel et al. (2001) proposed that deposition velocity occurs at a little higher velocity than the velocity at which pressure drop is a minimum. They developed a robust experimental technique for the accurate determination of the deposition velocity associated with the transport of slurries in pipes. They performed experiments with single species slurries made of washed garnet and water flowing through a 1 inch clear pipe. The deposition velocity was measured for garnet/water slurries of 10, 20, and 30 percent solids concentration by volume. Their experimental setup and the captured images are shown in Figure 2.2 and Figure 2.3 respectively. With the use of a high speed, high resolution digital camera, data acquisition system and clear test section one can clearly observe and calculate the critical deposition velocity of any slurry flow. Decreasing the flow velocity gradually and observing the settling of the particles, gives an estimate of deposition velocity. According to Kaushal et al. (2002), minimum operating velocity is usually kept as 0.5 m/s more than the deposition velocity.

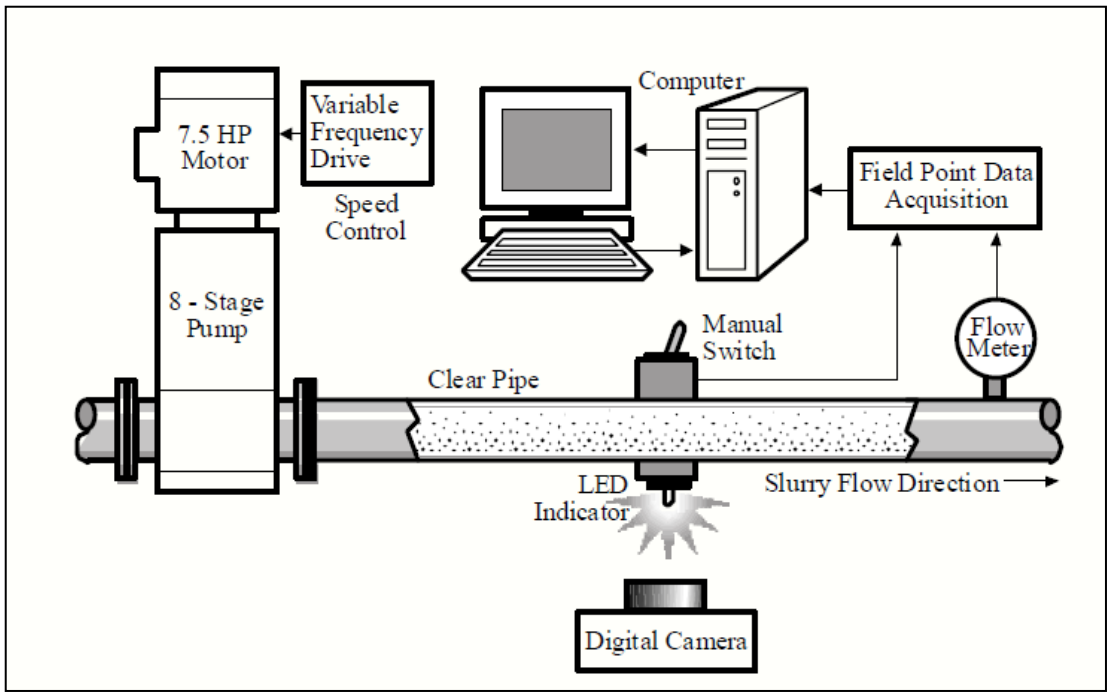

Figure 2.2: Schematic diagram for measuring deposition velocity (Fadel et al. 2001)

Figure 2.3: Captured images during homogeneous (top) and settled bed (bottom) flow conditions (Fadel et al. 2001)

A lot of research work has been done on horizontal slurry flows. Concentration profiles and pressure drop profiles have been measured in many cases by many researchers. Even though vertical slurry flows occur in hydraulic hoisting, stowing and well drilling operations there have been very few studies on vertical slurry flows. Sumner et al.'s (1990) investigation on vertical slurry flows was a major contribution. They measured the concentration and velocity profiles in vertical slurry pipe flows. They performed experiments using particles of different densities, diameters starting from 0.16mm to 1.7mm, and for different concentrations. The particle properties are shown in Table 2.1. A typical flow circuit used in their experiments is presented in Figure 2.4.

Particle	Diameter (d) (mm)	Density (ρ_s) (kg/m^3)
Fine sand	0.16	2650
Fine plastic	0.29	1050
Medium sand	0.47	2650
Coarse sand	0.78	2650
Coarse plastic	1.5	1050
Gravel	1.7	2650

Table 2.1: Particle properties used by Sumner et al. (1990)

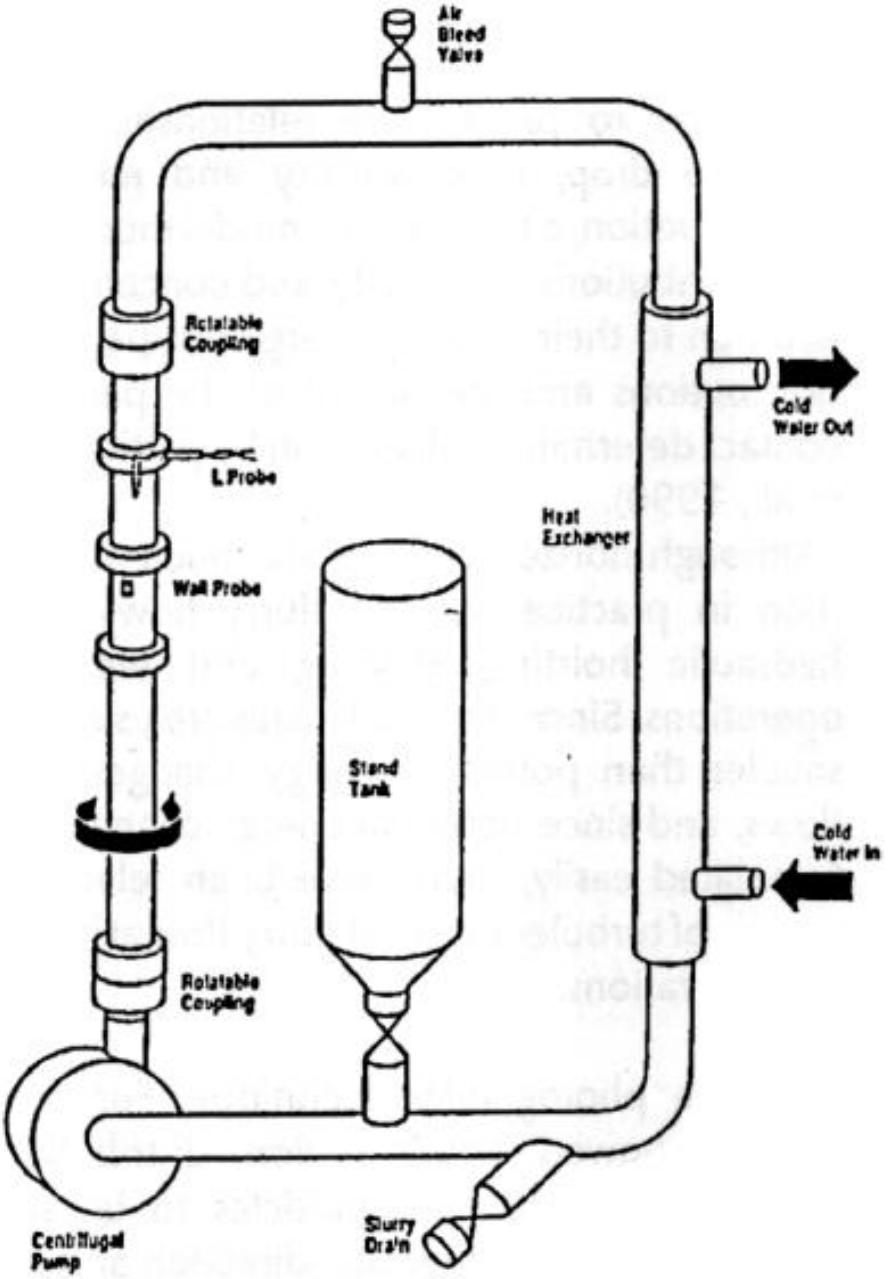

Figure 2.4: A typical flow circuit used in the experiment (Sumner et al. 1990)

Recirculating flow in the loop was produced by a centrifugal pump which discharged upward into the pipe section in which the measurements were made. The velocities were varied by adjusting the pump speed. Slurry concentrations were fixed by adding weighed quantities of solids to the loops whose volume was known. The temperature was maintained constant by cooling water through the double pipe heat exchanger. They plotted the velocity and concentration profiles for different particle sizes and densities. They observed a small change in concentration profile for bigger particles (coarse sand and gravel), but for smaller particles below 500 microns (fine sand, fine plastic, and medium sand) the concentration profiles looked similar and almost uniform. Figure 2.5 is the plot for concentration and velocity distributions for different particle sizes at 10% volume fraction. As it is a vertical slurry flow, the profiles are symmetric about the pipe axis, and both the velocity (left side of pipe axis) and concentration (right side of pipe axis) profiles are plotted on same graph. The x-axis represents the pipe diameter and the y-axis represents the non-dimensionalized velocity and concentration (where V is the mean velocity and C_b is the mean concentration).

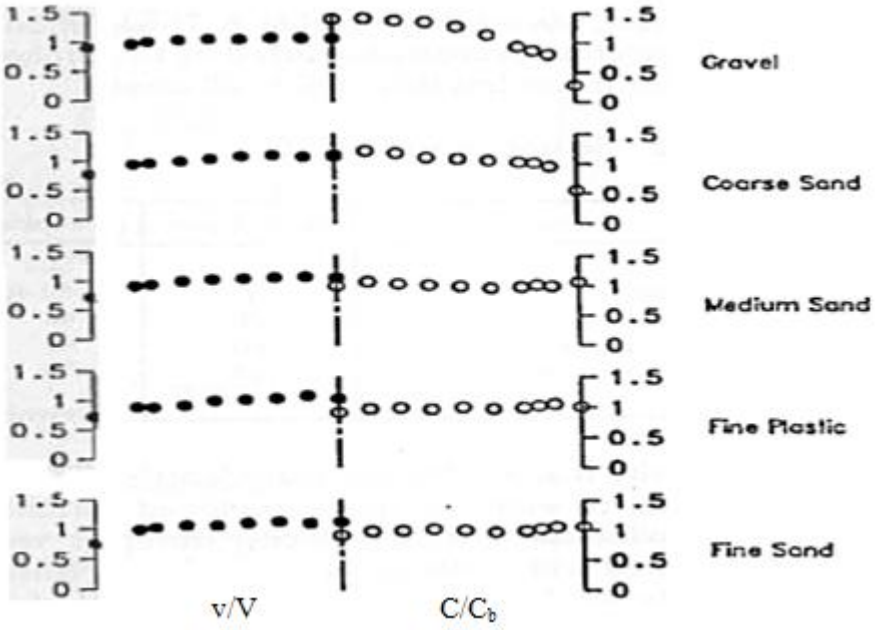

Figure 2.5: Velocity and concentration distributions in 40mm diameter pipe for 10% solids concentration (Sumner et al. 1990)

Profiles on the left side of the pipe axis are the velocity distributions and the profiles on the right side of the axis are the concentration distributions. They also performed experiments at solids volume fraction of 40%. Even at 40% solids volume fraction, there was a change in the concentration profiles only for particles above 500 microns (coarse sand and coarse plastic). For particles below 500 microns (fine sand, fine plastic, and medium sand), the concentration profiles are almost uniform and similar. Concentration and velocity distributions for 40% solid volume fraction are presented in Figure 2.6.

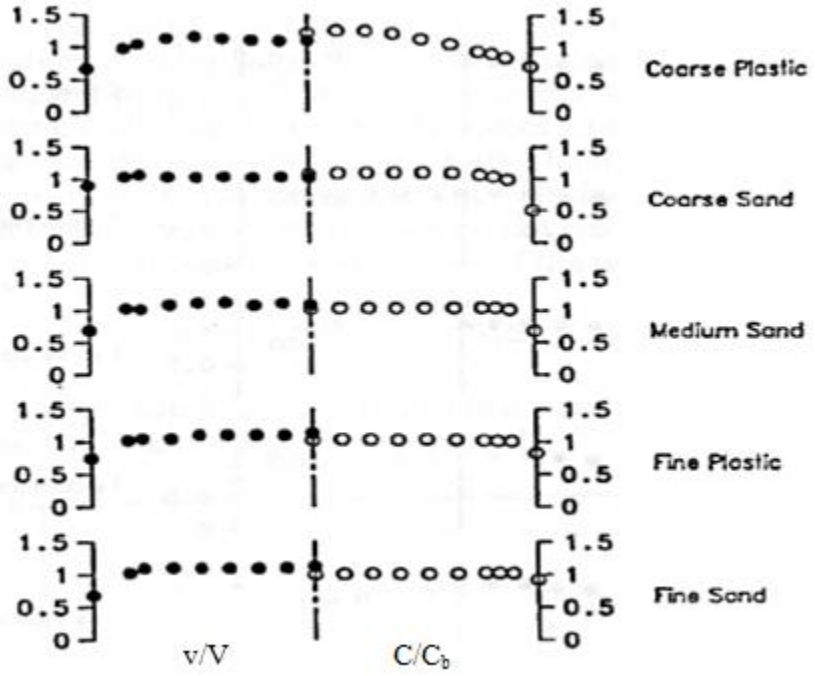

Figure 2.6: Velocity and concentration distributions in 40mm diameter pipe for 40% solids concentration (Sumner et al. 1990)

As compared to the concentration profiles in the vertical pipes, the concentration profiles in horizontal pipes follow a different trend. Figure 2.7 shows the concentration profiles of the sand water slurry for different sand concentrations in a horizontal pipe. One can observe a big slope in the concentration profiles of 0.165mm particles in horizontal pipes, while in a vertical slurry flow, the concentration profile is almost uniform even for 0.290mm particle size. This is a very surprising observation made by Sumner et al. (1990). According to them, concentration profiles are insensitive to mean flow velocity or pipe diameter.

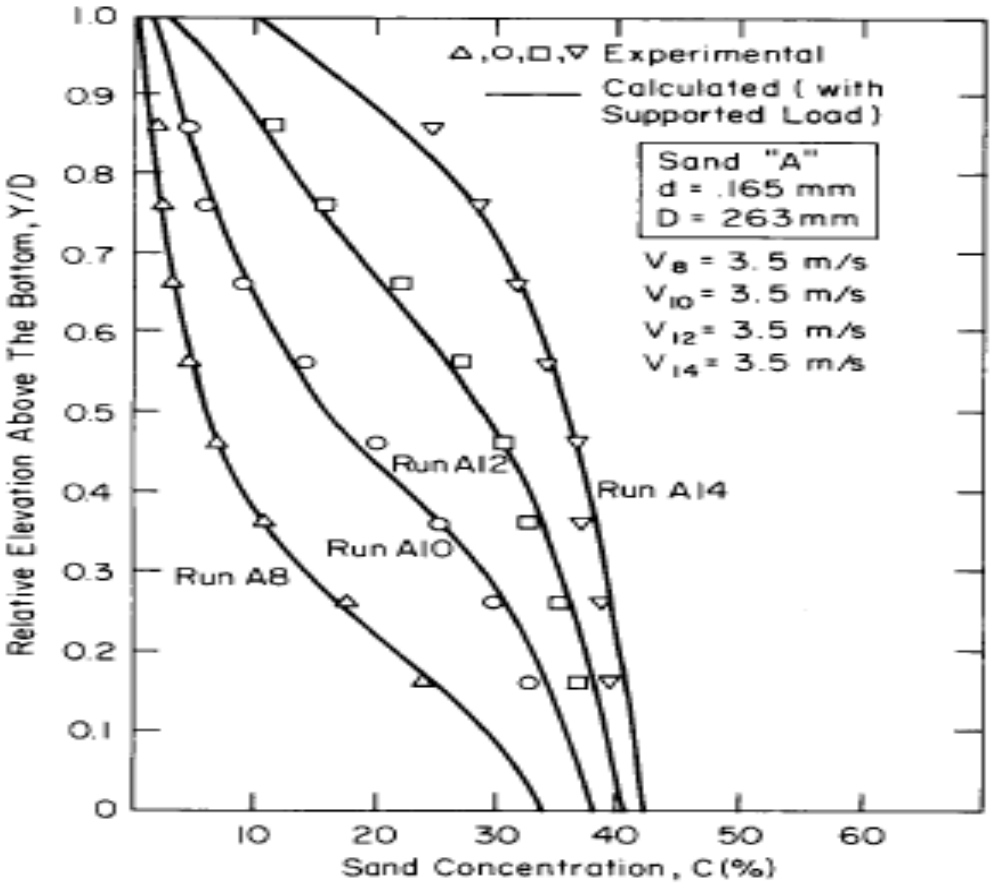

Figure 2.7: Concentration profiles of sand-water slurry flowing through a horizontal 263mm diameter pipe (Roco and Shook 1984)

As the concentration profiles are almost uniform in vertical pipes, vertical slurry flows can be very useful, when compared to horizontal slurry flows. Uniform concentration profiles allow better sampling and one can draw a sample that is a good representative of the slurry in the recirculation loop. In horizontal pipes because of the slope in concentration profiles, withdrawing a sample from the edge of the pipe can lead to erroneous results.

As this research work is concentrated on predicting the concentration profiles in the fully developed region of the vertical pipe and in the sampling pipe, it is important to know how the numerical analysis results agree with the experimental results in predicting the concentration profiles. Results of the numerical analysis of horizontal slurry pipe flows are presented below because numerical analysis of vertical slurry flows is not well documented. This makes the present research work more challenging.

Ekambara et al. (2009) predicted the behavior of horizontal solid-liquid (slurry) pipeline flows. Computational fluid dynamics (CFD) simulation results, obtained using a commercial CFD software package, ANSYS-CFX, were compared with a number of experimental data sets available in the literature. Very good agreement between the model predictions and the experimental data was obtained. The experimental and simulated results indicate that the particles are asymmetrically distributed in the vertical plane with the degree of asymmetry increasing with increasing particle size. The results are presented in Figure 2.8. The experimental and computational results are in good agreement, which shows that computational fluid dynamics can be a good predictor of concentration profiles of the solid particles present in the slurry. This gave a lot of encouragement for the present research work.

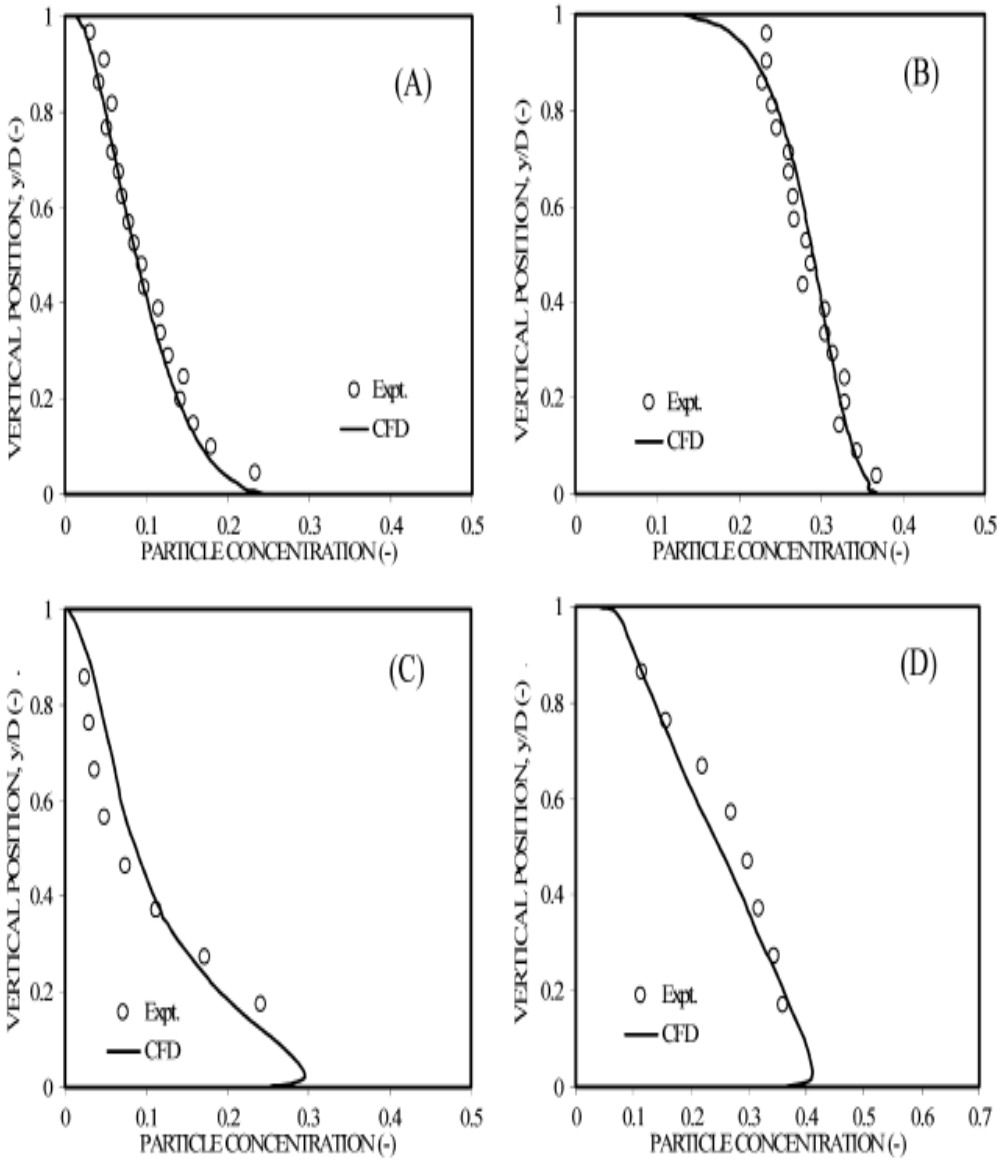

Figure 2.8: Computational validation of experimental results (sand-water slurry) of Roco and Shook (1983). Where (A) D=51.5 mm, α_s=0.0918, and V=3.78 m/s; (B) D=51.5 mm, α_s=0.286, and V=4.33 m/s; (C) D=263 mm, α_s=0.0995, and V=3.5 m/s; (D) D=263, α_s=0.268, and V=3.5 (Ekambara et al. 2009)

Lahiri (2009) studied the capability of commercial CFD software (FLUENT) to model complex solid-liquid flow in a horizontal pipeline. He found that CFD is capable to successfully model the slurry flow and the predicted concentration profiles of the particles show reasonably good agreement with the experimental data. The Euler-Euler model is used as the multi-phase model along with the standard k-ε turbulence model to simulate the turbulent solid-liquid flow. Concentration profiles were predicted for water-glass bead slurry at 125 and 440 micron particle and overall concentration up to 10 to 50% by volume. The results are presented in Figures 2.9 and 2.10.

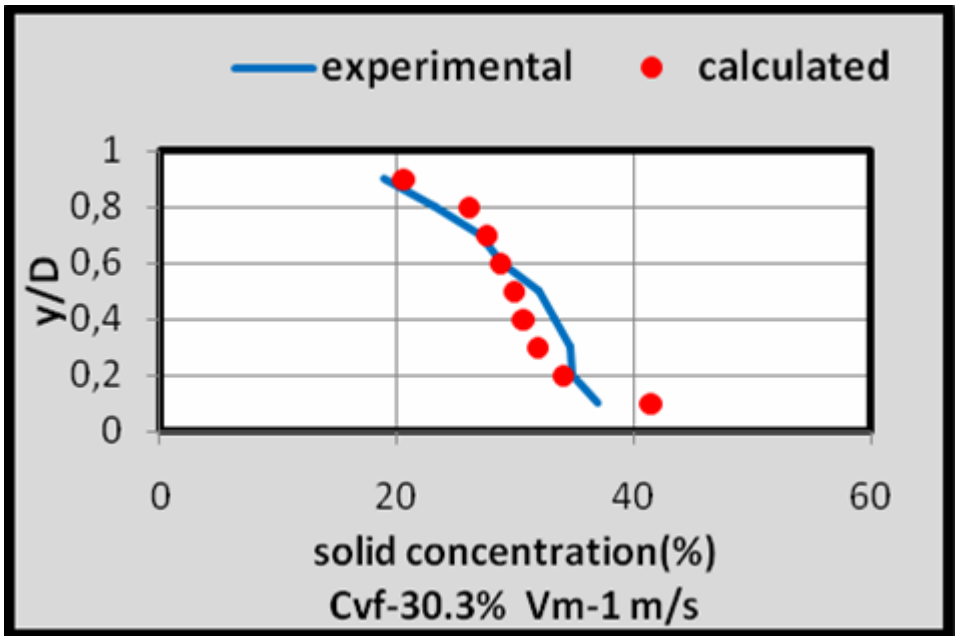

Figure 2.9: Computational validation of experimental results (water-glass bead slurry) of Kaushal et al. (2005) for 125 micron glass beads in 54.9mm diameter horizontal pipe (Lahiri 2009)

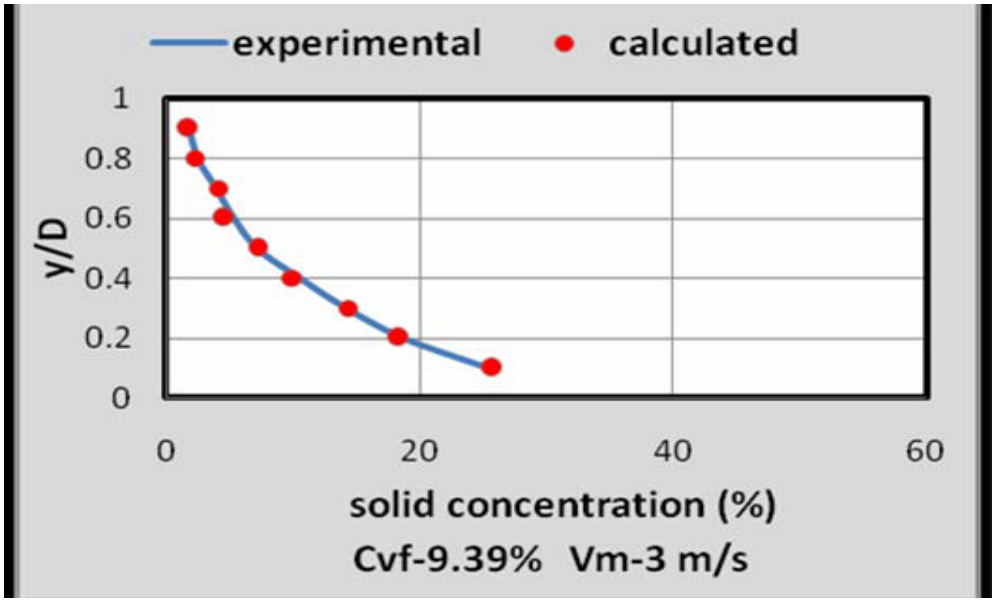

Figure 2.10: Computational validation of experimental results (water-glass bead slurry) of Kaushal et al. (2005) for 440 micron glass beads in 54.9mm diameter horizontal pipe (Lahiri 2009)

Kumar et al. (2008) used commercial CFD software FLUENT to study solid-liquid flow in a pipe bend. They used mixture multi-phase model along with k-ε turbulence model to predict the velocity and concentration distribution of particles in a 90 degree horizontal pipe bend. Simulations were performed in a 53 mm diameter pipe, at different initial solid concentrations in the range 0-8.82% with mean particle diameter of 448 μm. The velocity distribution shown in Figure 2.11 follows the typical pattern of slurry flow in a horizontal straight pipe just upstream of the pipe bend, but downstream of the pipe bend the typical velocity distribution pattern appears far away from the bend. Also, the velocity distribution is more uniform than the typical profile just downstream of the bend because of mixing of fluid in the bend. The effect of mixing extends further downstream of the bend, so that it requires a greater distance for the velocity distribution to regain its typical pattern. The concentration distributions are shown in Figure 2.12.

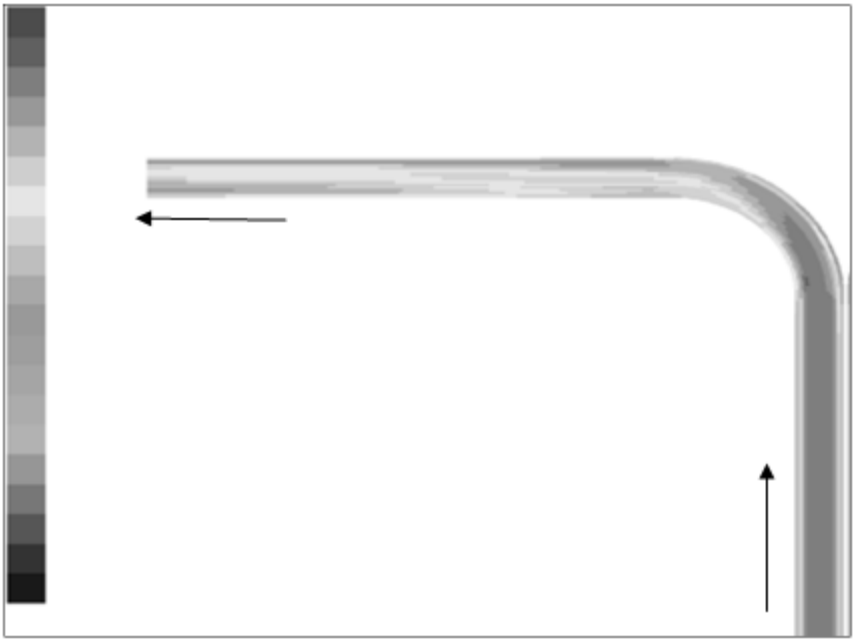

Figure 2.11: Particle velocity distribution at mid-horizontal plane at initial solid concentration of 8.82% and mean velocity of 3.56 m/s (Kumar et al. 2008)

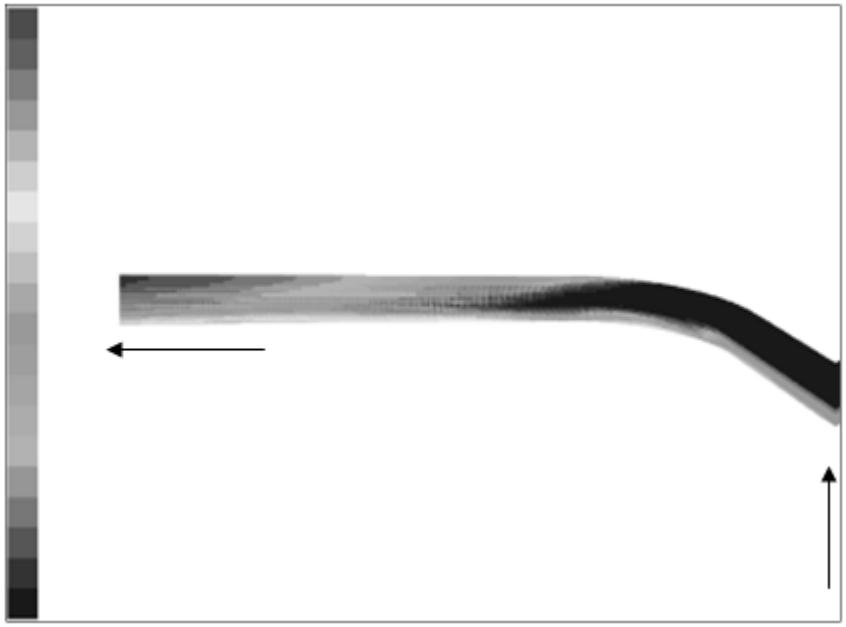

Figure 2.12: Three-dimensional concentration distribution at initial solid concentration of 8.82% (Kumar et al. 2008)

Similarly, the concentration distribution follows the typical pattern of slurry flow in a horizontal straight pipe (i.e. concentration of particles increasing exponentially from top to bottom of pipeline) just upstream of the pipe bend, but downstream the typical pattern of concentration distribution appears far away from the bend. It can also be seen that the concentration distributions become more uniform just downstream of the pipe bend because of the fluid mixing. Kumar et al. (2005) concluded that CFD modeling gives fairly accurate results within a percentage error of ±10%. This shows the capability of CFD on modeling solid-liquid flows in pipe bends. FLUENT software has a very strong ability to model solid-liquid mixture flowing upward and splitting in a tee-junction. The mixture multi-phase model along with k-ε turbulence model gives reliable results in predicting the slurry flow through these types of complex geometries (FLUENT Inc 2009).

Wang et al. (2008) studied oil-water flow through a horizontal pipe with a vertical branch using ANSYS CFX as shown in Figure 2.13. They used a 3D two fluid model along with k-ε turbulence model to simulate the flow through the horizontal pipe with a vertical branch at 90 degree. They used velocity boundary condition at the inlet and the outflow boundary condition at the two outlets, and slip flow boundary condition on the pipe wall. They performed simulations under these conditions and the results are shown in Figure 2.14. The phases tend to become more and more uniformly distributed from cross-section (a) to (c) (where (a) is the entrance cross section of the branch and (c) is the exit cross-section of the branch). Pure water is observed in the region adjacent to the pipe wall as shown in (c) and this result is in good agreement with the experimental observation shown in Figure 2.14.

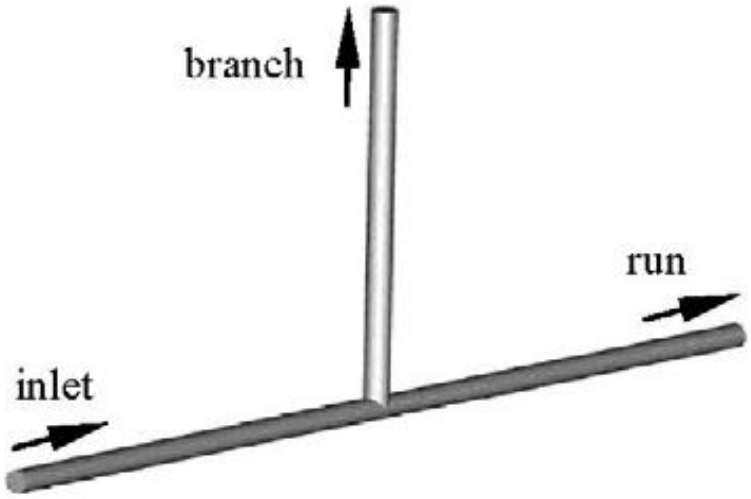

Figure 2.13: Geometrical model considered in the simulation (Wang et al. 2008)

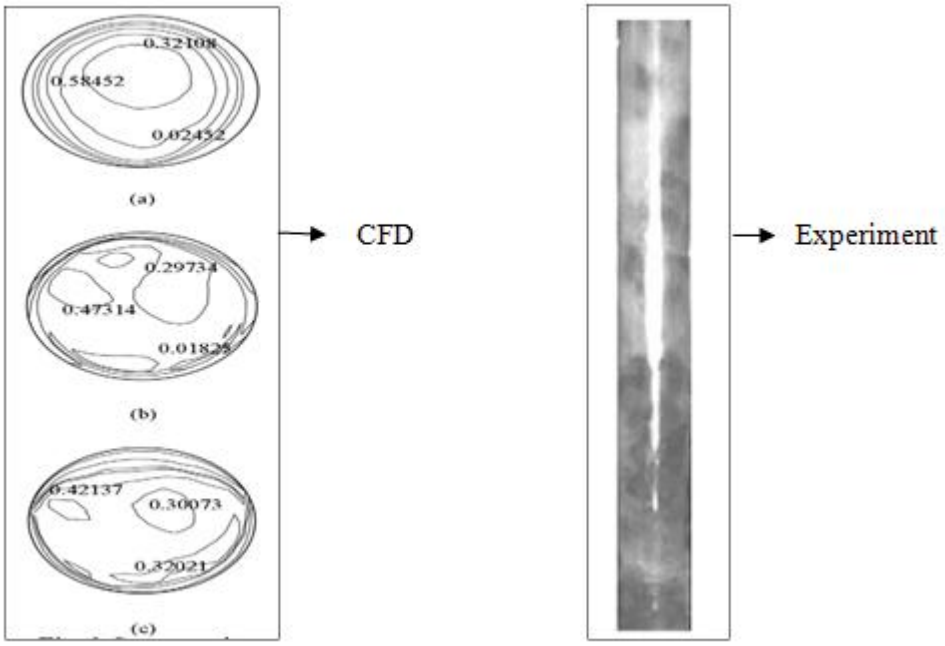

Figure 2.14: Cross-section oil volume fraction in the branch (left) and flow pattern in the branch (right) (Wang et al. 2008)

As we are dealing with liquid-solid flow in a pipe, it is important to consider particle dynamics. The Stokes number is a very important parameter in fluid-particle flows. The Stokes number related to particle velocity is defined as the ratio of particle response time (τ_v) to the characteristic fluid time scale (τ_F).

$$St_v = \frac{\tau_v}{\tau_F}$$

$$\tau_v = \frac{\rho_d d_p^2}{18\mu}$$

$$\tau_F = \frac{L_s}{U} \tag{2.1}$$

Where ρ_d is the particle density, d_p is the particle diameter, L_s is the characteristic length scale, and U is the flow velocity. According to Crowe et al. (1998) if the Stokes number is less than 1, the response of the particles is much less than the characteristic time associated with the flow field. Thus the particles will have ample time to respond to changes in flow velocity. Thus the particle and fluid velocities will be nearly equal. This is called velocity equilibrium. On the other hand, if the Stokes number is greater than one, then the particulate flow is highly inertial and will lag changes in the fluid flow.

An approximate relationship for the particle/fluid velocity ratio as a function of the Stokes number can be obtained from the "constant lag" solution. The velocity ratio is given by Crowe et al. (1998) as

$$\phi = \frac{1}{1 + St_v} \tag{2.2}$$

As the Stokes number reaches zero, the particle velocity approaches the carrier phase velocity and as the Stokes number reaches infinity, the particle velocity approaches zero. This means that the particle velocity is unaffected by the fluid. According to Tu and Fletcher (1996)

for large values of Stokes number (>2), the particulate flow is highly inertial and for low Stokes number (<0.25) the particles and the carrier fluid are strongly coupled and the particles would be expected to approximately follow the fluid flow.

Brown (2002) used a 3D CFD model based upon the commercial code CFX-4 to investigate the motion of caustic liquor and bauxite particles through a tee-junction as shown in Figure 2.15.

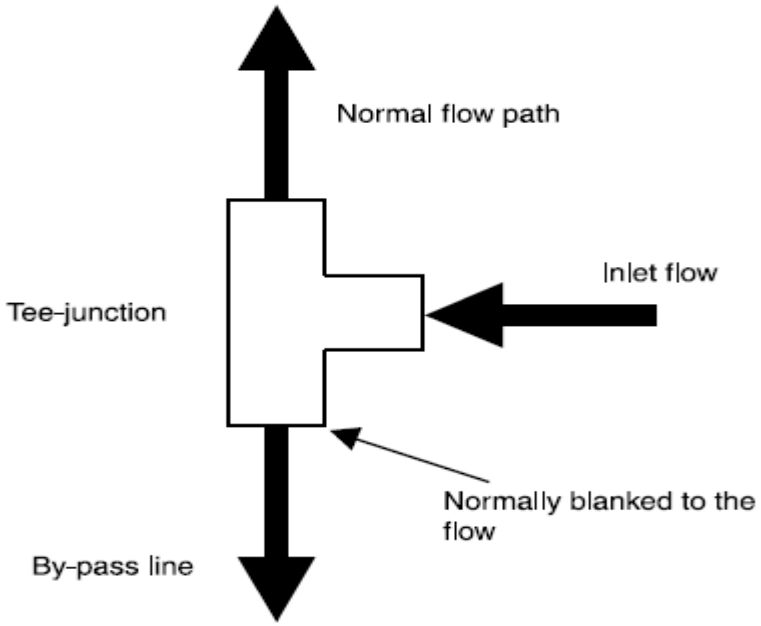

Figure 2.15: Schematic of slurry pipeline with tee-junction (Brown 2002)

The Eulerian-Eulerian multiphase model is used in conjunction with k-ε turbulence model to predict the motion of the slurry. He performed simulations considering 150 micron bauxite particles. All the variables are defined at the inlet. The particles are also assumed to be uniformly distributed and, due to the low Stokes number, the particle velocity distribution is assumed to be identical to that for the fluid phase. A zero gradient condition is applied at the outlet. Standard no-slip wall functions are applied at all solid surfaces for both the fluid and particle phases. Use of no-slip wall functions for the particle phase is justified in this case on the basis of the low Stokes number (0.026) which indicates that there is a strong coupling between

the particles and the fluid and hence that particle–wall rebound characteristics will have a negligible impact on the particle flow. The concentration of particles is shown in Figure 2.16.

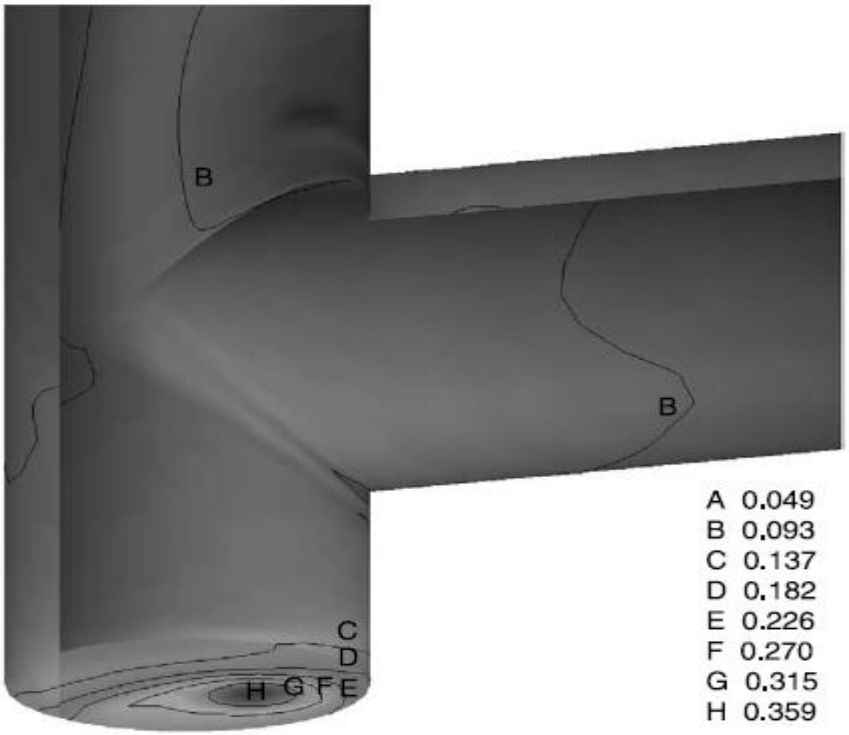

Figure 2.16: Particle concentration (Brown 2002)

He observed a higher concentration of particles in the blanked region of the tee-junction (blanked region at the bottom of tee is shown in Figure 2.16). This result is in agreement with the experimental observation. This shows the capability of CFD to model solid-liquid (slurry) flows in tee junctions. This gave a lot of encouragement, as our problem also deals with slurry flow in branches.

As a lot of information on slurry flows is covered, now it is time to know about Mass Spectroscopy. The next few pages deal with the important terminology used in Mass Spectroscopy.

2.2 Mass Spectroscopy:

Mass spectrometry (MS) is an analytical technique used to determinate the molecular mass of a sample. It is often abbreviated as Mass-Spec or simply MS. Mass Spectroscopy is widely used in biotechnology, pharmaceutical, clinical, environmental, and geological industries. The Mass Spectroscopy principle consists of ionizing chemical compounds to generate charged molecules and measuring their charge-to-mass (q/m) ratios. The typical Mass Spectroscopy procedure consists of 5 stages:

(i) Vaporization: A sample is presented on the MS instrument and undergoes vaporization

(ii) Formation of ions: The components of the sample are ionized by one of a variety of methods which results in the formation of charged particles (ions)

(iii) Acceleration: The positive ions are then accelerated by an electric field

(iv) Deflection: Ions are then deflected by magnetic fields. The lighter they are the more easily they get deflected. The amount of deflection also depends on how much charge the ion carries.

(v) Detection: The beam of ions is detected by a detector. The ions with smaller (q/m) ratio reach the detector faster. The detector displays a graph that has the (q/m) ratio on the horizontal axis and number of particles per second on the vertical. This graph is representative of the mass of the elements present in the sample.

MS instruments consist of three modules: an ion source, which can convert gas phase sample molecules into ions; a mass analyzer, which sorts the ions by their masses by applying electromagnetic fields; and a detector, which measures the value of an indicator quantity and thus provides data for calculating the numbers of each ion present. The technique has both qualitative and quantitative uses. These include identifying unknown compounds, determining the isotopic composition (different types of atoms of the same chemical element, each having a different number of neutrons) of elements in a molecule, and determining the structure of a compound by observing its fragmentation.

Dole et al. (1968) used Electron Spray Ionization (ESI) to produce sample ions. By means of electrospraying a dilute polymer solution into an evaporation chamber, negative ions were produced. Later Horning et al. (1973) used the Atmospheric Pressure Chemical Ionization technique (APCI) to produce sample ions. However, all these ionization methods require samples to be exposed to elevated temperatures, laser radiation, or a high velocity gas stream. Overcoming all these limitations Cody et al. (2005), developed a new ion source for rapid, non-contact analysis at ground potential and at ambient pressure. They named this technique Direct Analysis in Real Time (DART). DART is based on reactions of electronic excited-state species with reagent molecules and polar or non-polar analytes. The principle behind it is a jet of excited-state nitrogen gas is used to impact the surface of the sample to generate ions. DART gives good mass measurements when installed on a time-of-flight mass spectrometer (TOFMS). According to Nasrin et al. (2008) time-of-flight mass spectrometry (TOFMS) is a method of mass spectrometry in which ions are accelerated by an electric field of known strength. This acceleration results in an ion having the same kinetic energy as any other ion that has the same charge. The velocity of the ion depends on the mass-to-charge ratio. The time that it takes for the particle to reach a detector at a known distance is measured. This time will depend on the mass-to-charge ratio of the particle (heavier particles reach lower speeds).

From this time and the known experimental parameters one can find the mass-to-charge ratio of the ion. DART has been applied to analyze gases, liquids, and solids. Apart from all these advantages the most unique feature of the DART technique is the direct detection of chemicals without requiring sample preparation. Since its response is instantaneous, DART provides real-time information. The basic DART source consists of a tube divided into several chambers through which a gas such as nitrogen or helium flows. The gas is introduced into a discharge chamber containing a cathode and an anode. An electrical potential of several kilovolts initiates an electrical discharge producing ions, electrons, and excited-state species in a plasma. The

electronic excited state species (metastable helium atoms or nitrogen molecules) are the working reagent in DART.

The basic DART source is presented in Figure 2.17. The gas flows into a second chamber where a second perforated electrode can be biased to remove ions from the gas stream. The gas flow then passes through a third region that can be optionally heated. Gas exiting through a third perforated electrode or grid is directed toward the mass spectrometer sampling orifice; an insulating cap protects the sample and operator from any exposure to the grid. The grid serves several functions: it acts as an ion repeller and it serves to remove ions of the opposite polarity thereby preventing signal loss by ion-ion recombination. The DART gas flow can be aimed directly toward the mass spectrometer orifice, or the gas flow can be reflected off a sample surface and into the mass spectrometer. Although optimum geometries exist for specific applications, the exact positioning, distance, and angle of DART with respect to the sample surface and the mass spectrometer are not critical.

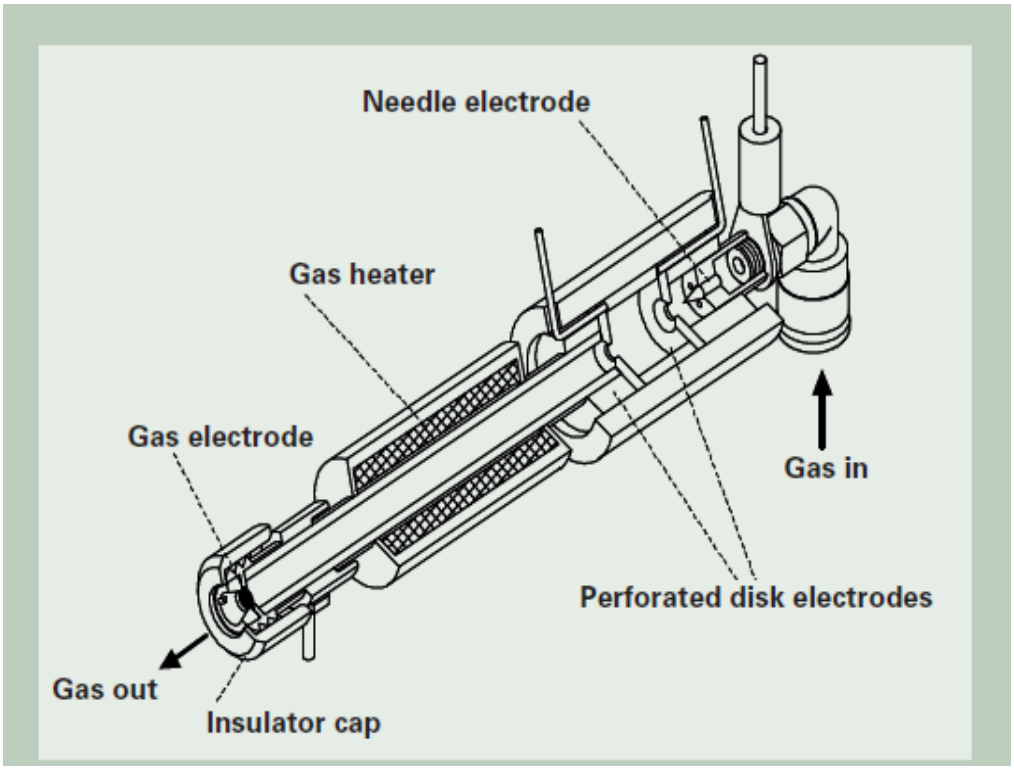

Figure 2.17: Cutaway view of DART source (Cody et al. 2005)

After reviewing the DART technique, it looks highly possible to analyze slurry samples. The schematic of the DART technique used by Cho (2010) is shown in Figure 2.18.

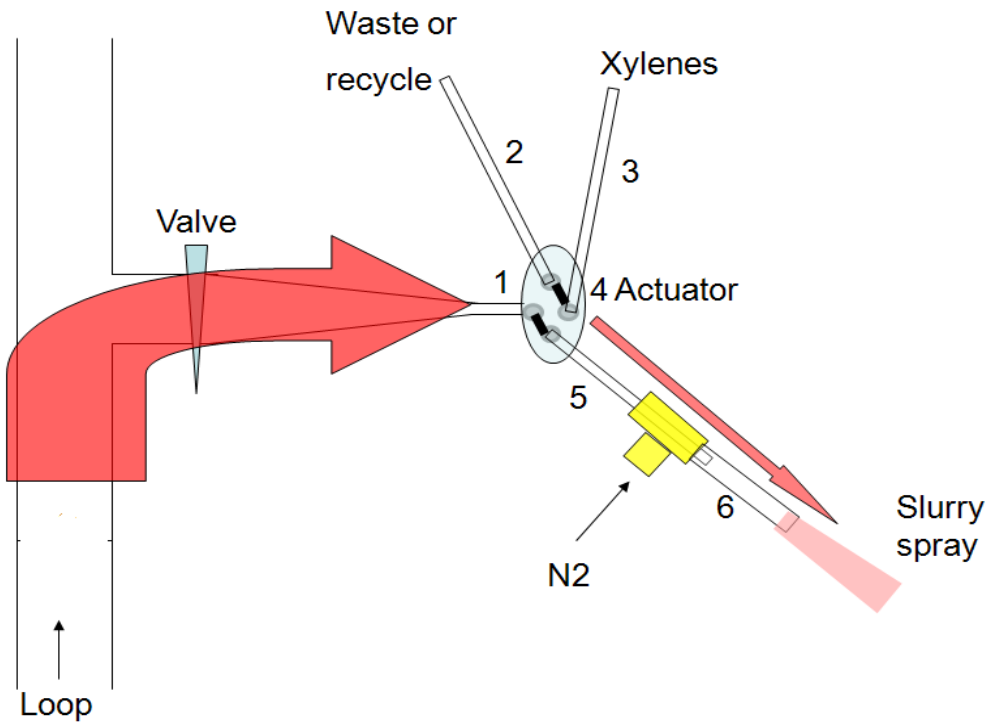

Figure 2.18: Schematic of DART technique used by Cho (2010)

Figure 2.18 shows a sample withdrawn from the recirculation loop, converted to spray by the use of an excited-state nitrogen gas, and finally sent to the Mass-Spectrometer. Figure 2.19 shows the experimental setup of a laboratory scale reactor, where a sample is withdrawn from the recirculation loop using a small diameter sampling pipe. Everything seems perfectly all right until now. But an important question is whether the sample being withdrawn is an exact representative of the slurry in the batch reactor. In other words, if the total slurry has 10% of particles by weight or volume, what is the percentage of particles by weight or volume present in the sample withdrawn using a sampling pipe (branch). This can be determined only by experimental analysis or predicted by CFD analysis.

Figure 2.19: Experimental set used to perform off-line sampling (Cho 2010)

Computational Fluid Dynamics can help in determining the concentration profiles in the sampling pipe located in the fully developed region of the recirculation loop. Comparing the concentration profiles in the fully developed region of the recirculation loop and concentrations profiles in the sampling pipe will provide a good knowledge of the sample being withdrawn. The effect of particle size and initial solids concentration on the concentration profiles in the sampling pipe will also provide a better understanding of the off-line sampling method. The next chapters explain how this is achieved.

CHAPTER III

NUMERICAL APPROACH

3.1 Introduction:

Study of fluids and the forces acting on them is called fluid mechanics. Fluid mechanics is divided into fluid statics and fluid dynamics. Study of fluids at rest is called fluid statics and study of fluids in motion is called fluid dynamics. Computational Fluid Dynamics is a branch of fluid mechanics which uses numerical methods and algorithms to solve the fluid flow problems. With the development of super computers and better codes, CFD analysis proved valuable by producing accurate results to the fluid flow problems. There are many advantages in performing CFD analysis. Simple and complex problems are solved faster at lower cost when compared to performing experiments. Performing CFD analysis followed by experiments gives better results in less time and also helps in designing better systems.

One may think it is easy to solve problems by performing CFD analysis. However, one should keep in mind that CFD can give reliable results only when the problem is presented correctly. In other words one must understand the flow characteristics properly before performing CFD analysis. CFD solves the governing equations that are characteristic of the flow. The governing equations are the conservation of mass, conservation of momentum, and conservation of energy. Conservation of momentum equation is also called the Euler equations for inviscid flows and the Navier-Stokes equations for viscous flows. The present study deals with viscous flows.

The three main steps that are followed in performing CFD analysis are given below:

(i) Pre-processing

(ii) Solving

(iii) Post-processing

In the pre-processing stage the geometry of the problem is created and the volume occupied by the fluid is divided into small units called cells. This process of dividing the flow

volume into discrete cells is called meshing. The region of interest where numerical data has to be computed is also defined in the pre-processing phase. The next step is the solving stage. In this step the created mesh file is loaded into the solving software. Appropriate boundary conditions are then applied. This involves defining the fluid behavior and specifying the properties at the boundaries of the problem. Then, the governing equations are solved iteratively. Finally, the resulting solution is analyzed and visualized in the post-processing stage.

As we are dealing with the slurry flow in pipes, the most important factor that is to be considered is the Reynolds number (Re). Reynolds number is a non-dimensional number, defined as the ratio of inertial forces to viscous forces and it is given as:

$$\mathrm{Re} = \frac{\rho U L}{\mu} \tag{3.1}$$

Flows with low Reynolds numbers are called laminar flows and flows with high Reynolds number are called turbulent flows. For pipe flows, Reynolds numbers below 2100 correspond to laminar flow and Reynolds numbers above 4000 correspond to turbulent flow. Computational Fluid Dynamics has a strong ability to model laminar flows as well as turbulent flows. Reynolds Stress Model (RSM), k-epsilon model, k-omega model, and Spalart-Allmaras model are used to characterize turbulent flows. Each model has its own importance and works well (characterize turbulence) only for specific problems. Choosing a turbulence model is a very important step and is explained clearly in the following sections of this chapter.

Since we are dealing with multiphase flow (solid-liquid flow), it is important to know the capabilities of Computational Fluid Dynamics to characterize these flows. Computational Fluid Dynamics has been widely used to model single phase flows. With the advancements in computers and development of models which can model multi-phase flows, Computational Fluid Dynamics is now being used to model even multi-phase flows. Modeling multi-phase flows,

slurry flows in particular, is one of the hot research topics in the field of fluid mechanics. With the development of multi-phase models Computational Fluid Dynamics is very effective in studying multi-phase flows. Performing experiments to study multi-phase flows, extracting concentration profiles of the particles in particular is very difficult. It requires a lot of skill, instrumentation, money, and time. With proper understanding of the problem and presenting it correctly, Computational Fluid Dynamic analysis will give reliable results.

As mentioned before, the three main steps in performing Computational Fluid Dynamic Analysis are pre-processing, solving, and post-processing. In the present study, ICEM CFD and FLUENT are used to perform all the steps. Both ICEM CFD and FLUENT 12.0 belong to ANSYS family. ANSYS FLUENT is the most widely used CFD package in industry and educational institutions.

3.2 Governing equations:

Governing equations are the differential equations that describe the flow field. The three main governing equations are

(i) Conservation of mass

(ii) Conservation of momentum

(iii) Conservation of energy

Conservation of mass is also known as the continuity equation. The continuity equation in its differential form is presented in Equation 3.2 below.

$$\frac{\partial \rho}{\partial t} + \frac{\partial (\rho u)}{\partial x} + \frac{\partial (\rho v)}{\partial y} + \frac{\partial (\rho w)}{\partial z} = 0 \qquad (3.2)$$

For incompressible flows (constant density), the continuity equation simplifies to Equation 3.3.

$$\frac{\partial u}{\partial x}+\frac{\partial v}{\partial y}+\frac{\partial w}{\partial z}=0 \tag{3.3}$$

Conservation of momentum is also known as the Navier-Stokes equation for a Newtonian fluid. The Navier-Stokes equation for an incompressible flow of a Newtonian fluid is presented in Equation 3.4. A Newtonian fluid is a fluid for which stress is linearly proportional to strain and the constant of proportionality is called viscosity.

$$\rho(\frac{\partial v}{\partial t}+v.\nabla v)=-\nabla p+\mu\nabla^2 v+f \tag{3.4}$$

It is very important to understand the terms in Equation 3.4.

$$\overbrace{\rho\Big(\underbrace{\frac{\partial \mathbf{v}}{\partial t}}_{\text{Unsteady acceleration}}+\underbrace{\mathbf{v}\cdot\nabla\mathbf{v}}_{\text{Convective acceleration}}\Big)}^{\text{Inertia (per volume)}}=\overbrace{\underbrace{-\nabla p}_{\text{Pressure gradient}}+\underbrace{\mu\nabla^2\mathbf{v}}_{\text{Viscosity}}}^{\text{Divergence of stress}}+\underbrace{\mathbf{f}}_{\text{Other body forces}} \tag{3.5}$$

The left hand side of the equation represents the acceleration of the fluid, while the right hand side represents the forces acting on the fluid. This is explained by Newton's second law. Newton's second law states that the net force acting on a particle is equal to rate of change of its linear momentum.

$$ma = F \tag{3.6}$$

The Navier-Stokes equations are commonly used in three coordinate systems: Cartesian, cylindrical, and spherical. The Navier-Stokes equations in a Cartesian coordinate system are presented below.

$$\rho(\frac{\partial u}{\partial t}+u\frac{\partial u}{\partial x}+v\frac{\partial u}{\partial y}+w\frac{\partial u}{\partial z})=-\frac{\partial p}{\partial x}+\mu(\frac{\partial^2 u}{\partial x^2}+\frac{\partial^2 u}{\partial y^2}+\frac{\partial^2 u}{\partial z^2})+\rho g_x$$

$$\rho\left(\frac{\partial v}{\partial t}+u\frac{\partial v}{\partial x}+v\frac{\partial v}{\partial y}+w\frac{\partial v}{\partial z}\right)=-\frac{\partial p}{\partial y}+\mu\left(\frac{\partial^2 v}{\partial x^2}+\frac{\partial^2 v}{\partial y^2}+\frac{\partial^2 v}{\partial z^2}\right)+\rho g_y$$

$$\rho\left(\frac{\partial w}{\partial t}+u\frac{\partial w}{\partial x}+v\frac{\partial w}{\partial y}+w\frac{\partial w}{\partial z}\right)=-\frac{\partial p}{\partial z}+\mu\left(\frac{\partial^2 w}{\partial x^2}+\frac{\partial^2 w}{\partial y^2}+\frac{\partial^2 w}{\partial z^2}\right)+\rho g_z \tag{3.8}$$

The energy equation is given below, where Φ represents viscous dissipation.

$$\rho\frac{Dh}{Dt}=\frac{Dp}{Dt}+div\left(k\nabla T\right)+\Phi \tag{3.9}$$

Using the Navier-Stokes equation, in the form described previously, it is not computationally feasible to account for turbulence which is characteristic of high Reynolds number pipe flows. Most of the research on turbulent-flow analysis in the past century has used the concept of time averaging. Applying time averaging to the basic equations of motion yields the Reynolds equations. It involves both the mean ($\bar{u}$) and fluctuating (u') quantities (White 2006). Applying Reynolds decomposition:

$$u=\bar{u}+u'$$

$$v=\bar{v}+v'$$

$$w=\bar{w}+w'$$

$$p=\bar{p}+p'$$

$$T=\bar{T}+T' \tag{3.10}$$

Now substituting and applying the rules of averaging (average of a fluctuating term multiplied to a mean term vanishes, while the average of two fluctuating terms remains) into the continuity equation yields two equations:

$$\frac{\partial\bar{u}}{\partial x}+\frac{\partial\bar{v}}{\partial y}+\frac{\partial\bar{w}}{\partial z}=0 \tag{3.11}$$

$$\frac{\partial u'}{\partial x}+\frac{\partial v'}{\partial y}+\frac{\partial w'}{\partial z}=0 \tag{3.12}$$

This shows both mean and fluctuating components satisfying separately the continuity equation. Now applying the same procedure to non-linear Navier-Stokes equations yields

$$\rho \frac{D\overline{V}}{Dt} = \rho g - \nabla \overline{p} + \nabla . \tau_{ij} \tag{3.13}$$

$$\tau_{ij} = \mu(\frac{\partial \overline{u_i}}{\partial x_j} + \frac{\partial \overline{u_j}}{\partial x_i}) - \rho \overline{u_i' u_j'} \tag{3.14}$$

Mathematically, the turbulent inertia terms behave as if the total stress on the system were composed of the Newtonian viscous stresses plus an additional or apparent turbulent-stress tensor $\rho \overline{u_i' u_j'}$ (White 2006).The effects of these turbulent stresses on the flow field can be simulated either by modeling them algebraically or through additional partial differential transport equations.

Reynolds-averaged Navier-Stokes (RANS) requires less computational power, and gives reliable results for a certain class of problems such as the one in hand. Therefore, in the present study RANS approach is used to model turbulence. In Direct Numerical Simulation (DNS), Navier-Stokes equations are solved numerically without any turbulence models. In other words, the whole range of spatial and temporal scales of turbulence is resolved. This is the most computationally expensive approach of all the three. Large Eddy Simulation (LES) requires less computational power when compared to Direct Numerical Simulation (DNS). In this technique large eddies are simulated, while the small eddies are mathematically modeled.

3.3 Turbulence models and their selection:

Von Karman in 1937 defined turbulence as, *"Turbulence is an irregular motion which in general makes its appearance in fluids, gaseous or liquid, when they flow past solid surfaces or even when neighboring streams of the same fluid flow past or over one another."* Many researchers found the word "irregular motion" to be too imprecise. Later, Hinze in 1975 provided a sharper definition of turbulence as, *"Turbulent fluid motion is an irregular condition of flow in which the various quantities show a random variation with time and space coordinates, so that statistically distinct averaged values can be discerned."*

It is very important to model turbulence which is the characteristic of high Reynolds number flows. Though DNS and LES can give higher degrees of accuracy, they are computationally very expensive. On the other hand, Reynolds-Averaged Navier-Stokes can give accurate results with less computational power, when the problem is presented correctly. While performing Computational Fluid Dynamics, there should be a balance between accuracy and computational power. As the RANS model has all the capabilities to solve the problem in hand, it is chosen as the approach to model turbulence.

The Computational Fluid Dynamics software (ANSYS FLUENT) used in the present study offers a number of RANS models. The Reynolds stresses which appear as unknowns in the Reynolds equations are determined by a turbulence model, either via the turbulent viscosity hypothesis or more directly from modeled Reynolds-stress transport equations (Pope 2000). The turbulent viscosity hypothesis is also called the Boussinesq hypothesis. The Boussinesq method involves using an algebraic equation for the Reynolds stresses which includes determining the turbulent viscosity, and depending on the level of sophistication of the model, solving transport equations for determining the turbulent kinetic energy and dissipation. In Reynolds stress models, model transport equations are solved for the individual Reynolds stresses and for the dissipation

(Pope 2000). Therefore, the turbulent-viscosity hypothesis is eliminated. As the Reynolds Stress Model solves additional seven transport equations, it requires very high computational resources.

In many cases, models based on the Boussinesq hypothesis perform very well, and the additional computational expense of the Reynolds stress model is not justified. However, the RSM is clearly superior for situations in which the anisotropy of turbulence has a dominant effect on the mean flow. As we are not dealing with such flows, using a model based on the Boussinesq hypothesis is justified. Most of the turbulence models that FLUENT offers are based on the Boussinesq hypothesis. These models are either one equation models or two equation models. The Spalart-Allmaras model is a one equation model. It solves a modeled transport equation for the kinematic eddy viscosity. This model is used to solve external flows and is not suitable for solving 3D flows. Two equation models have served as the foundation for much turbulence model research. Two equation models can be used to predict properties of a given turbulent flow with no prior knowledge of the turbulence structure (Wilcox 2006). The k-ε turbulence model is the most widely used complete turbulence model in which transport equations are solved for two turbulence quantities – k and ε.

In addition to the Boussinesq hypothesis, the k-ε model consists of (Pope 2000)

(i) The model transport equation for k

(ii) The model transport equation for ε and

(iii) The specification of turbulent viscosity as

Kinematic Eddy Viscosity:

$$\upsilon_t = C_\mu \frac{k^2}{\varepsilon} \tag{3.15}$$

Turbulence Kinetic Energy:

$$\frac{\partial k}{\partial t} + U_i \frac{\partial k}{\partial xj} = \frac{\partial}{\partial x_j}[(\upsilon + \frac{\upsilon_t}{\sigma_k})\frac{\partial k}{\partial x_j}] + \tau_{ij}\frac{\partial U_i}{\partial x_j} - \varepsilon \tag{3.16}$$

Dissipation Rate:

$$\frac{\partial \varepsilon}{\partial t} + U_j \frac{\partial \varepsilon}{\partial x_i} = \frac{\partial}{\partial x_j}[(\upsilon + \frac{\upsilon_t}{\sigma_\varepsilon})\frac{\partial \varepsilon}{\partial x_j}] + C_{1\varepsilon}\frac{\varepsilon}{k}\tau_{ij}\frac{\partial U_i}{\partial x_j} - C_{2\varepsilon}\frac{\varepsilon^2}{k} \tag{3.17}$$

The k-ε model is the most widely used complete turbulence model, and it is incorporated in most commercial CFD software (Pope 2000). Other variations of k-ε turbulence model are the RNG k-ε model and the realizable k-ε model. The RNG k-ε model has an additional term in its ε equation that significantly improves the accuracy for rapidly strained flows. The realizable k-ε model contains a new formulation for the turbulent viscosity. Walls affect the turbulent flows because viscous damping and kinematic blocking near the wall reduce velocity fluctuations and large gradients in the temperature and velocity fields occur near the wall.

The region near the wall (inner layer) can be divided into three layers:

(i) Viscous sublayer, where molecular viscosity makes the flow behave close to laminar.

(ii) Buffer layer, where the laminar and turbulent stresses of the flow both are important.

(iii) Fully turbulent region, where the turbulence plays a dominant role.

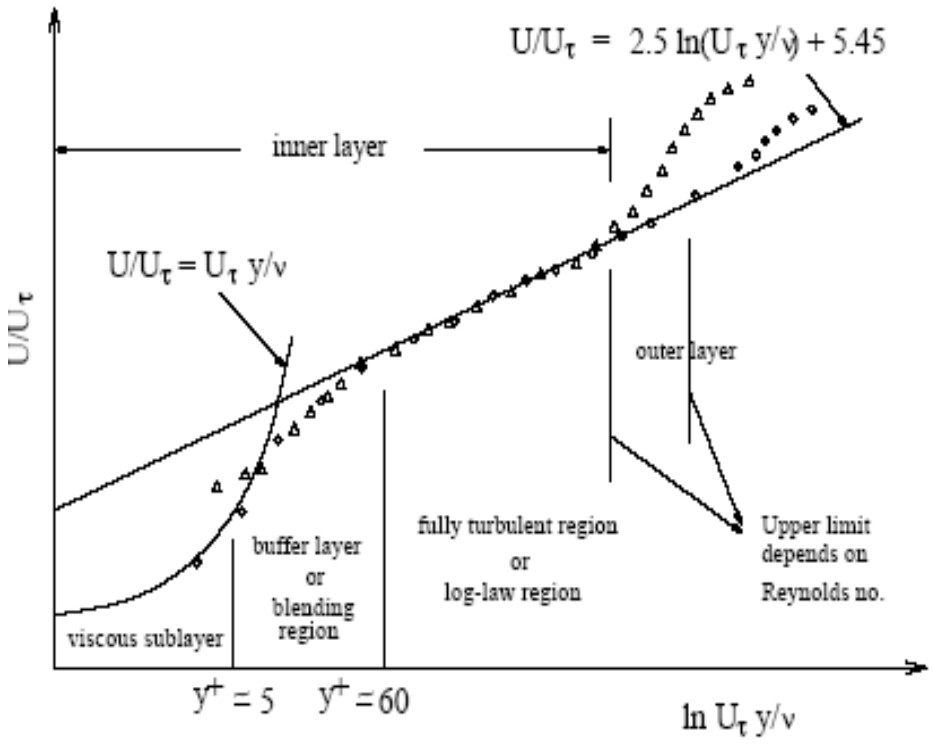

Figure 3.1: Illustration of the near-wall region (Wilcox 2006)

Near wall modeling impacts the accuracy of the numerical solution. The near-wall region generates large gradients. Therefore, accurate representation of the flow in the near-wall region determines successful prediction of wall bounded turbulent flows. Solving turbulent flows where the resolution close to the wall is fine demands large computational power. Thus, the computational fluid dynamic software (FLUENT) is equipped with what are known as "wall functions". These functions are semi-empirical formulas used to bridge the viscosity-affected region between the wall and the fully-turbulent region. The use of wall functions obviates the need to modify the turbulence models to account for the presence of the wall. The wall functions can be understood by observing Figure 3.2.

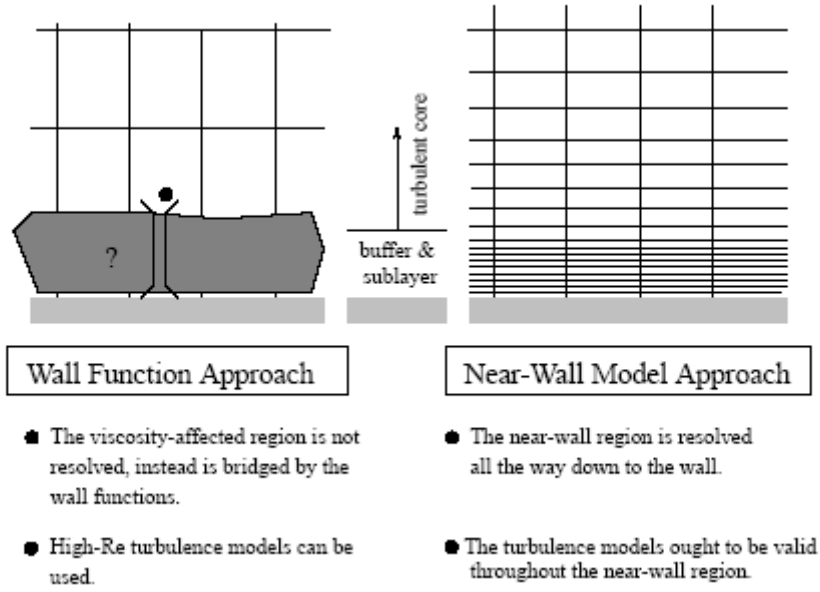

Figure 3.2: Near-wall treatments (Hirsch 2007)

FLUENT offers k-ε turbulence model with different wall functions that are suitable for modeling high Reynolds number flows. Therefore, the k-ε turbulence model with wall function approach is selected as the turbulence model. As we are dealing with solid-liquid flow in pipes, the next step to be considered is choosing the right multi-phase model. FLUENT offers a number of multi-phase models, but the model that satisfies the present needs is required. The next section deals with the selection of the multi-phase model.

3.4 Multi-phase flow models and their selection:

Mixture of the phases of solid, liquid and gas is called a multi-phase system. Gas bubbles rising in liquid, water droplets falling in air, and solid particles transported by a fluid are the real time examples of a multi-phase system. There are two approaches for the numerical calculation of multiphase flows:

(i) Euler-Lagrange approach

(ii) Euler-Euler approach

Euler-Lagrange Approach:

In the Euler-Lagrange approach, the fluid phase is treated as a continuum by solving the time-averaged Navier-Stokes equations, while the dispersed phase is solved by tracking a large number of particles, bubbles, or droplets through the calculated flow field. The dispersed phase can exchange momentum, mass, and energy with the fluid phase. A fundamental assumption made in this model is that the dispersed secondary phase occupies a low volume fraction. The particle or droplet trajectories are computed individually at specified intervals during the fluid phase calculation. This makes the model appropriate for the modeling of spray dryers, coal and liquid fuel combustion, and some particle-laden flows, but inappropriate for the modeling of liquid-liquid mixtures, fluidized beds, or any application where the volume fraction of the secondary phase is not negligible. As we are dealing with a flow where there is a significant amount of secondary phase volume fraction (up to 30%), using the Euler-Lagrange approach is completely eliminated. The next option is the Euler-Euler approach.

Euler-Euler Approach:

In the Euler-Euler approach, the different phases are treated mathematically as interpenetrating media. Since the volume of a phase cannot be occupied by the other phases, the concept of phase volume fraction is introduced. These volume fractions are assumed to be continuous functions of space and time and their sum is equal to one. Conservation equations for each phase are derived to obtain a set of equations, which have similar structure for all phases. These equations are closed by providing constitutive relations that are obtained from empirical information.

FLUENT offers three different Euler-Euler multiphase models. They are:

(i) The Volume of Fluid Model

(ii) The Mixture Model

(iii) The Eulerian Model

The Volume of Fluid Model (VOF): The VOF model is a surface-tracking technique applied to a fixed Eulerian mesh. It is designed for two or more immiscible fluids where the position of the interface between the fluids is of interest. In the VOF model, a single set of momentum equations is shared by the fluids, and the volume fraction of each of the fluids in each computational cell is tracked throughout the domain. Applications of the VOF model include stratified flows, free-surface flows, filling, sloshing, the motion of large bubbles in a liquid, the motion of liquid after a dam break, the prediction of jet breakup (surface tension), and the steady or transient tracking of any liquid-gas interface. From this it is clear that the VOF model is not suitable to model slurry flows. Hence, we have to choose between the Mixture model and the Eulerian model.

The Mixture Model: The Mixture model is designed for two or more phases (fluid or particulate). In the Mixture model, the phases are treated as interpenetrating media. The mixture model solves for the mixture momentum equation and prescribes relative velocities to describe the dispersed phases. Applications of the mixture model include particle-laden flows with moderate loading (up to 50%), bubbly flows, sedimentation, and cyclone separators.

The Eulerian Model: The Eulerian model is the most complex of all the multiphase models in FLUENT. It solves a set of n momentum and continuity equations for each phase. Coupling is achieved through the pressure and interphase exchange coefficients. The manner in which this coupling is handled depends upon the type of phases involved; granular (fluid-solid) flows are handled differently than non-granular (fluid-fluid) flows. For granular flows, the properties are obtained from application of kinetic theory. Momentum exchange between the phases is also dependent upon the type of mixture being modeled. Applications of the Eulerian multiphase model include bubble columns, risers, particle suspension, and fluidized beds.

From the above discussion it is clear that both the models can be used to model a solid-liquid flow. To choose the best model out of the two, a few other factors are also considered. The Stokes number is a very important parameter in fluid-particle flows (Crowe 1998). It is used as an important parameter in deciding the multiphase model. The Stokes number related to the particle velocity is defined again (previously in section 2.1) as

$$St_v = \frac{\tau_v}{\tau_F}$$

$$\tau_v = \frac{\rho_d d_p^2}{18\mu}$$

$$\tau_F = \frac{L_s}{U} \qquad (2.1)$$

Where τ_v is the momentum response time, τ_F is the time characteristic of the flow field, L_s is the characteristic length scale, and U is the flow velocity. Considering the diameter of the sampling pipe as the characteristic length scale, 300 micron particle size, and substituting all the values into (3.19) gives the Stokes number which is less than 1. Flows having Stokes number less than 1 can be modeled accurately by the mixture model. One more advantage of using the mixture model is that it is computationally very economical compared to the Eulerian model. The Eulerian model requires very high computational power and it is used for flows having particles with Stokes number greater than one. As we are dealing with liquid-solid flow having Stokes number less than one, the mixture model is selected as the multiphase model.

Modeling with mixture multiphase model:

As mentioned before, the mixture model can model n phases (fluid or particulate) by solving the momentum, continuity, and energy equations for the mixture, the volume fraction equations for the secondary phases, and algebraic expressions for the relative velocities. The mixture model allows the user to select granular phases and calculates all properties of the granular phases. This is specially designed for liquid-solid flows.

The equations that are solved in the mixture model are given below. The continuity equation is given by Equation 3.19, where $\overline{v_m}$ is the mass-averaged velocity, ρ_m is the mixture density, α_k and is the volume fraction of the phase k.

$$\frac{\partial(\rho_m)}{\partial t} + \nabla.(\rho_m \overline{v_m}) = 0$$

$$v_m = \frac{\sum_{k=1}^{n} \alpha_k \rho_k \overline{v_k}}{\rho_m}$$

$$\rho_m = \sum_{k=1}^{n} \alpha_k \rho_k \tag{3.19}$$

The momentum equation for the mixture is obtained by adding the momentum equations of both the phases. It is represented by Equation 3.20, where n is the number of phases, $\overline{F}$ is a body force, μ_m is the viscosity of the mixture, and $\overline{v_{d,k}}$ is the drift velocity for secondary phase.

$$\frac{\partial(\rho_m \overline{v_m})}{\partial t} + \nabla.(\rho_m \overline{v_m}.\overline{v_m}) = -\nabla p + \nabla.[\mu_m(\nabla \overline{v_m} + \nabla \overline{v_m^T})] + \rho_m \overline{g} + \overline{F} + \nabla.[\sum_{k=1}^{n} \alpha_k \rho_k \overline{v_{dr,k}}\,\overline{v_{dr,k}}]$$

$$\mu_m = \sum_{k=1}^{n} \alpha_k \mu_k$$

$$\overline{v_{d,k}} = \overline{v_k} - \overline{v_m} \tag{3.20}$$

The energy equation is represented by Equation 3.21, where k_{eff} is the effective conductivity, k_t is the turbulence thermal conductivity, and S_E includes any other volumetric heat sources.

$$\frac{\partial}{\partial t}\sum_{k=1}^{n}(\alpha_k \rho_k E_k) + \nabla.\sum_{k=1}^{n}(\alpha_k \overline{v_k}(\rho_k E_k + p)) = \nabla.(k_{eff}\nabla T) + S_E$$

$$k_{eff} = \sum(\alpha_k (k_k + k_t)) \tag{3.21}$$

As mentioned before, the mixture model can model n phases by solving the algebraic expressions for relative velocities. They are given by the Equation 3.22. $\overline{v_{pq}}$ is the slip velocity and is defined as the velocity of the secondary phase relative to the velocity of the primary phase, c_k is the mass fraction, f_{drag} and is the drag function.

$$\overline{v_{pq}} = \overline{v_p} - \overline{v_q}$$

$$c_k = \frac{\alpha_k \rho_k}{\rho_m}$$

$$\overline{v_{dr,p}} = \overline{v_{pq}} - \sum_{k=1}^{n} c_k \overline{v_{qk}}$$

$$v_{pq} = \frac{(\rho_p - \rho_m) d_p^2 \vec{a}}{18 \mu_q f_{drag}} - \frac{v_m}{\alpha_p \sigma_D} \nabla \alpha_q \tag{3.22}$$

Finally, the volume fraction equation for the secondary phase is given by Equation 3.23 and it is obtained from the continuity equation for the secondary phase.

$$\frac{\partial}{\partial t}(\alpha_p \rho_p) + \nabla.(\alpha_p \rho_p \overline{v_m}) = -\nabla.(\alpha_p \rho_p \overline{v_{dr,p}}) + \sum_{q=1}^{n} (\dot{m}_{qp} - \dot{m}_{pq}) \tag{3.23}$$

Modified k and ε equations are given by Equations 3.24 and 3.25 respectively.

$$\frac{\partial}{\partial t}(\rho_m k) + \nabla.(\rho_m \overline{v_m} k) = \nabla.(\frac{\mu_{t,m}}{\sigma_k} \nabla k) + G_{k,m} - \rho_m \varepsilon \tag{3.24}$$

$$\frac{\partial}{\partial t}(\rho_m \varepsilon) + \nabla.(\rho_m \overline{v_m} \varepsilon) = \nabla.(\frac{\mu_{t,m}}{\sigma_\varepsilon} \nabla \varepsilon) + \frac{\varepsilon}{k}(C_{1\varepsilon} G_{k,m} - C_{2\varepsilon} \rho_m \varepsilon) \tag{3.25}$$

Where mixture density (ρ_m), mass-averaged velocity ($\overline{v_m}$), and turbulent viscosity ($\mu_{t,m}$) are given by Equation 3.26.

$$\rho_m = \sum_{i=1}^{n} \alpha_i \rho_i$$

$$\overline{v_m} = \frac{\sum_{i=1}^{n} \alpha_i \rho_i \overline{v_i}}{\sum_{i=1}^{n} \alpha_i \rho_i}$$

$$\mu_{t,m} = \rho_m C_\mu \frac{k^2}{\varepsilon} \tag{3.26}$$

So far we have looked at the governing equations, different turbulence models and selected k-ε turbulence model with wall functions approach as the final turbulence model, and we have also selected the mixture model as our multiphase model. The next step is creating geometries, applying suitable meshes, and solving for final results. Before creating geometries, it will be useful to have a good look at the problems being considered and the phases involved. Therefore, the next section deals with the different geometries (horizontal pipe, vertical pipe, and vertical pipe with a branch) and the phases considered for the present study.

3.5 Geometries and phases:

Liquid-Solid flow in three pipe geometries is considered in the present study. They are

(i) Horizontal pipe

(ii) Vertical pipe

(iii) Vertical pipe with a branch section (sampling pipe)

Horizontal and vertical pipes are 0.0508 m in diameter and 2.54 m in length. Flow in a pipe becomes fully-developed at around 30 – 35 diameters length. Therefore, to ensure the flow is fully-developed, 50 diameter long pipes are considered. To compare the concentration profiles in the fully-developed region and in the sampling pipe, a small diameter pipe is placed in the fully-developed region of the vertical pipe. The diameter of the sampling pipe is 0.0127 m. All the three geometries are shown in Figure 3.3.

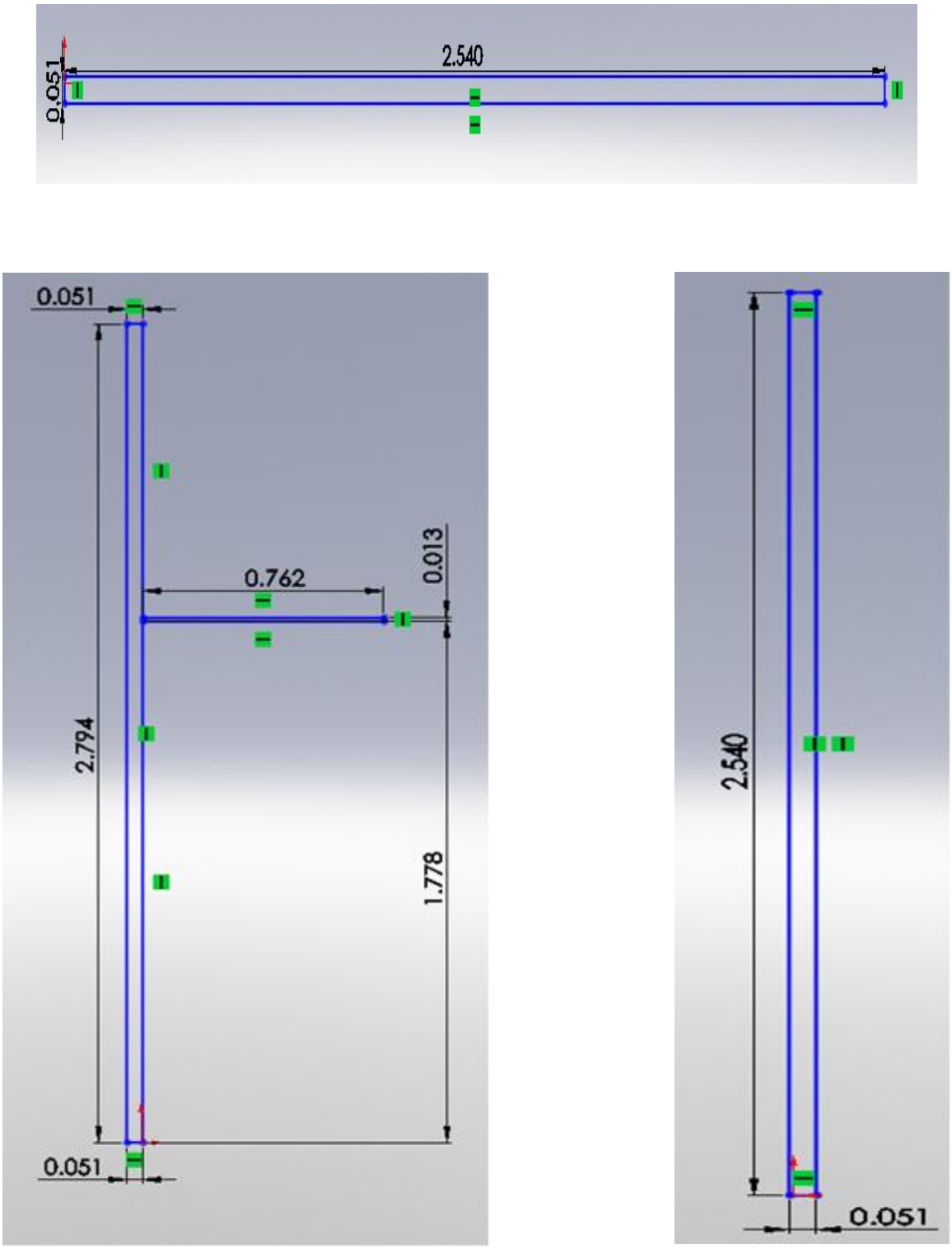

Figure 3.3: Geometries considered in the present study (Top: Horizontal pipe, Left: Vertical pipe with a branch section (sampling pipe), and Right: Vertical pipe) (All units in meters)

As we are dealing with liquid-solid flow, it is important to specify the two phases involved. Xylene is the primary phase and 2-Amino-4, 6-dimethylpyrimidine (ADP) is the secondary phase. Properties of both the phases are specified in Table 3.1 below.

	Viscosity (Pa-S)	Density (Kg/m^3)
Xylene	6.2×10^{-4}	870
ADP	N/A	1480

Table 3.1 Properties of the phases

3.6 Pre-processing:

Pre-processing is the first step in performing Computational Fluid Dynamic analysis. Creating the geometry, dividing the volume into discrete cells also called meshing, and applying boundary conditions comes under Pre-Processing stage. In the present study ICEM CFD is used to perform Pre-Processing.

The horizontal and vertical pipes are created easily by creating an edge and revolving it around the axis. But the vertical pipe with a branch section (sampling pipe) is a complex geometry to create. First a long vertical plane pipe is created and then a small pipe (horizontal) is created at the fully-developed region (35 diameters away from pipe inlet). Now we have two volumes. These two volumes are merged (united) to form a single volume. All the geometries are three dimensional. As the geometries are ready, the next step is to apply a suitable mesh. As we are dealing with 3D models, the mesh is created using tetrahedral elements. For grid independence study, coarse, medium, and fine grids for each model are created. More about grid independence is presented in Sections 3.8 and 4.3. After meshing, boundary conditions are applied. Boundary conditions are specified in Table 3.2.

	INLET	OUTLET	WALL	VOLUME
Vertical pipe	Velocity	Pressure	Wall	Fluid
Horizontal Pipe	Velocity	Pressure	Wall	Fluid
Vertical pipe with a branch section for sampling	Velocity	Outflow	Wall	Fluid

Table 3.2: Boundary conditions

Meshed models with boundary conditions are shown below.

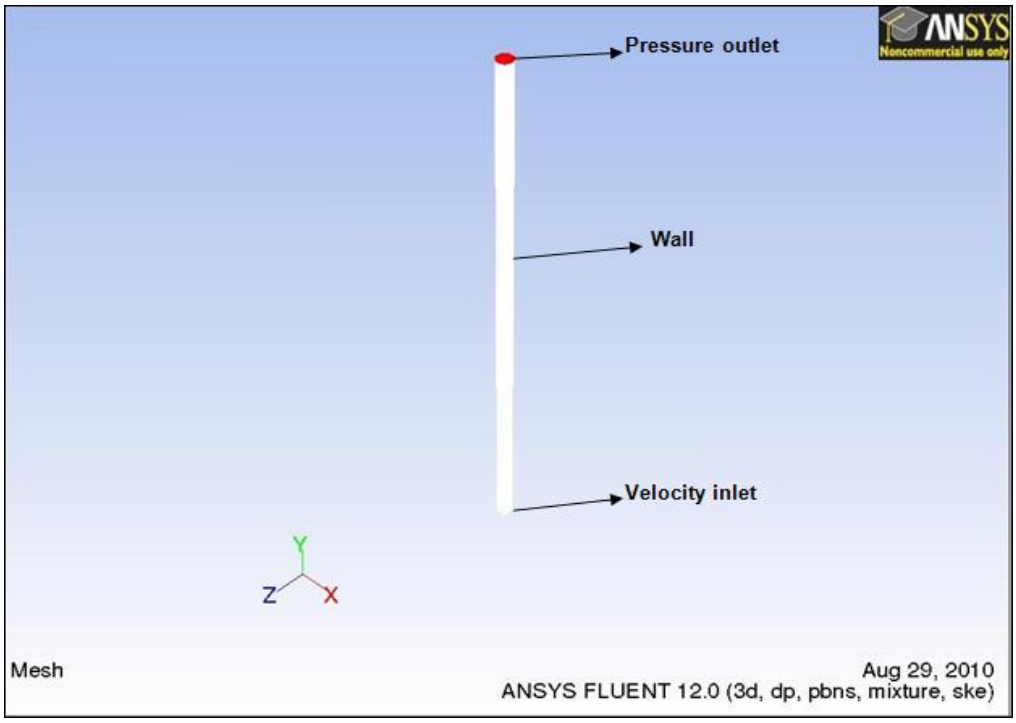

Figure 3.4: Vertical pipe meshed geometry

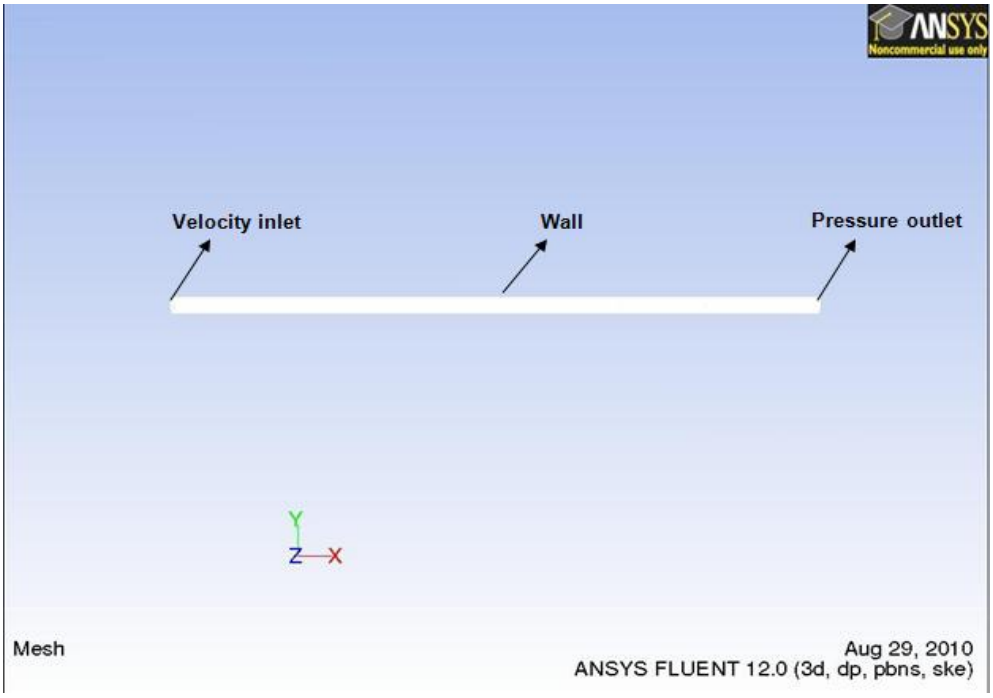

Figure 3.5: Horizontal pipe meshed geometry

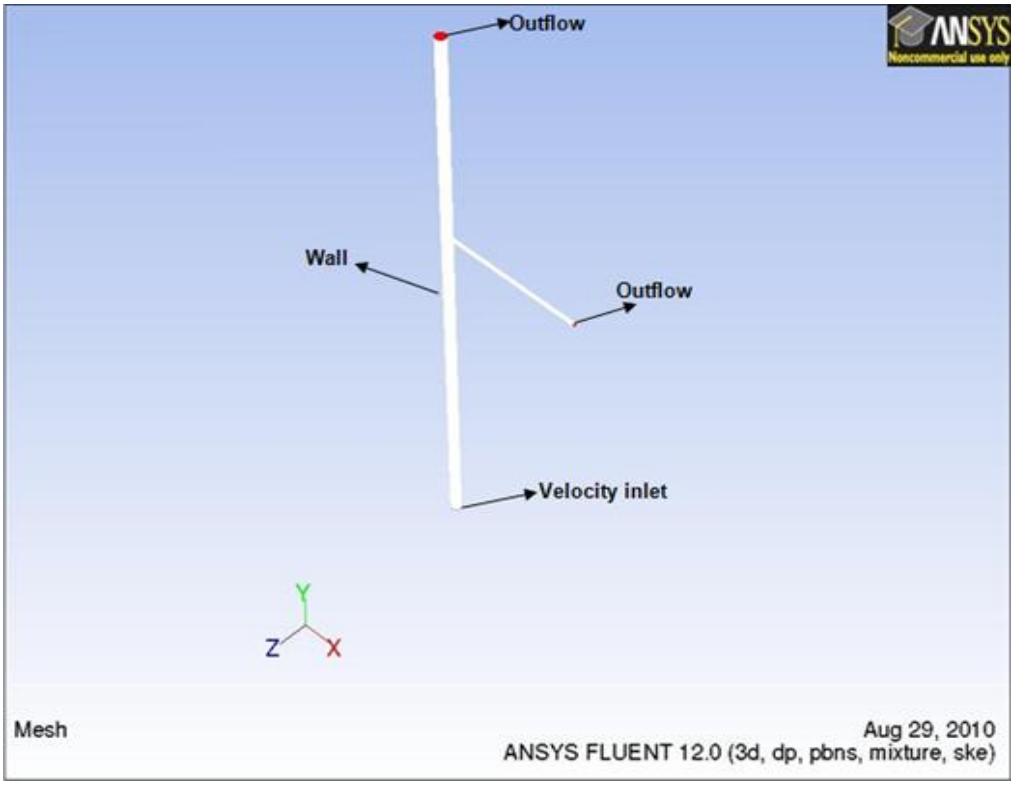

Figure 3.6: Vertical pipe with a branch section (sampling pipe) meshed geometry

The meshed models are saved as mesh files and are uploaded into the solver. The solving step is presented next.

3.7 Solving:

For the present study, FLUENT is used as the solver. The generated mesh file is uploaded into the solver. As we are dealing with three dimensional models, the 3d double precision solver is used. It is also called 3ddp. The double precision solver gives better results than the normal 3d solver. The solver reads the mesh files and gives the number of cells and nodes created. Steady state solver is used to obtain the solution. As mentioned before, we will be using the mixture model for multi-phase modeling. As the mixture model is not compatible with the density-based solver, the pressure-based solver is selected. For modeling turbulence, the k-ε turbulence model is selected with standard wall functions. The most important factor to be considered while modeling turbulence using the k-ε model with standard wall function approach is the value of the lowest y^+, which should be in the range of 30 to 60. Therefore, y^+ is checked first by running the simulation using Xylene as the only fluid. If the y^+ is not in the range of 30 to 60, the "adapt function" is used to adapt the boundaries and once again the simulation is performed. This process is continued until the required y^+ is achieved. The change in the mesh when grid adaptation is performed is shown in Figure 3.7.

Once the required y^+ is achieved, that particular grid is used for all the simulations. As we are dealing with three geometries, grid adaptation is performed for all the models. Next, the multiphase model is activated. In our case it is the mixture model. The material properties of two phases are entered into the solver. Xylene is selected as the primary phase and ADP is selected as the secondary phase. While selecting ADP as the secondary phase, we can enter the diameter of the ADP particles. As gravity plays a very important role, the gravity option is checked. The next step is to specify the boundary conditions.

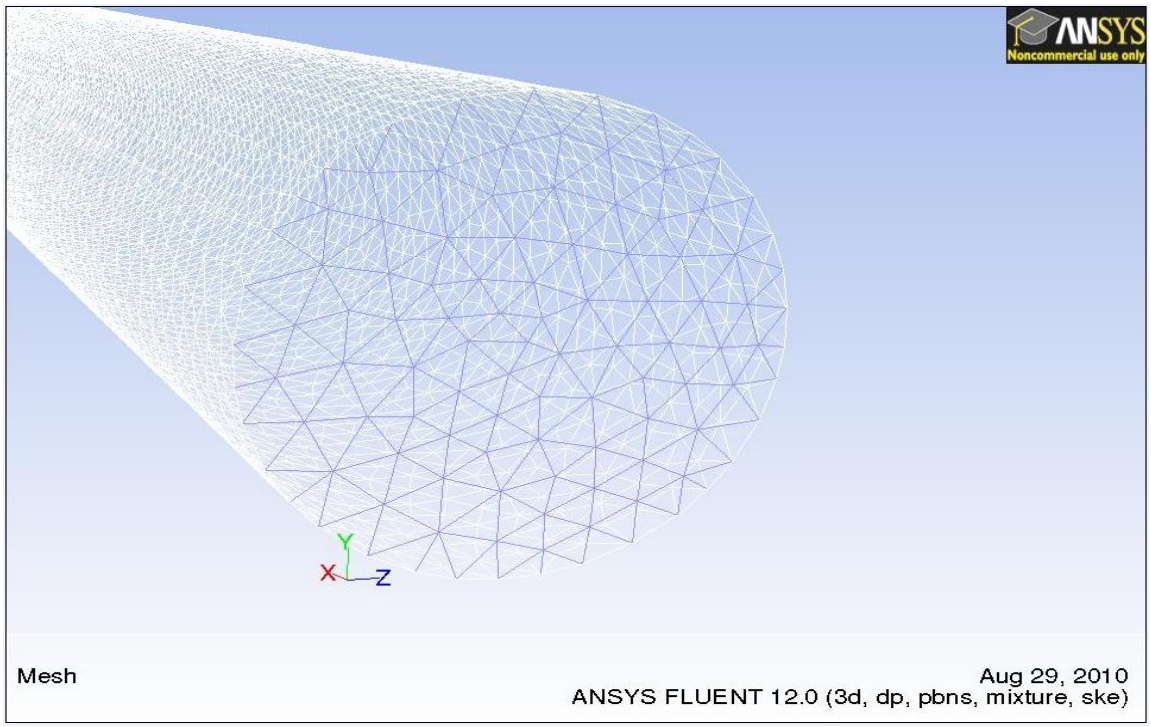

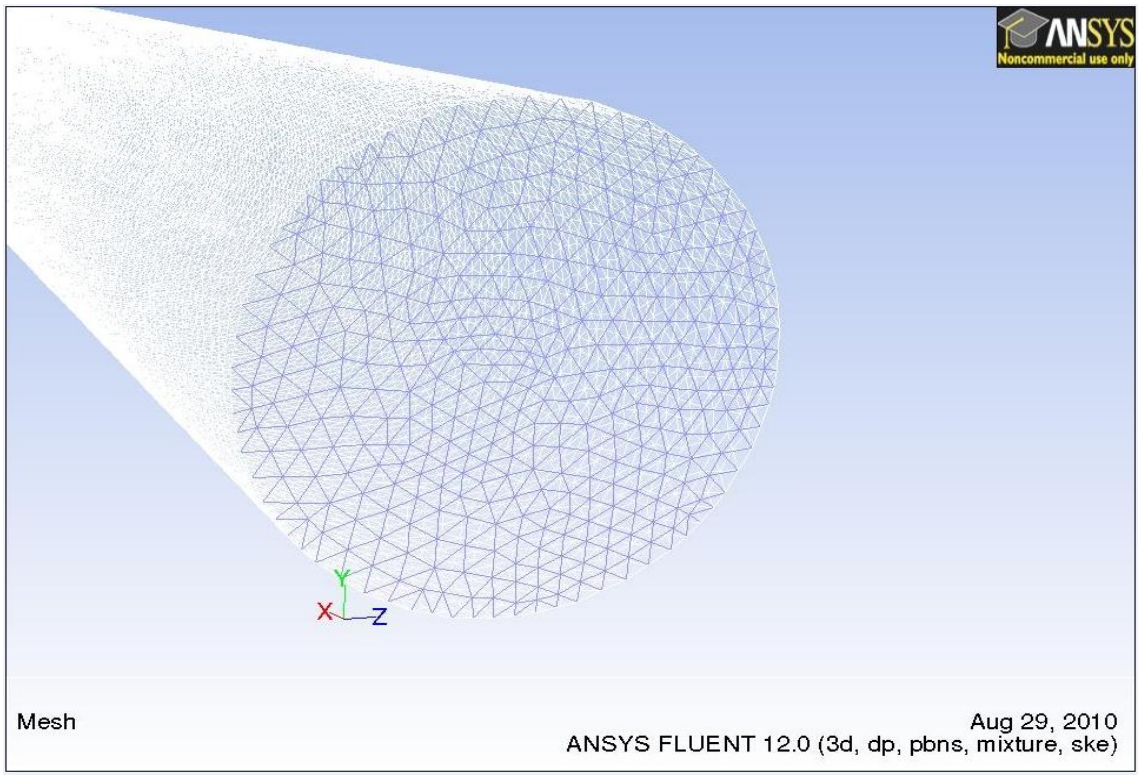

Figure 3.7: Changes in the grid after performing grid adaptation (Top: Original grid, Bottom: After adaptation)

For horizontal and vertical pipes the same boundary conditions are specified. For vertical pipe with a branch section (sampling pipe), different outlet boundary condition is used. Boundary conditions for horizontal and vertical pipes are explained first, followed by the vertical pipe with a branch section. For vertical and horizontal pipe, inlet velocity for the primary phase (Xylene) is given as 2 m/s. The initial guess for the secondary phase (ADP) velocity can be any arbitrary value less than 2 m/s. Thus the secondary phase is provided with a velocity of 1.5 m/s. The initial volume fraction of the secondary phase is provided. This value should be less than 40%, which is the limiting value for the mixture model. For the mixture phase, turbulent intensity and hydraulic diameter values are provided at the inlet. Turbulent intensity is calculated from the equation below (Lu 2009).

$$T.I = 0.16 * (\mathrm{Re})^{(-1/8)} \tag{3.28}$$

From the above equation turbulent intensity is specified as 3.4% and the hydraulic diameter is specified as 0.0508 m. The outlet is kept at atmospheric pressure (1 atm). At the outlet, for the mixture phase, turbulent intensity and hydraulic diameter values are provided. To achieve fully-developed flow conditions, backflow volume fraction is assumed to be the same as the input value (FLUENT will use the backflow conditions if the fluid is flowing into the computational domain through the outlet, since backflow might occur at some point during the solution procedure, one should set reasonable backflow conditions to prevent convergence from being adversely affected).

The inlet boundary conditions for the third model (vertical pipe with a branch) are the same as mentioned above. The outflow boundary condition is used at the outlet. Outflow boundary condition is used because we have two outlets. As we are not sure about the backflow volume fractions for the secondary phase, pressure outlet boundary condition is not used. The outflow boundary condition works well when there are two outlets. Flow rate weighting (ratio of flow rates) for the mixture phase is the only value that is to be provided. Flow rate weighting at

the two exits is calculated based on the flow rate. The deposition velocity for the sampling pipe is calculated using the correlations mentioned in the literature review section. For higher concentration (up to 40%) slurry flows, deposition velocity is calculated from the correlation given by Wasp et al. (1977).

$$V_D = 4.0\left(\frac{d}{D}\right)^{1/6}(C_v)^{1/5}\sqrt{2gD\left(\frac{\rho_s}{\rho_l}-1\right)} \tag{2.3}$$

For 300 micron size particles, initial solid concentration of 30%, 0.0127 diameter sampling pipe, the deposition velocity is 0.7 m/s. As it is advisable to have velocity greater than deposition velocity, 1 m/s is selected as the velocity in the sampling pipe. The next step is to specify the solution controls, residual monitors, and the number of iterations. Initially, the solution is solved for a first order upwind discretization scheme. Later, it is solved using second order upwind discretization. All the presented results are for second order discretization scheme. The SIMPLE algorithm is used for pressure-velocity coupling. The under-relaxation factors are adjusted so that steady convergence is obtained. The residuals of all the governing equations are set to 1e-06 to obtain maximum accuracy. After specifying all these values, the solution is initialized and the governing equations are solved iteratively. The parameters mentioned above are presented in Table 3.3.

Solver	Pressure based solver
Discretization scheme	Second order
Residuals	1e-06
Under-relaxation factors	Suitable

Table 3.3: The parameters employed to simulate the multi-phase flow

3.8 Post-processing:

After convergence of the solution, the case and data files are saved. These data files have the information of all the variables at each and every cell present in the control volume. One can create a point, a line, or a plane in the control volume and can gain useful information about the variation of the flow variables at these locations. The software presents the results in the form of X-Y plots, contour plots, vector displays, etc. These results are presented in the next section.

CHAPTER IV

RESULTS AND DISCUSSION

4.1 Introduction:

This section presents the results achieved in the present research study. First, the validation results are presented for the solid-liquid flows in both horizontal and vertical pipes, to show how well the present computational model is working. Then, the effect of particle diameter on the concentration profiles in both horizontal and vertical pipes is presented to find a good location to perform off-line sampling analysis. And finally, the effect of particle diameter and initial solid concentration on the concentration profiles in the sampling pipe located at the fully-developed region are presented. The concentration profiles in the sampling pipe are compared with the concentration profiles in the fully-developed region of the pipe.

4.2 Grid independence:

An important factor that is to be considered while performing CFD analysis is the grid independence test. To perform this test, three meshed models of both the horizontal and verticle pipes are created i.e., a total of six unstructured grids (tetrahedral elements) are considered. Three grids for vertical pipe grid independence and three grids for horizontal pipe. The three grids are coarse grid (0.5 million), medium grid (1 million), and fine grid (1.5 million). The grid independence test for both horizontal and vertical pipes is performed at a Reynolds number (Re_D) of 150,000 using Xylene and 70 μm ADP particles at 25% initial solids concentration. Figures 4.1 - 4.3 present the results for vertical pipe grid independence test and Figures 4.4 - 4.6 present the results for hortizontal pipe grid independence test.

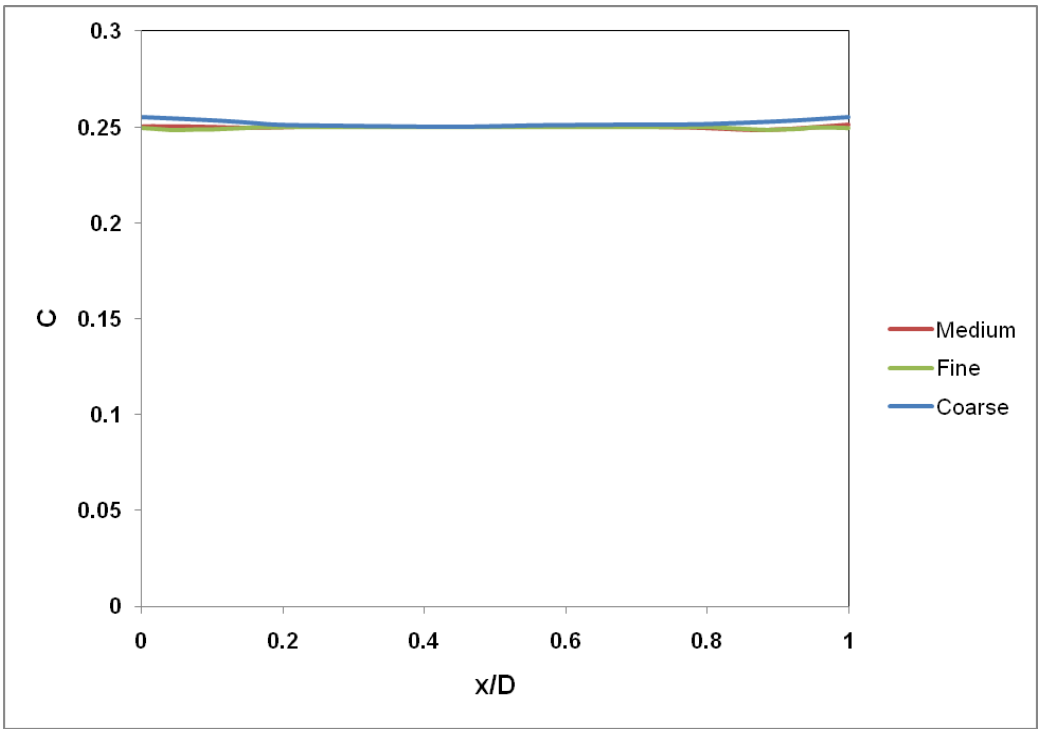

Figure 4.1: Grid independence test for the flow in vertical pipe (Concentration profiles)

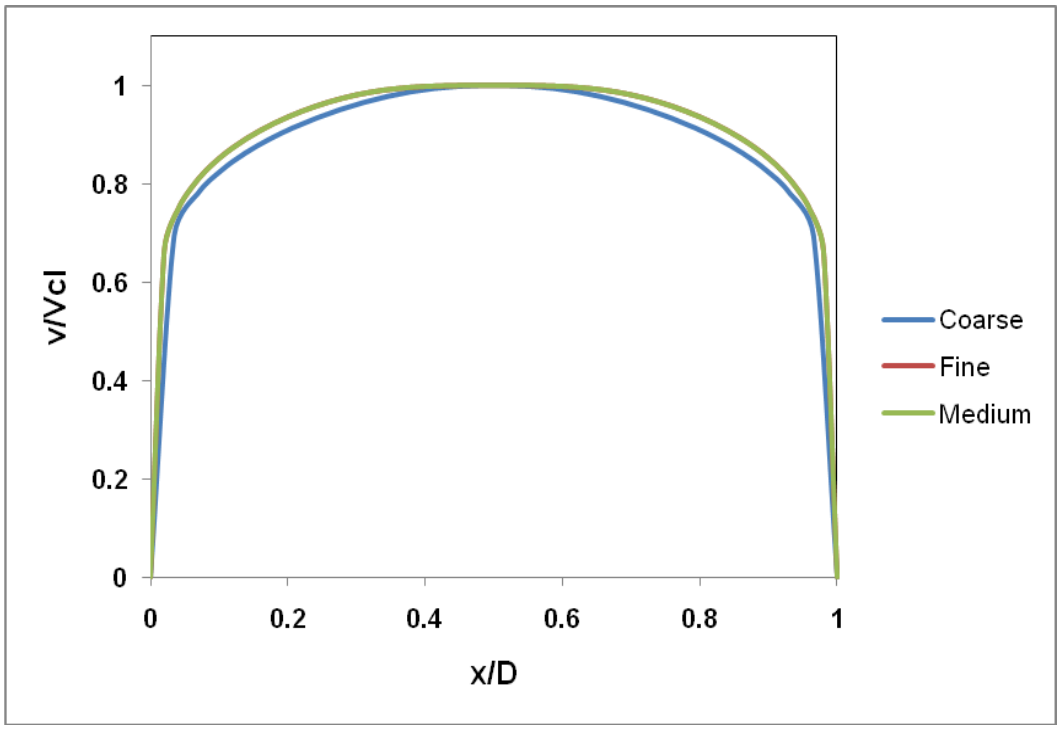

Figure 4.2: Grid independence test for the flow in vertical pipe (Velocity profiles)

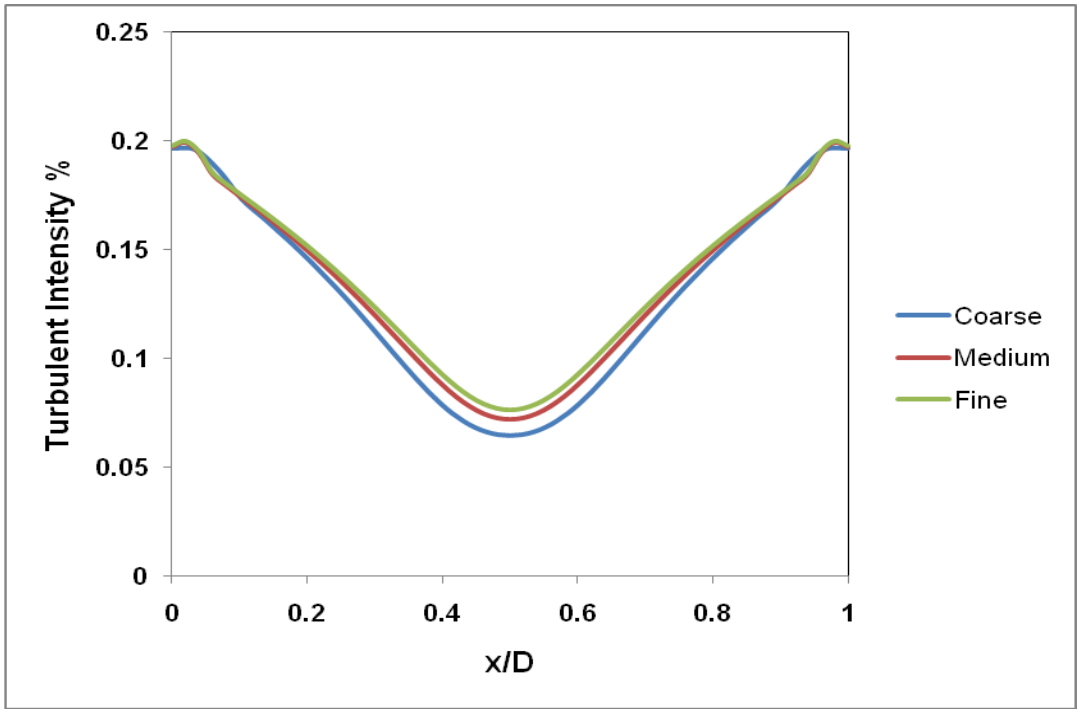

Figure 4.3: Grid independence test for the flow in vertical pipe (Turbulent Intensity profiles)

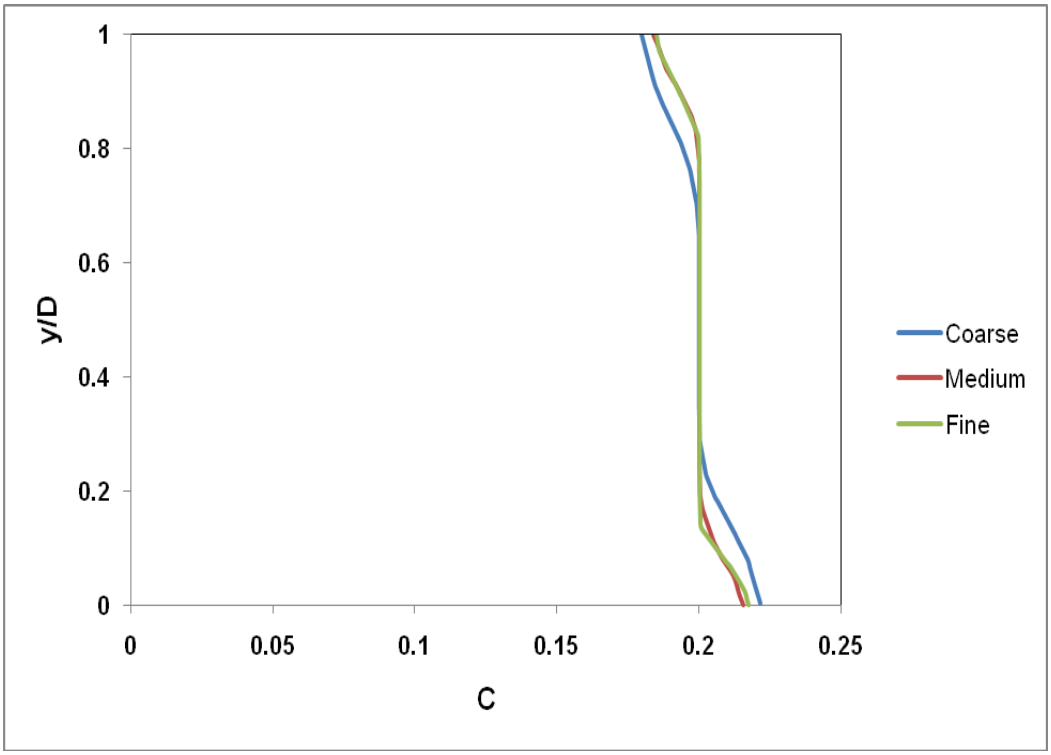

Figure 4.4: Grid independence test for the flow in horizontal pipe (Concentration profiles)

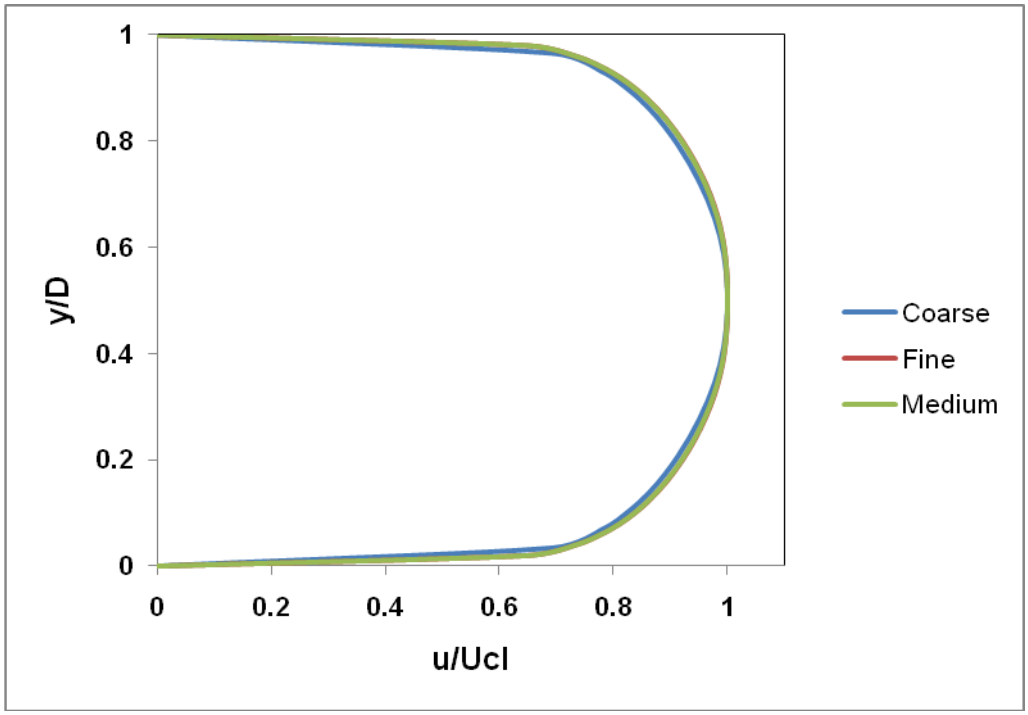

Figure 4.5: Grid independence test for the flow in horizontal pipe (Velocity profiles)

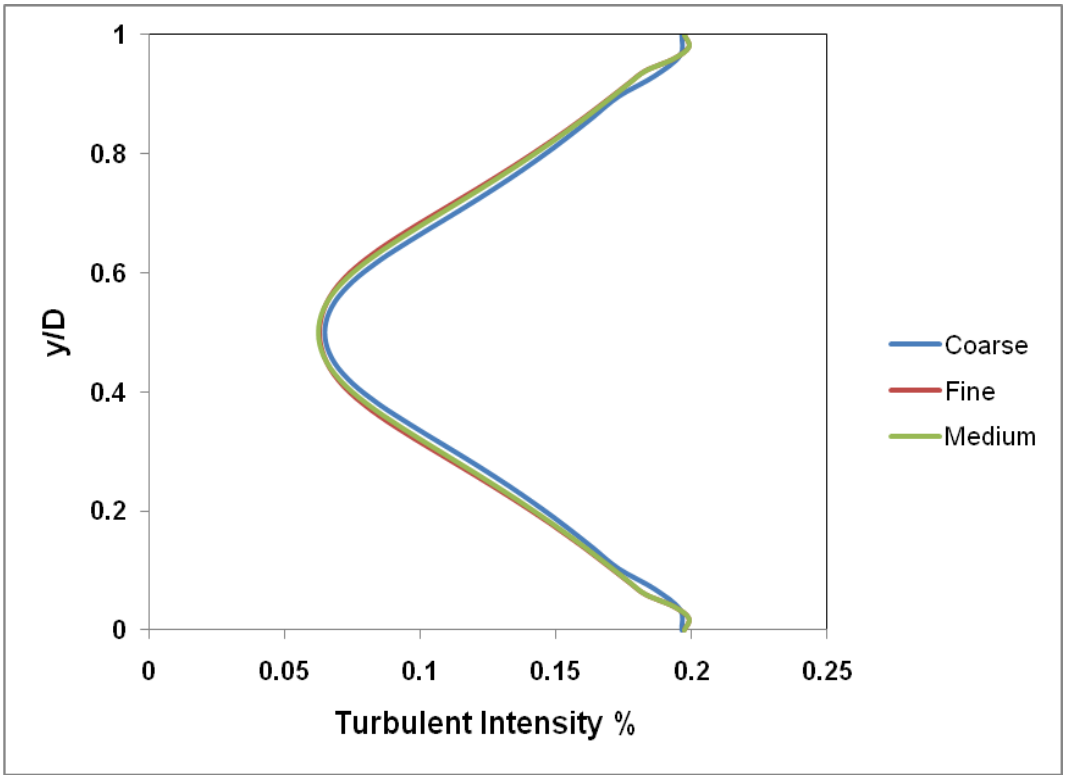

Figure 4.6: Grid independence test for the flow in horizontal pipe (Turbulent Intensity profiles)

One can clearly observe in Figures 4.1 – 4.3 that all the three grids predict almost similar profiles for the flow of slurry in vertical pipe. Close observation reveals a small deviation in the profile predicted by the coarse mesh. As the profiles predicted by the medium and fine grids are similar, all the computations are performed using medium grid, since it saves a lot of computational power which is one of the main reasons behind performing grid independence test. In the case of horizontal pipe, the coarse grid showed a big variation in the concentration profile near the walls. While the profiles predicted by the medium and fine grids are in good agreement. Therefore, all the computations are performed using medium grid.

4.3 Fully-developed location:

Finding the fully-developed location is the most important task. All the measurements should be performed at the full-developed region. The fully-developed region is the location beyond which the velocity profiles and turbulent intensity profiles do not change in the flow direction. Considering Xylene as the fluid and no particles, simulations are performed at a Reynolds number (Re_D) of 150,000 and profiles are plotted at regular intervals from the pipe inlet. For vertical pipe (upward flow), the fully-developed condition is achieved at around Y/D = 30. In other words, there is no change in the velocity and turbulent intensity profiles after 30 diameters away from the pipe inlet. The fully-developed velocity and turbulent intensity profiles are shown in Figures 4.7 and 4.8.

In the figures, the x-axis represents the pipe diameter and the y-axis represents the function (velocity and turbulent intensity). For the x-axis, 0 corresponds to the left wall and 1 corresponds to the right wall of the vertical pipe and the flow is in the upward direction.

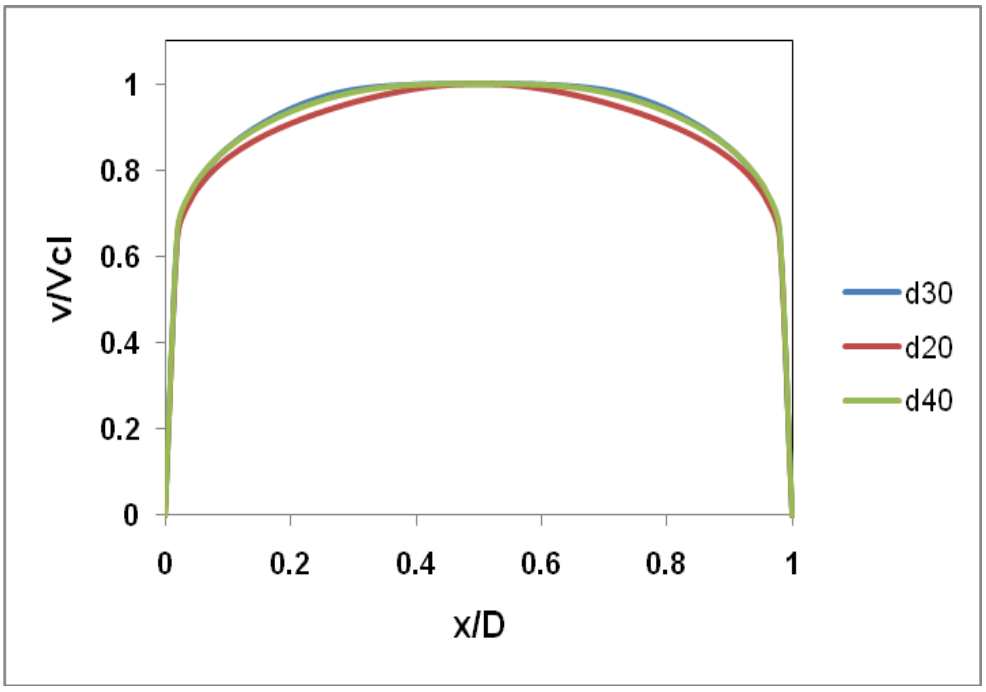

Figure 4.7: Fully-developed velocity profiles in the vertical pipe

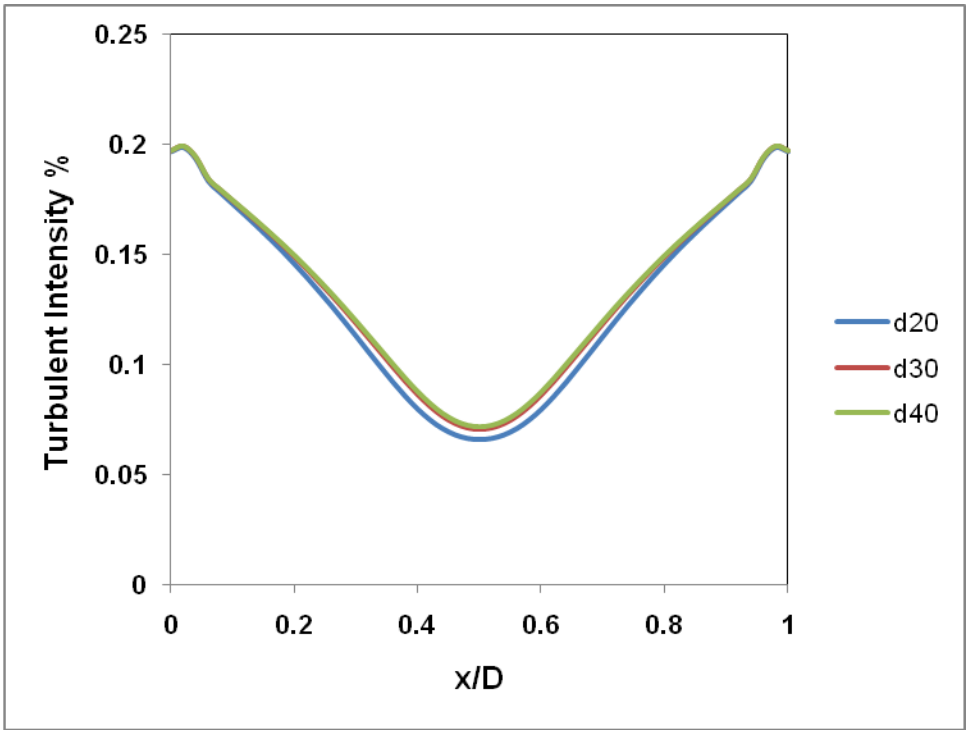

Figure 4.8: Fully-developed turbulent intensity profiles in the vertical pipe

The turbulence intensity (I) is presented in Equation 4.1. Where, k is Turbulence kinetic energy (m^2/s^2) and $\overline{U}$ is Reynolds averaged centre line mean fluid velocity (m/s).

$$I = \frac{\sqrt{\frac{2k}{3}}}{\overline{U}} \tag{4.1}$$

Similarly, simulations are performed using Xylene as the fluid in the horizontal pipe at a Reynolds number (Re_D) of 150,000. The velocity and turbulent intensity profiles are plotted at regular intervals from the pipe inlet. The fully-developed condition is achieved at around X/D = 30. The velocity and turbulent intensity profiles for the flow in horizontal pipe are shown in Figures 4.9 and 4.10. In the figures, the y-axis represents the pipe diameter and the x-axis represents the function (velocity and turbulent intensity). For the y-axis, 0 corresponds to the bottom wall and 1 corresponds to the top wall of the horizontal pipe and the flow direction is from left to right. Therefore, Y/D = 30 (vertical pipe) and X/D = 30 (horizontal pipe) are considered as the fully-developed locations in both the pipes.

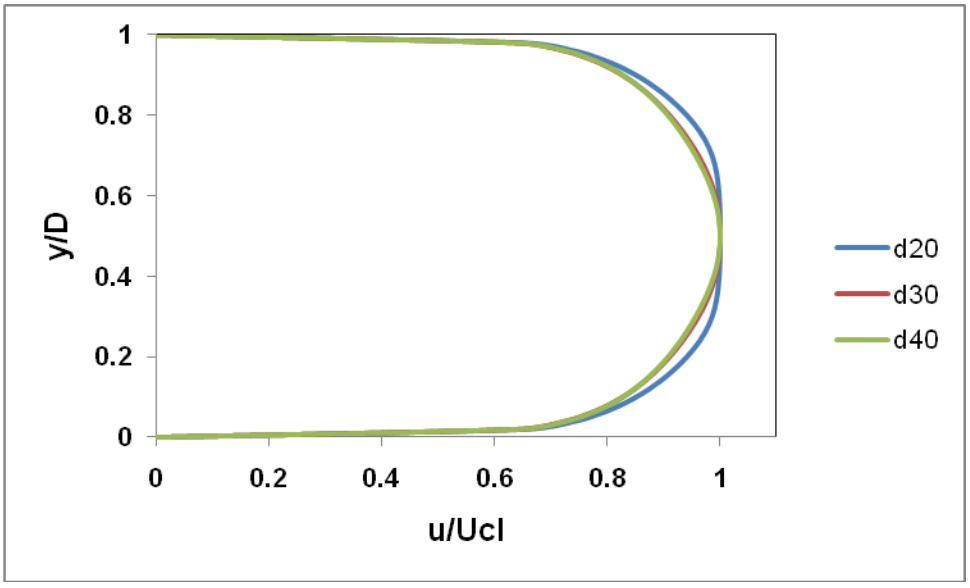

Figure 4.9: Fully-developed velocity profiles in the horizontal pipe

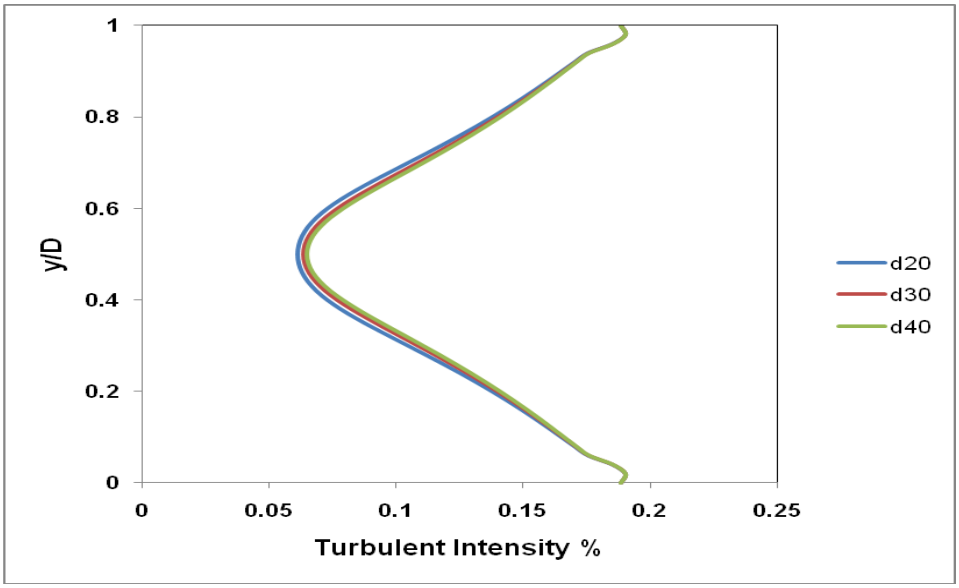

Figure 4.10: Fully-developed turbulent intensity profiles in the horizontal pipe

As we have located the fully-developed region and selected the grids to perform computational analysis, the next step is to validate the results with the results in the literature.

4.4 Validation of velocity profiles:

First, the velocity profiles are compared with the power law. For this, simulations are performed using Xylene as the fluid and k-ε with standard wall functions as the turbulence model. The comparision of velocity profile with the power law for the flow in vertical and horizontal pipes is shown in Figures 4.11 and 4.12 respectively.It is observed that the velocity profiles generated at a Reynolds number (Re_D) of 150,000 by numerical analysis are in good agreement with the power law profile (n=8) of Schlichting 1979. This shows that the k-ε turbulence model is working well to characterize the turbulence in the flow.

Re_D	$4x10^3$	$2.3x10^4$	$1.1x10^5$	$1.1x10^6$	$2.0x10^6$	$3.2x10^6$
n	6.0	6.6	7.0	8.8	10	10

Table 4.1: Reynolds number dependence of velocity profile exponent, n (Schlichting 1979)

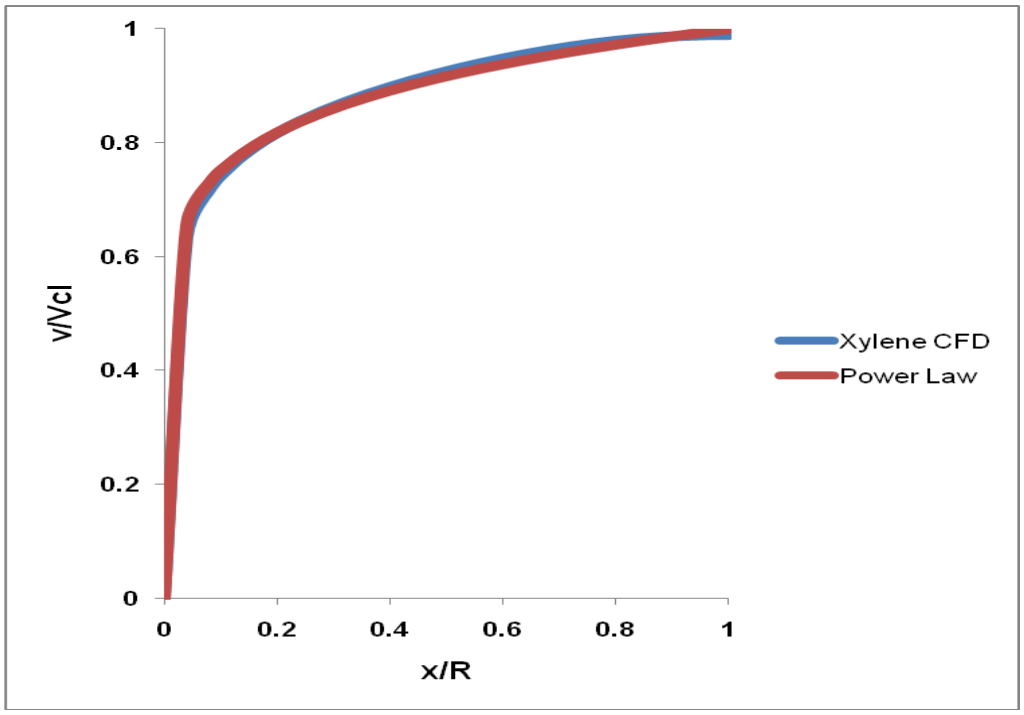

Figure 4.11: Power law profile compared with the profile generated through numerical computation (Vertical pipe)

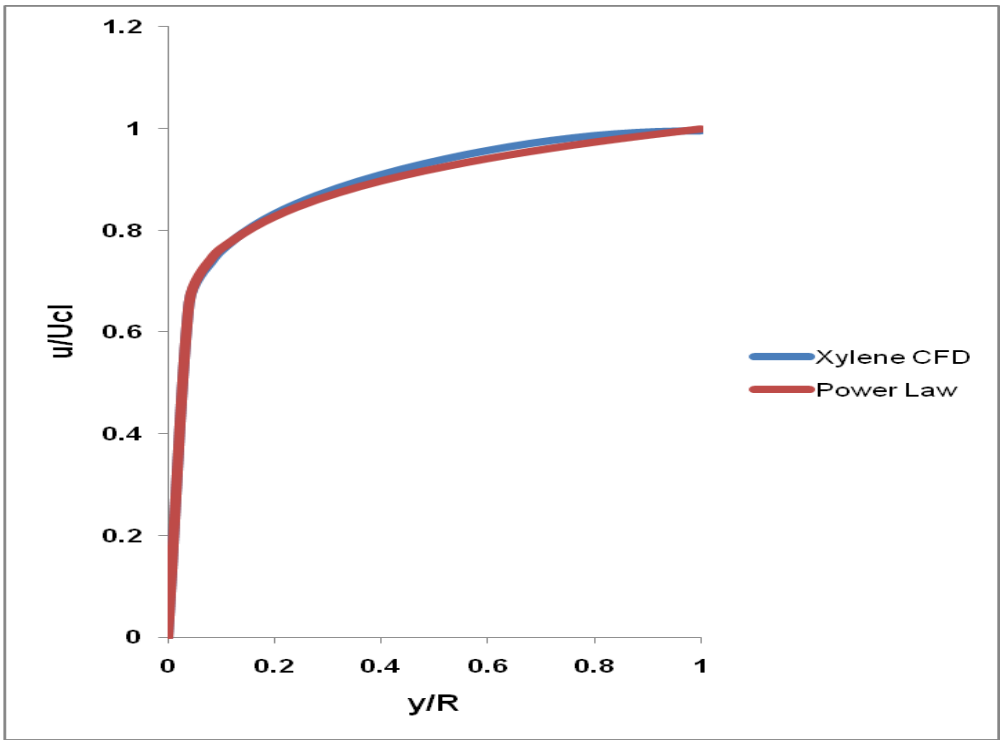

Figure 4.12: Power law profile compared with the profile generated through numerical computation (Horizontal pipe)

Validating the velocity profiles of the slurry (solid-liquid flow) is important to check the performance of the present models. Therefore, velocity profiles of the slurry flowing in a vertical pipe are compared to the experimental results of Sumner et al. (1995). Sumner et al. experimentally plotted the velocity profiles of the slurry with different particle sizes, densities, and concentrations. The properties of the particles are presented in Table 2.1 of the literature review Section 2.1. Velocity profiles under similar conditions are generated using the present computational model. Figures 4.13 to 4.16 presents the validations of the present computational results with the experimental results of Sumner et al. Validating the computational results with the experimental results of slurry flows in vertical pipes is a challenging task, because CFD analysis of slurry flows in vertical pipes is not well documented. As the profiles are symmetric about the pipe axis, only half velocity profiles are presented by Sumner et al. In all the figures 0 represents the left wall, 0.5 represents the pipe axis, and V is the mean velocity.

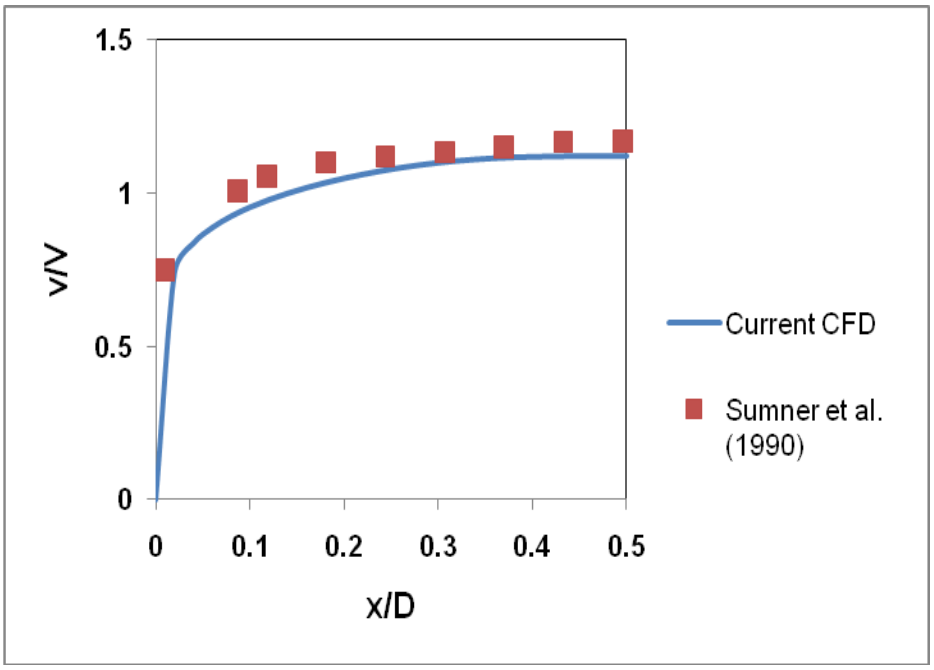

Figure 4.13: Comparison of fine sand-water slurry (d_p = 0.16 mm) at pipe flow Reynolds number of (Re_D = 160,000) and initial volumetric concentration of (C = 10%)

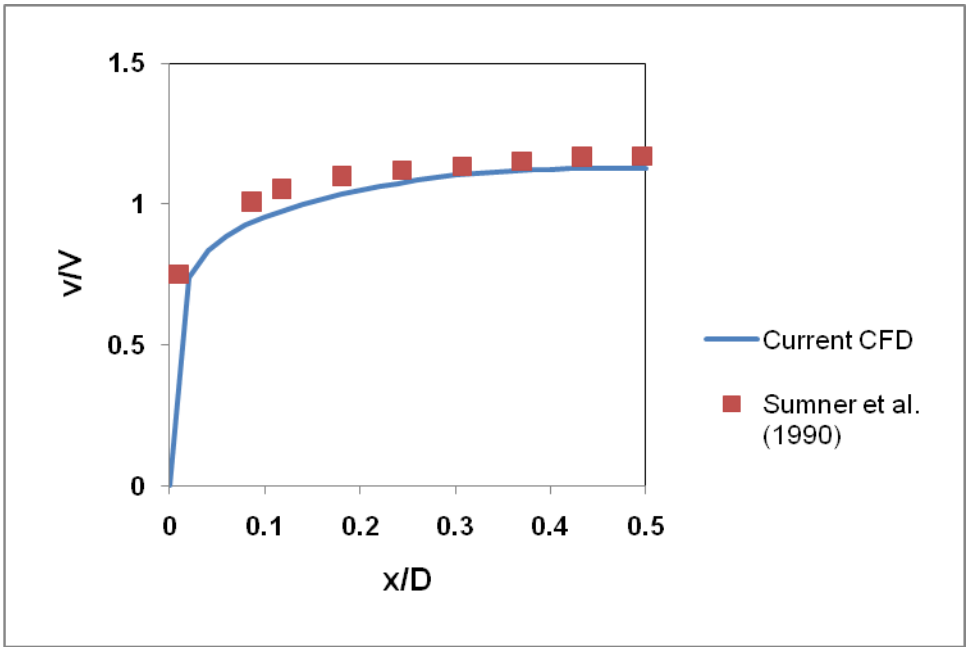

Figure 4.14: Comparison of fine plastic-water slurry (d_p = 0.29 mm) at pipe flow Reynolds number of (Re_D = 160,000) and initial volumetric concentration of (C = 10%)

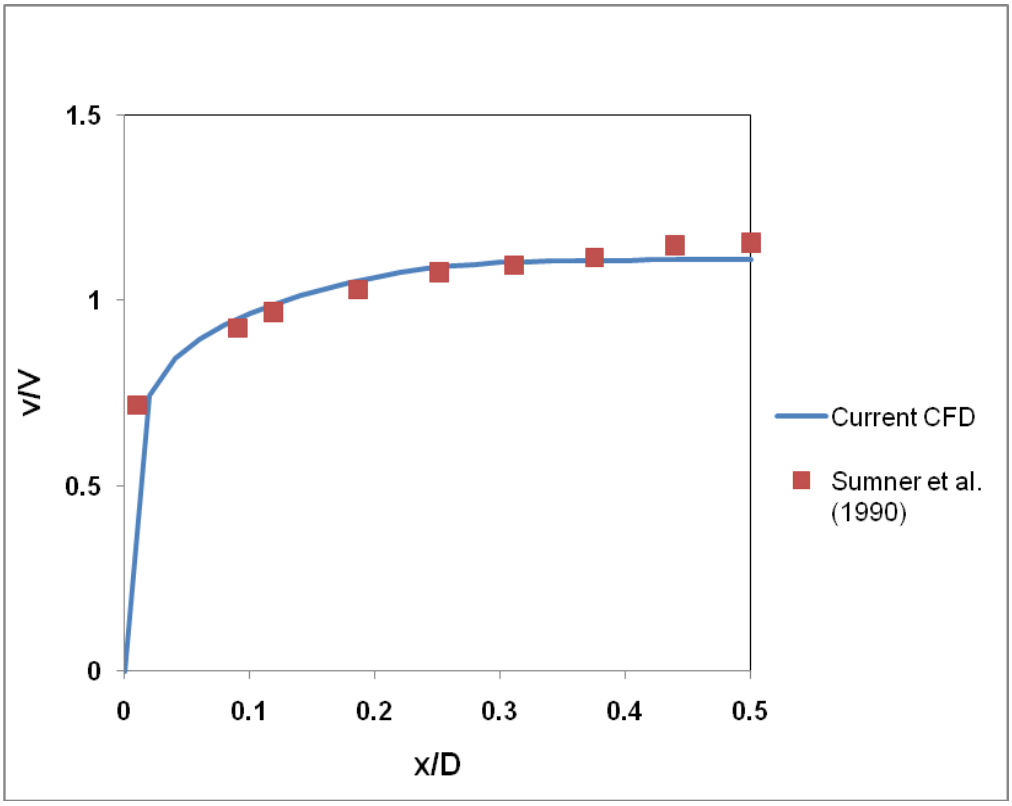

Figure 4.15: Comparison of medium sand-water slurry (d_p = 0.29 mm) at pipe flow Reynolds number of (Re_D = 160,000) and initial volumetric concentration of (C = 10%)

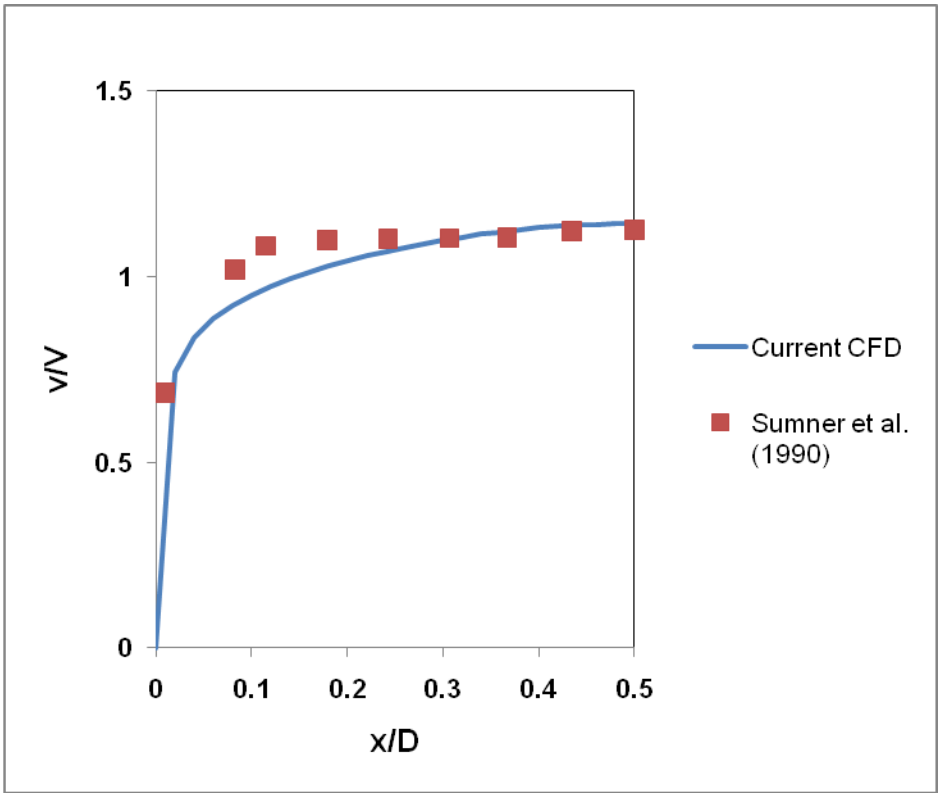

Figure 4.16: Comparison of velocity profiles of fine sand-water slurry (d_p = 0.29 mm) at Reynolds number of (Re_D = 80,000) and initial volumetric concentration of (C = 40%)

It is obseved from the above results that the present computational results are in good agreement with the experimental results except for the slurry with 40% intial solid concentration. This disagreement results from the performance limit of the mixture multiphase model. The mixture models works well for moderate concentrations up to 30%. This shows that the present computational models are working well (up to 30% concentration) to predict the velocity profiles of the slurry flow in vertical pipes. For these computations, the grid developed for Re_D of 150,000 was used. Since it was for 150,000 it should be very good for 80,000, a lower Re_D. Similarly, velocity profiles of the slurry flowing in horizontal pipe are validated with the results in the literature. Gillies et al. (2003) conducted experiments with 0.19% sand-water slurries (d_p = 90 microns) at a Reynolds number of (Re_D = 307,521). Ekambara et al. (2009) performed computational analysis with sand-water slurry and validated their results with the experimental results of Gillies et al. Therefore, simulations are performed under similar conditions with the

present computational model and the velocity profiles are validated with both the numerical results of Ekambara and experimental results of Gillies. The comparision is presented in Figure 4.17, where U_{cl} is the centre line velocity.

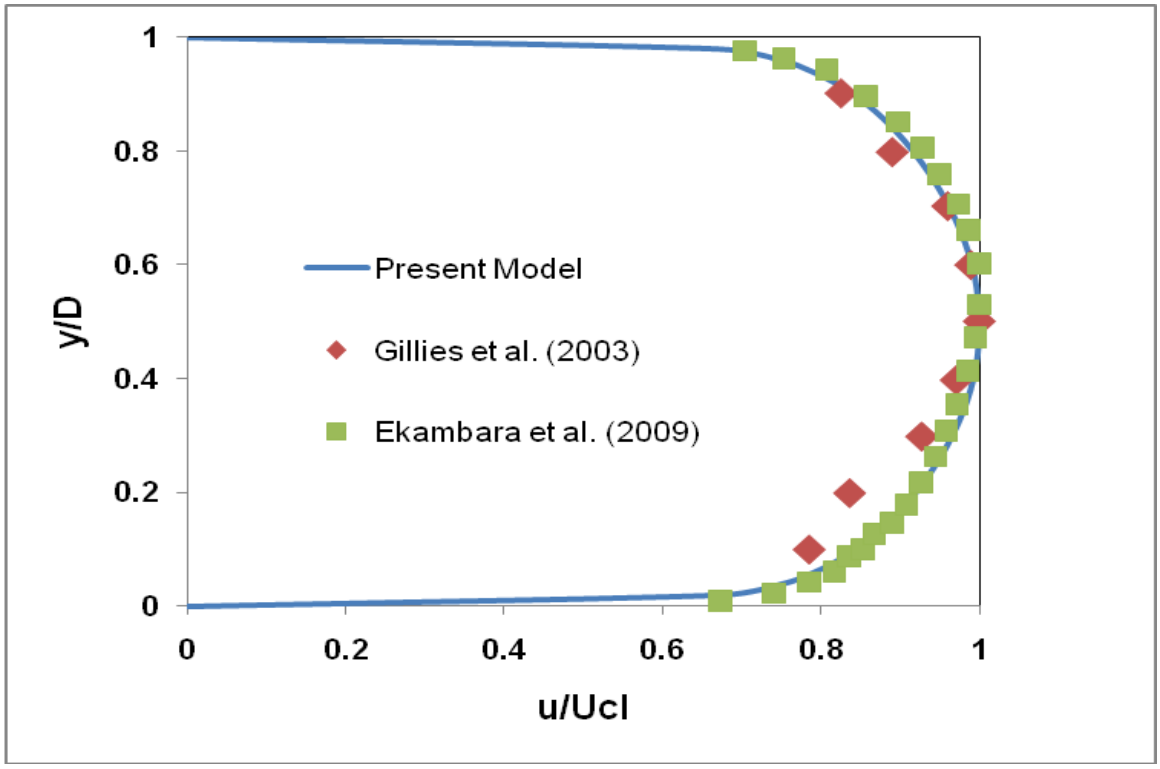

Figure 4.17: Comparison of velocity profiles of a sand-water slurry at a Reynolds number (Re_D) of 300000

After observing the graph in the above figure, one can say that the two computational results, Ekambara et al. and the present model, are in good agreement with each other. The computational results and the experimental results (Gillies at al. 2003) are also in good agreement but a deviation is observed near the bottom wall. This could be due to the presence of a fraction of particles larger than the mean particle diameter. According to Wildman et al. (1992) slight imperfections on the surface of the wall makes the experimental measurements more challenging. The apparent difference also may result from experimental uncertainty for the second measurement point from the bottom. The points above and below it are in better agreement with the compared profile. We have looked at the velocity profiles and their validations for the slurry flows in vertical and horizontal pipes. The next step is to validate the concentration profiles.

4.5 Validation of concentration profiles:

In this section, the concentration profiles of the slurry flowing in vertical and horizontal pipes are compared with the results in the literature, to make sure that the present mixture multiphase model is doing an acceptable job.

For vertical pipe, the concentration profiles are validated with the experimental results of Sumner et al. (1995). Computational analysis to predict the concentration profiles of the slurry flowing in vertical pipes is not well documented according to our literature survey. This makes the present research work more challenging. The simulations are performed under similar conditions used in the experimental analysis. The results are shown in Figures 4.18 – 4.20. As the profiles are symmetric about the pipe axis, only half profiles are plotted by Sumner et al. In all the Figures 0.5 represents the pipe axis and 1 represents the right wall (C_b is the mean concentration).

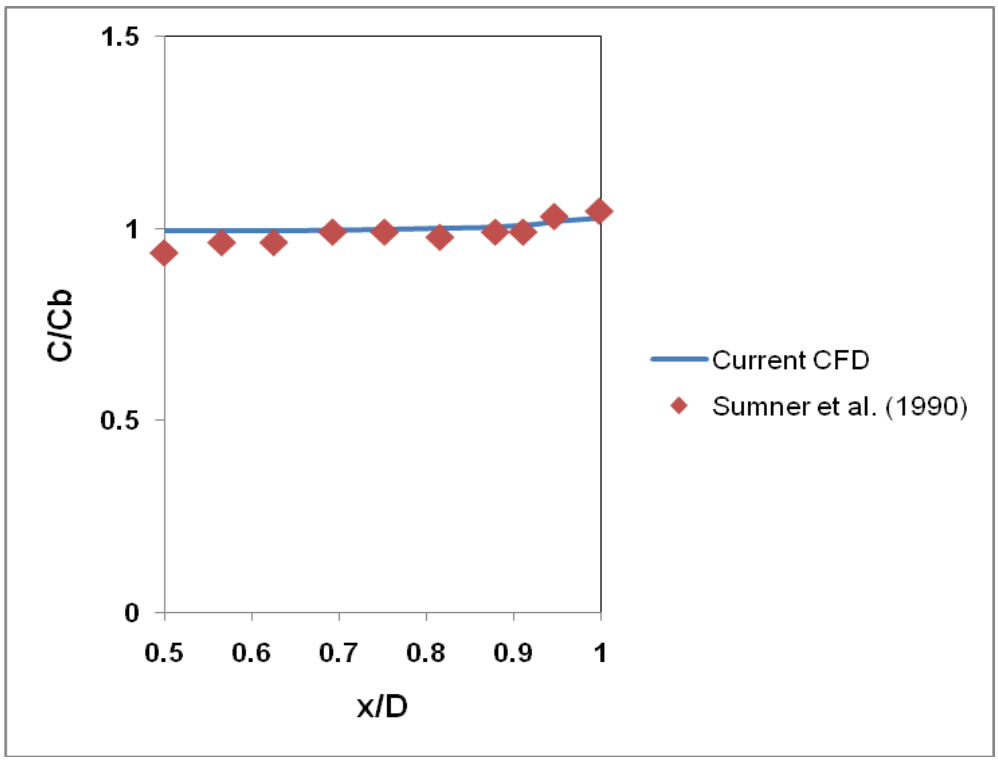

Figure 4.18: Comparison of concentration profiles of fine sand-water slurry (d_p = 0.16 mm) at pipe flow Reynolds number of (Re_D = 160,000) and initial volumetric concentration of (C = 10%)

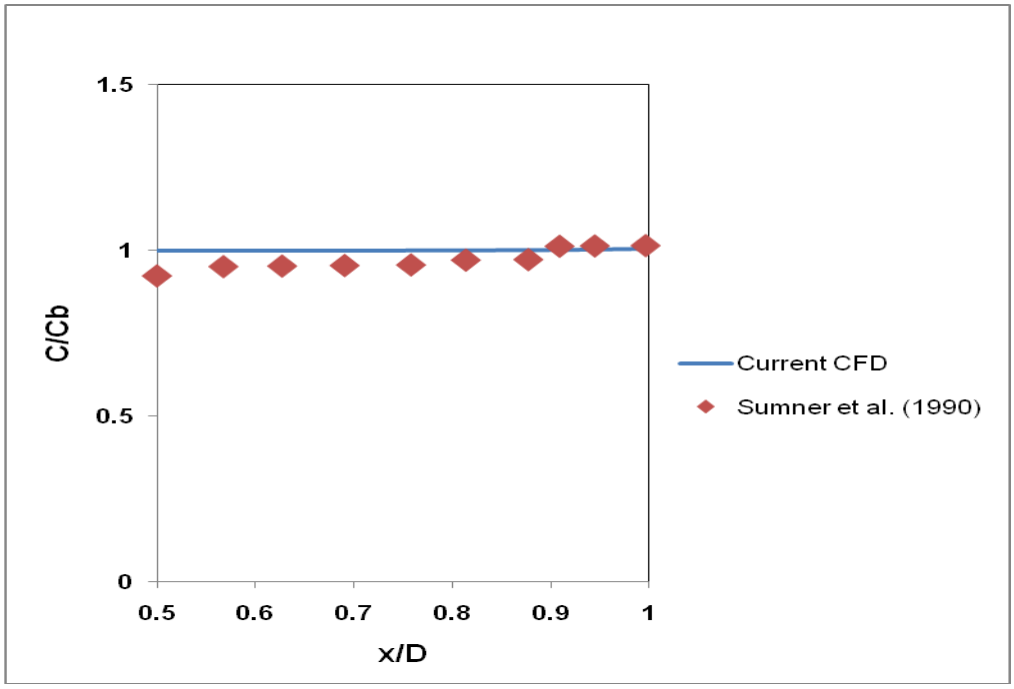

Figure 4.19: Comparison of concentration profiles of fine plastic-water slurry (d_p = 0.29 mm) at pipe flow Reynolds number of (Re_D = 160,000) and initial volumetric concentration of (C = 10%)

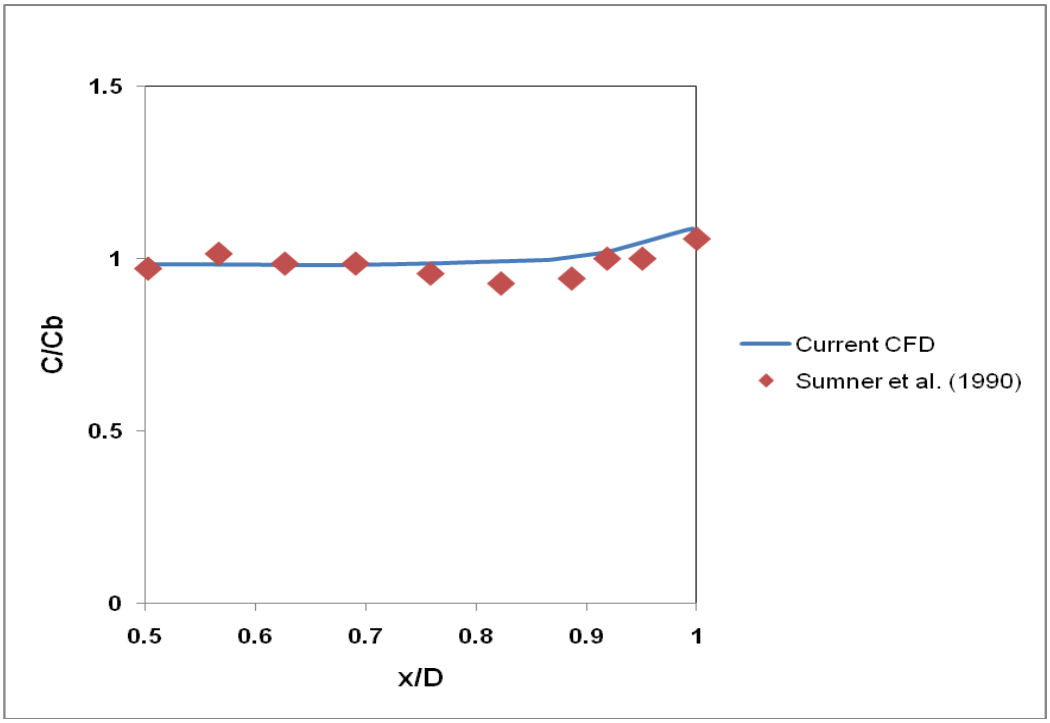

Figure 4.20: Comparison of concentration profiles of fine sand-water slurry (d_p = 0.47 mm) at pipe flow Reynolds number of (Re_D = 160,000) and initial volumetric concentration of (C = 10%)

One can clearly observe that the present computational results are in good agreement with the experimental results. This shows that the present mixture multiphase model is working well in predicting the concentration profiles of the slurry flowing in vertical pipes. Similarly, the concentration profiles for the flow of slurry in horizontal pipe are validated with the experimental result of Gillies et al. (2003). The concentration profiles are predicted using the present model for sand-water slurry (d_p = 90 micron) at 0.19 initial volume concentration. The comparision is shown in Figure 4.21. Note that the grid, which was developed for Re_D of 150,000, appears to work well at this higher Re_D.

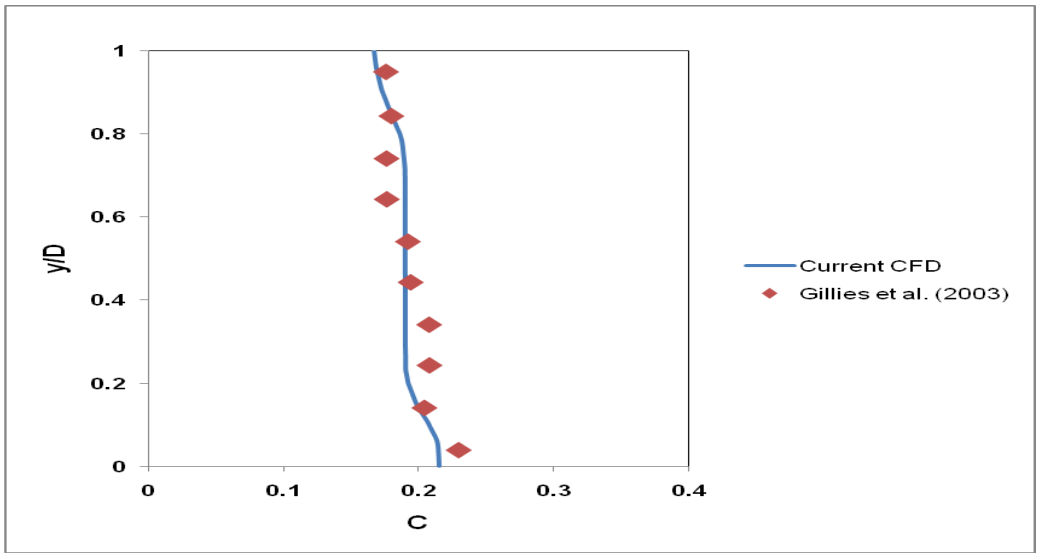

Figure 4.21: Comparison of concentration profiles of sand-water slurry (d_p = 90 microns) at initial volumetric concentration of 0.19 (Re_D = 300,000)

Until now we have validated the velocity profiles and the concentration profiles of the slurry flowing in vertical and horizontal pipes. These results prove that the present computational model (k-ε turbulence model and the mixture multiphase model) is doing a good job in predicting the concentration profiles, which is the main objective of the present research study. Therefore, we can say that the results presented from now can be considered substantially accurate. Next, the results pertaining to finding a good location to perform off-line sampling and NIR Spectroscopic analysis are presented.

4.6 Good location to perform off-line sampling:

The first objective of the present research is finding a good location to perform NIR Spectroscopy and off-line sampling analysis. In the previous sections we have located the right location to perform measurements by finding the fully-developed region, which is at X/D = 30 for horizontal pipe and Y/D = 30 for vertical pipe, from the pipe inlet. The right location to perform off-line sampling and NIR Spectroscopic analysis is determined by comparing the concentration profiles in the fully developed region of vertical and horizontal pipes, by performing simulations under similar conditions. The effect of particle diameter on the concentration profiles is determined in both the geometries. The computational analysis is performed by using Xylene as the primary phase and 2-Amino-4, 6-dimethylpyrimidine (ADP) particles as the secondary phase. The properties of the two phases are are presented again to give a better understanding.

	Viscosity (Pa-S)	Density (Kg/m^3)
Xylene	6.2×10^{-4}	870
ADP	N/A	1480

Table 4.2: Properties of the phases

The simulations are performed at the same Reynolds number and intial solid concentration. The effect of particle diameter on the concentration profile is observed by considering three particle sizes. The different cases computed in this section are outlined in Table 4.3. The two geometries are shown in Figures 4.22 and 4.23.

Pipe Reynolds number, Re_D= 150000 (Velocity = 2 m/s)	
Particle diameter (d_p) microns	***Initial solid concentration (C)***
30	0.3
100	0.3
150	0.3

Table 4.3: Cases studied for the flow of slurries in horizontal and vertical pipes

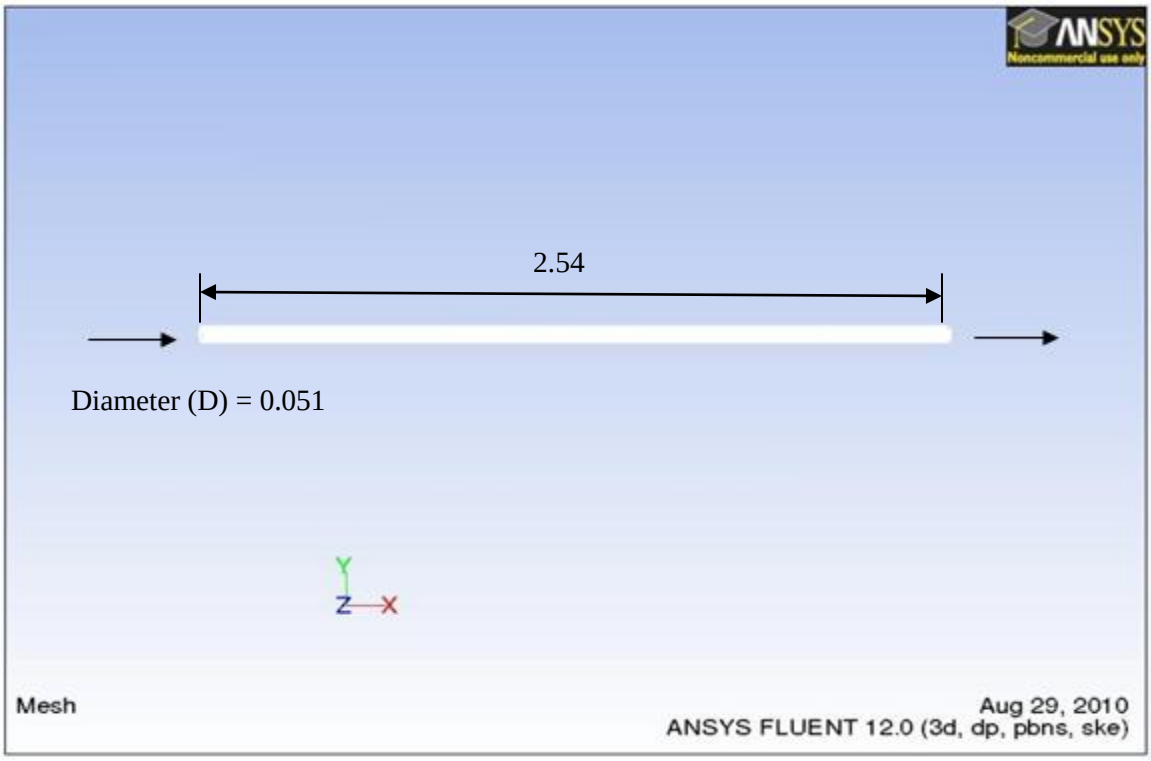

Figure 4.22: Horizontal pipe (units in meters)

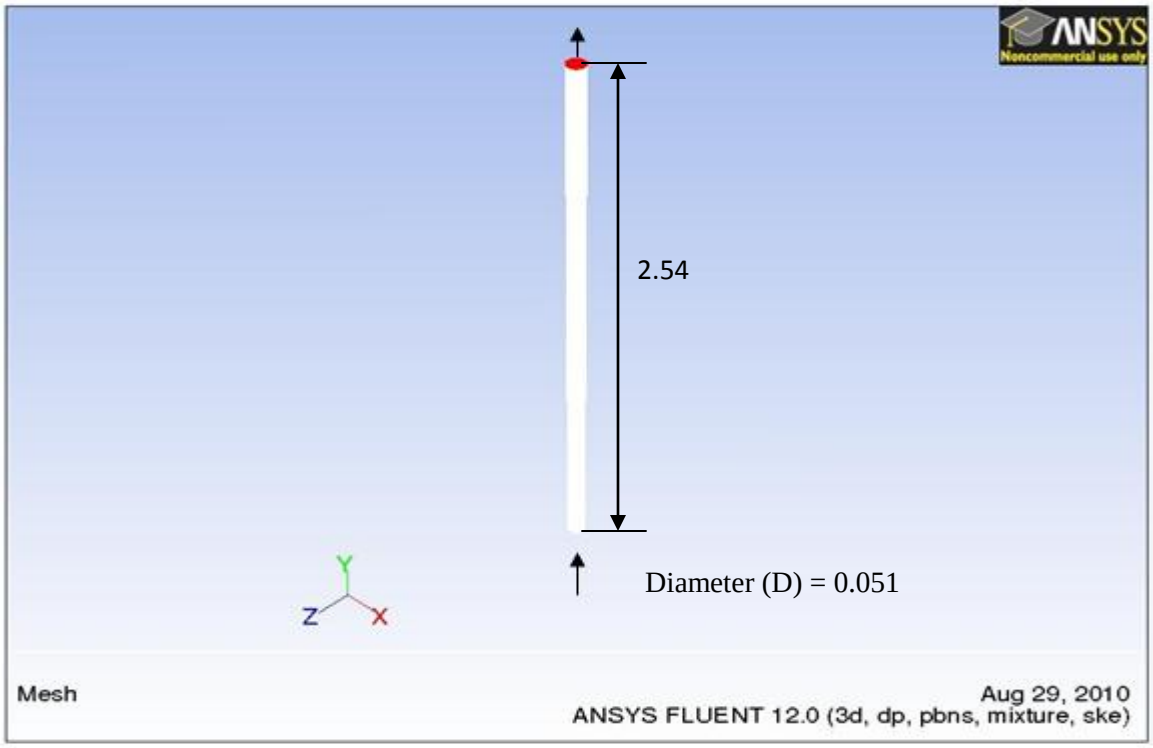

Figure 4.23: Vertical pipe (units in meters)

Figures 4.24, 4.25, and 4.26 present the concentration profiles in horizontal pipe. The flow is from left to right. The x- axis represents the concentration and the y-axis represents the pipe diameter (0 corresponds to the bottom wall and 1 corresponds to the top wall of the pipe).

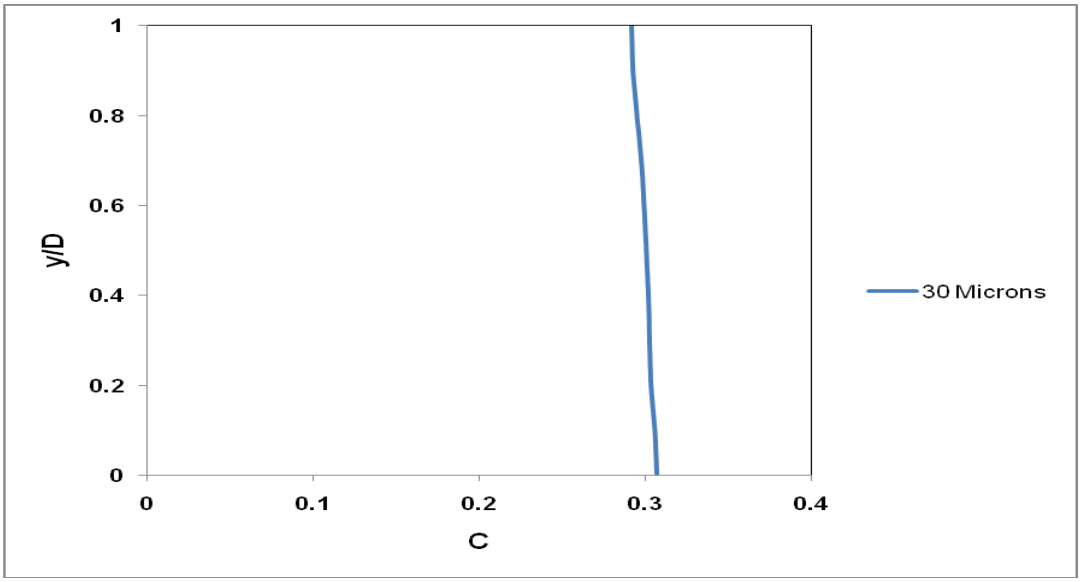

Figure 4.24: Concentration profile of 30 µm ADP particles at 0.3 initial solids concentration at the fully developed region (X/D = 30) of the horizontal pipe

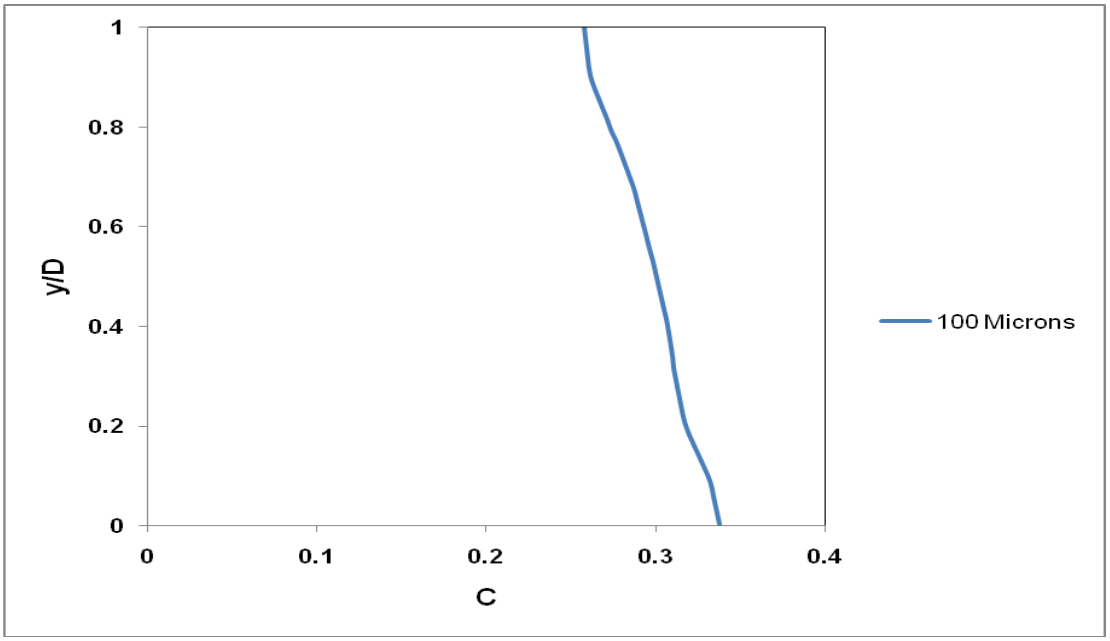

Figure 4.25: Concentration profile of 100 µm ADP particles at 0.3 initial solids concentration at the fully developed region (X/D = 30) of the horizontal pipe

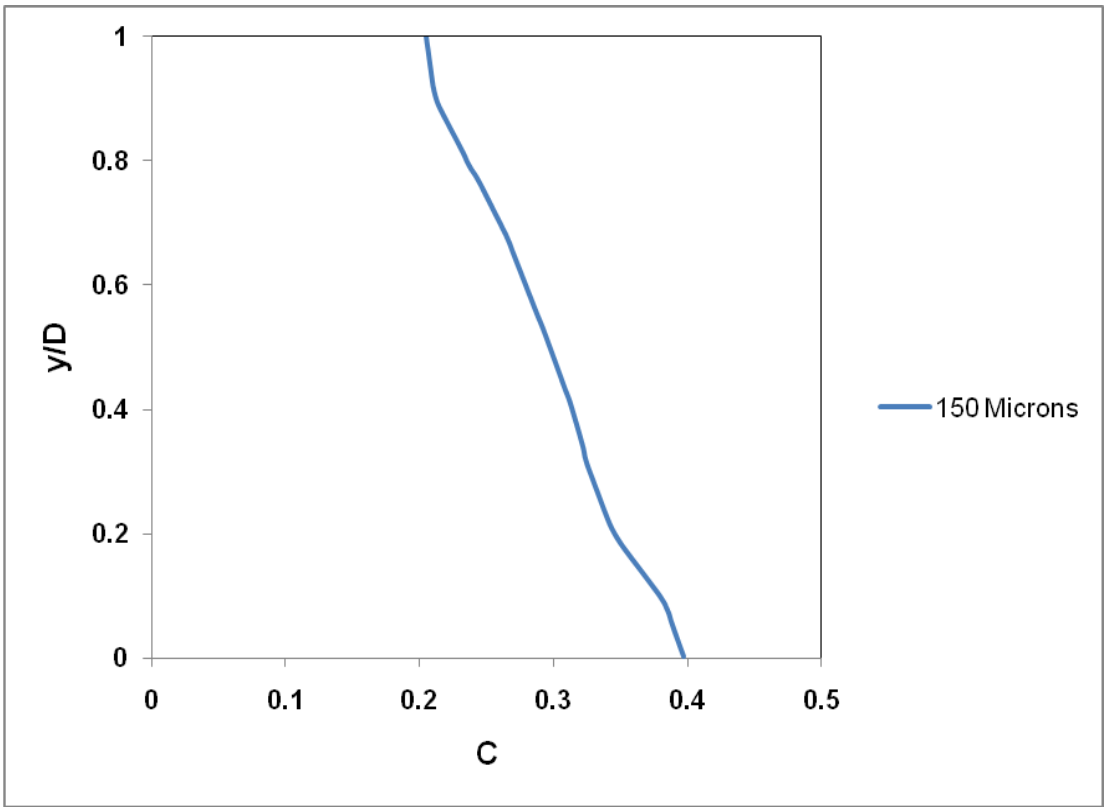

Figure 4.26: Concentration profile of 150 µm ADP particles at 0.3 initial solids concentration at the fully developed region (X/D = 30) of the horizontal pipe

After observing the graph from Figure 4.18, one can say that the particles are almost uniformly distributed across the pipe diameter. There is a slight slope to the profile with more particle concentration at the bottom wall when compared to the top wall. This effect is more pronounced for 100 and 150 micron particles. The slope is more for 100 micron particles when compared to 30 micron particles. The concentration profile for 150 micron particles shows a greater slope. Gravity plays an important role for the flow of slurry in horizontal pipes. For 30 micron particles gravity effects are less when compared to 150 micron particles. This is the reason for the slope in the concentration profiles.

The magnitude of the deposition velocity is high for larger diameter particle size (150 μm). The velocities were calculated using the correlation given by Durand (1952).

$$V_D = 4.0\left(\frac{d}{D}\right)^{1/6}(C_v)^{1/5}\sqrt{2gD\left(\frac{\rho_s}{\rho_l}-1\right)} \qquad (2.3)$$

The variation of deposition velocity for different particle sizes is shown below in Table 4.4.

Particle size (μm) ***(d_p)***	***30 % Initial solid volume fraction (C)***
	Deposition velocity (V_D) ***m/s***
30	0.8
100	0.95
150	1

Table 4.4: Variation of deposition velocity for different particle sizes

The simulations are performed under similar conditions in the vertical pipe and the results are presented in Figures 4.27, 4.28, and 4.29 below. The flow is in the upward direction. The y-axis represents the concentration and the x-axis represents the pipe diameter (0 corresponds to the left wall and 1 corresponds to the right wall of the pipe).

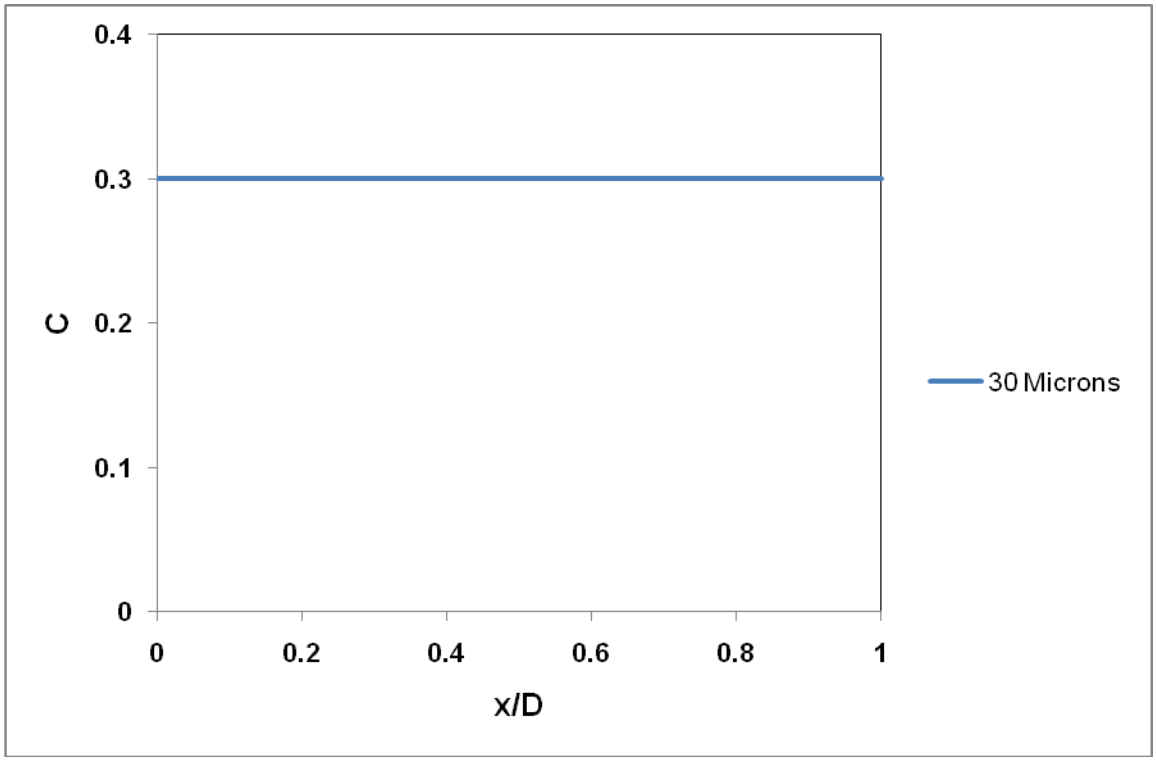

Figure 4.27: Concentration profile of 30 µm ADP particles at 0.3 initial solids concentration at the fully developed region (Y/D = 30) of the vertical pipe

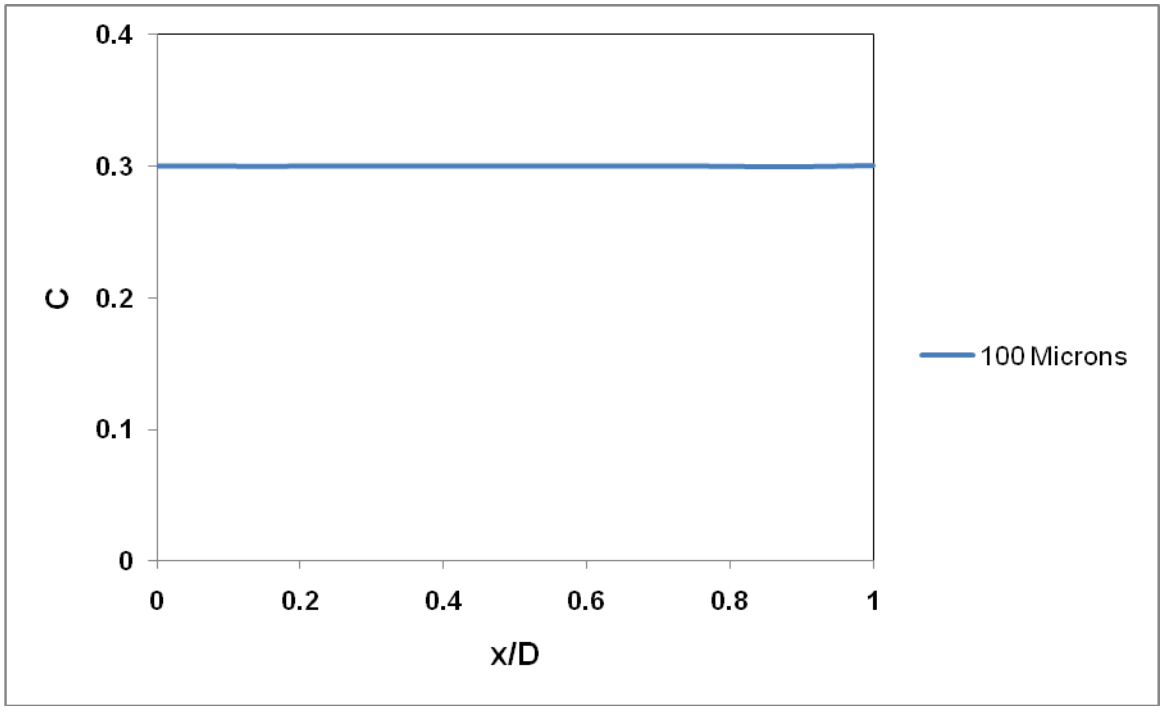

Figure 4.28: Concentration profile of 100 µm ADP particles at 0.3 initial solids concentration at the fully developed region (Y/D = 30) of the vertical pipe

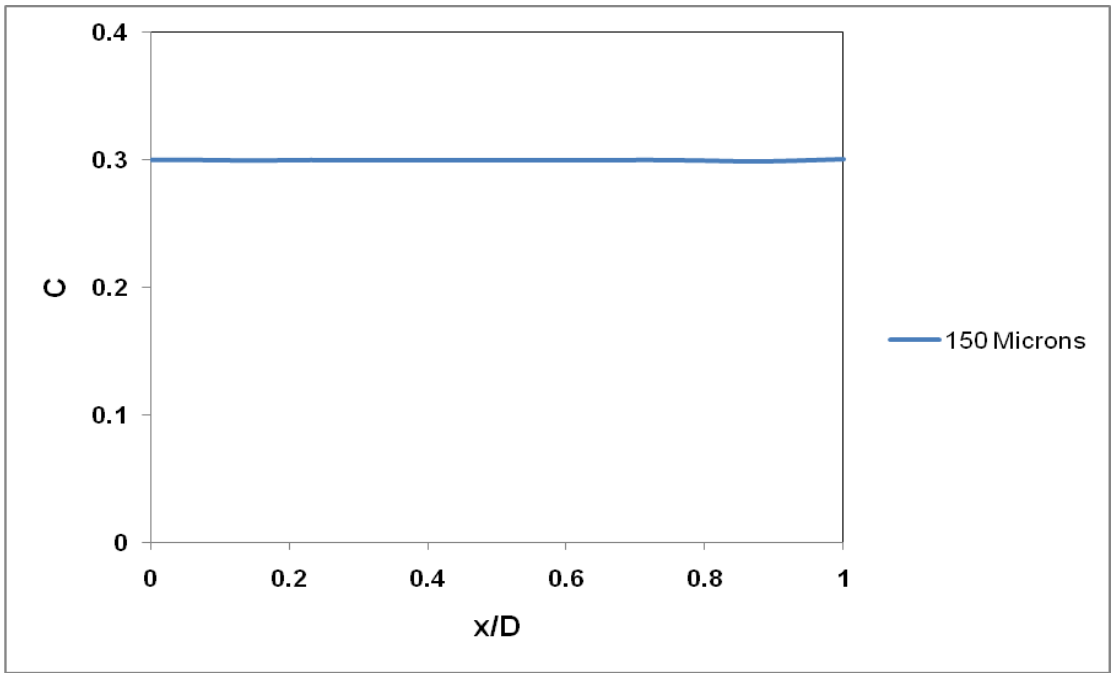

Figure 4.29: Concentration profile of 150 µm ADP particles at 0.3 initial solids concentration at the fully developed region (Y/D = 30) of the vertical pipe

The concentration profiles are almost uniform for all the three particle sizes in the vertical pipe and therefore this location is suitable for performing NIR Spectroscopic analysis. Even though we observe a small variation in the profile near the walls for 150 micron particles, the variation is negligible when compared to the concentration profiles in horizontal pipe. The concentration distributions are not much affected by the increase in particle diameters because the effect of gravity is the same across the pipe cross-section. This is a very different result for the slurry flows in vertical pipes when compared to the horizontal pipes. Fortunately, this result favors performing off-line sampling analysis in vertical pipes. Taking a sample from the edge of the horizontal pipe can give erroneous results because of the slope in the concentration profile. While in the vertical pipe because of the uniform distribution of particles performing off-line sampling may give a sample that is a good representative of the slurry in the batch reactor. Therefore, this analysis proves that the vertical pipes are the best for performing off-line sampling and in-line measurements. Finally, the fully-developed region of the vertical pipe is recognized as the best location to perform sampling and NIR Spectroscopic analysis.

4.7 Concentration profiles in the sampling pipe:

As the right location to perform off-line sampling is determined, the next step is to compare the concentration profiles in the fully-developed region of the recirculation loop and the sampling pipe. Figure 4.30 shows the sampling pipe located at the fully-developed region of the vertical pipe.

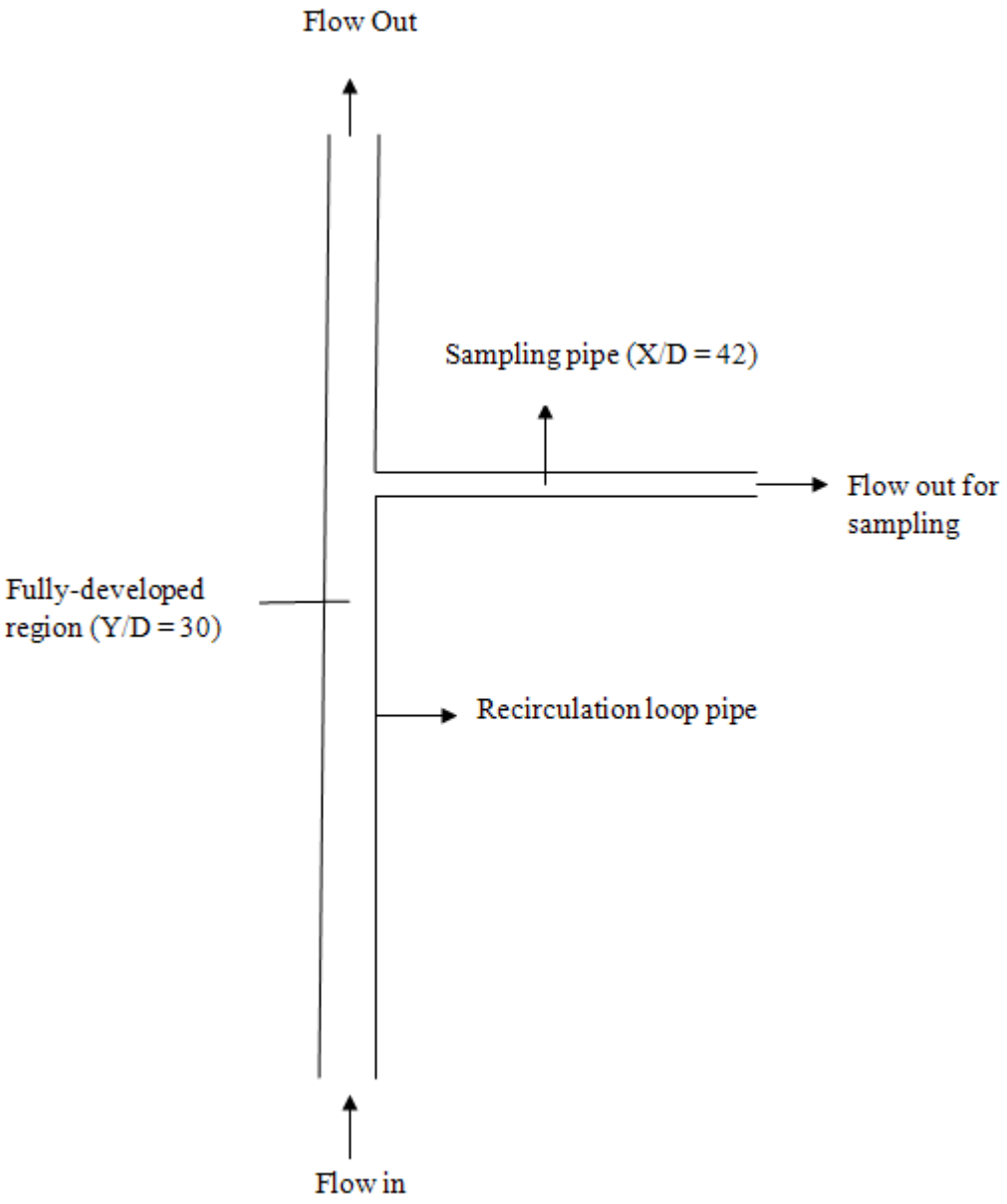

Figure 4.30: Position of the sampling pipe with respect to the vertical pipe

The present section deals with the effect of particle diameter and initial solid concentration on the profiles of the slurry in the sampling pipe. The concentration profiles in the sampling pipe for different cases are presented, and are compared with those at the fully-developed region of the vertical pipe. Suitable reasoning to explain the variation of the concentration profiles in the sampling pipe is also presented. The different cases that are computed in this section are outlined in Table 4.5.

Velocity in the main pipe = 2 m/s (Re_D = 150,000) ***Velocity in the sampling pipe = 1 m/s (Re_D = 18,000)***			
Particle diameter (d_p) (μm)	***Initial solid concentration (C) %***		
30	5	15	30
100	5	15	30
300	5	15	-

Table 4.5: Different cases studied

The concentration profiles in the recirculation loop pipe (verticle pipe) are presented at Y/D = 30 (fully-developed region) and the concentration profiles in the sampling pipe are presented at X/D = 42. The concentration profiles in the sampling pipe do not change after X/D = 40. Figure 4.31 shows the concentration profiles in the sampling at X/D = 40 and X/D = 50.

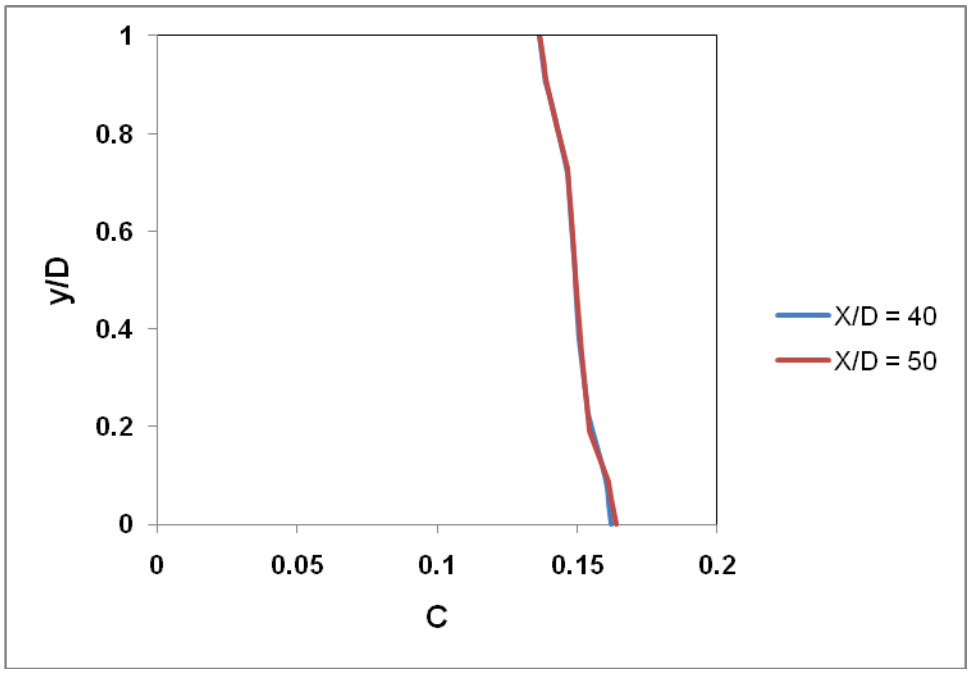

Figure 4.31: Concentration profiles in the sampling pipe (X/D = 40 and X/D = 44)

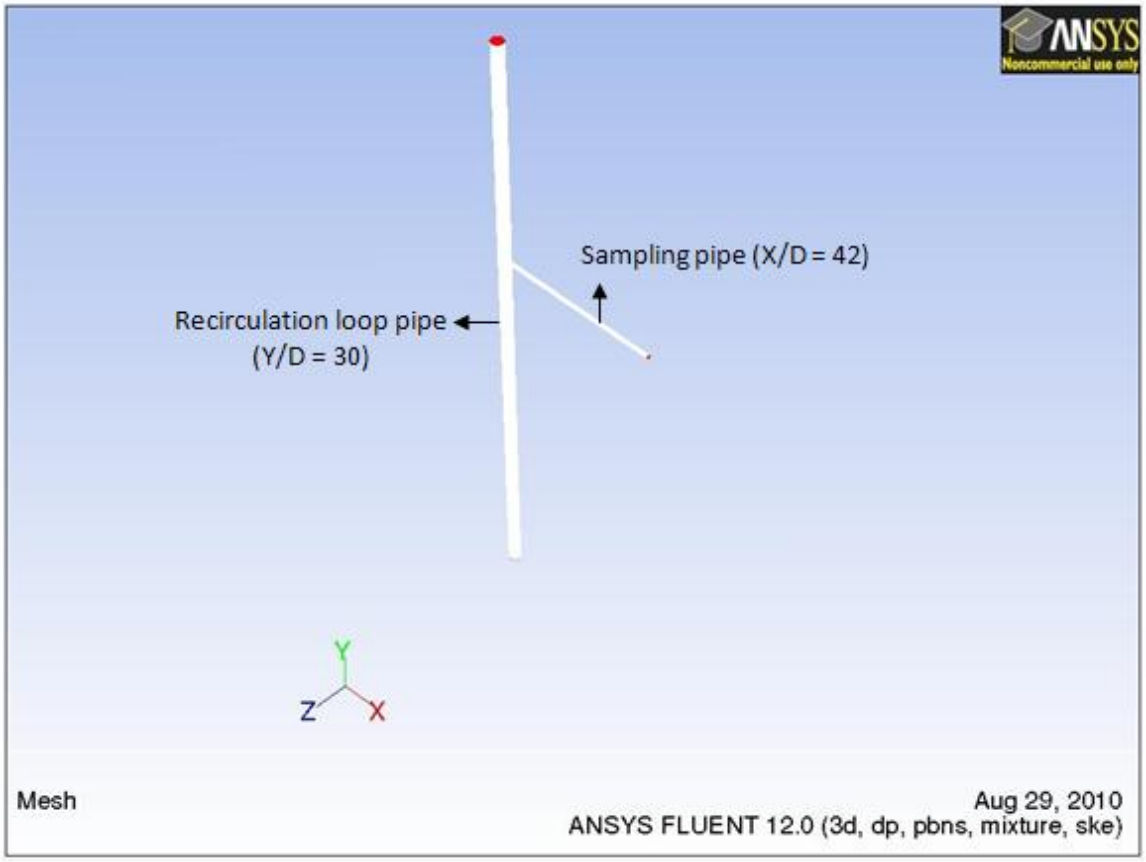

Figure 4.32: Locations where concentration profiles are presented

The concentration profiles registered at the fully-developed region of the recirculation loop and the sampling pipe for 30 micron particle size are shown below. Figures 4.33, 4.34, and 4.35 present the concentration profiles at 5%, 15%, and 30% intial solid concentrations respectively.

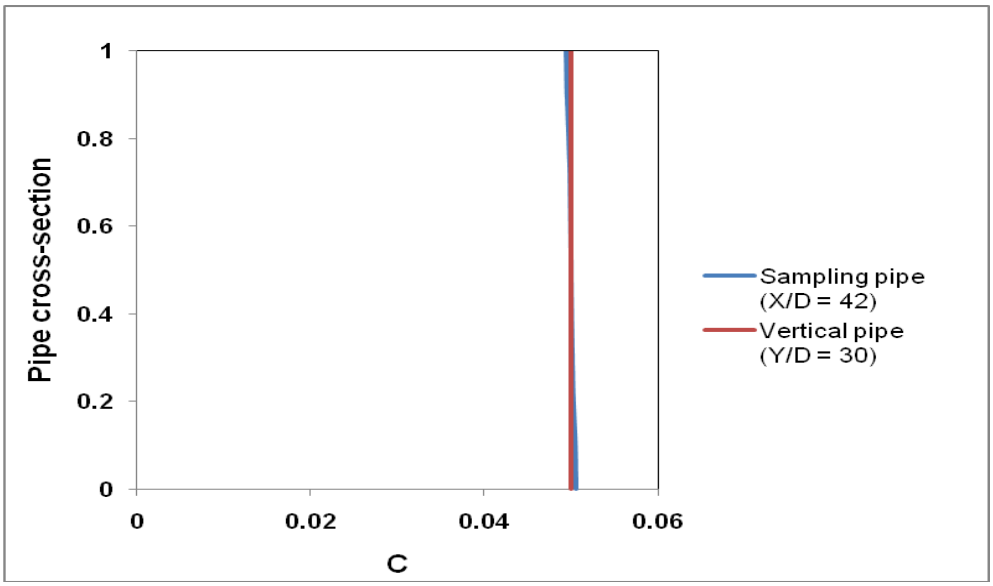

Figure 4.33: Concentration profiles of 30 µm ADP particles at 0.05 initial solids concentration as realized at the vertical pipe and the sampling pipe

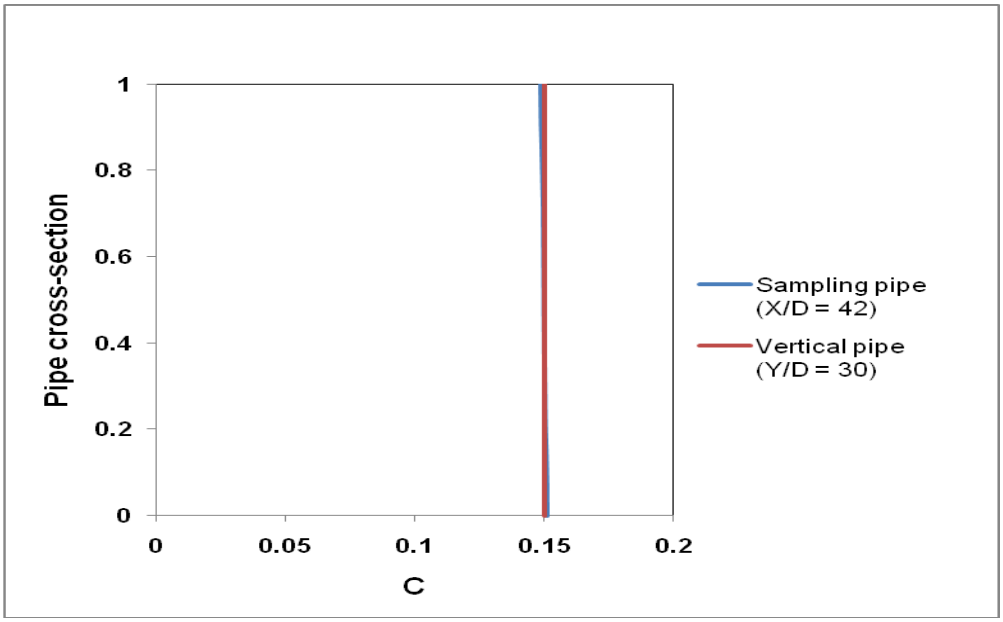

Figure 4.34: Concentration profiles of 30 µm ADP particles at 0.15 initial solids concentration as realized at the vertical pipe and the sampling pipe

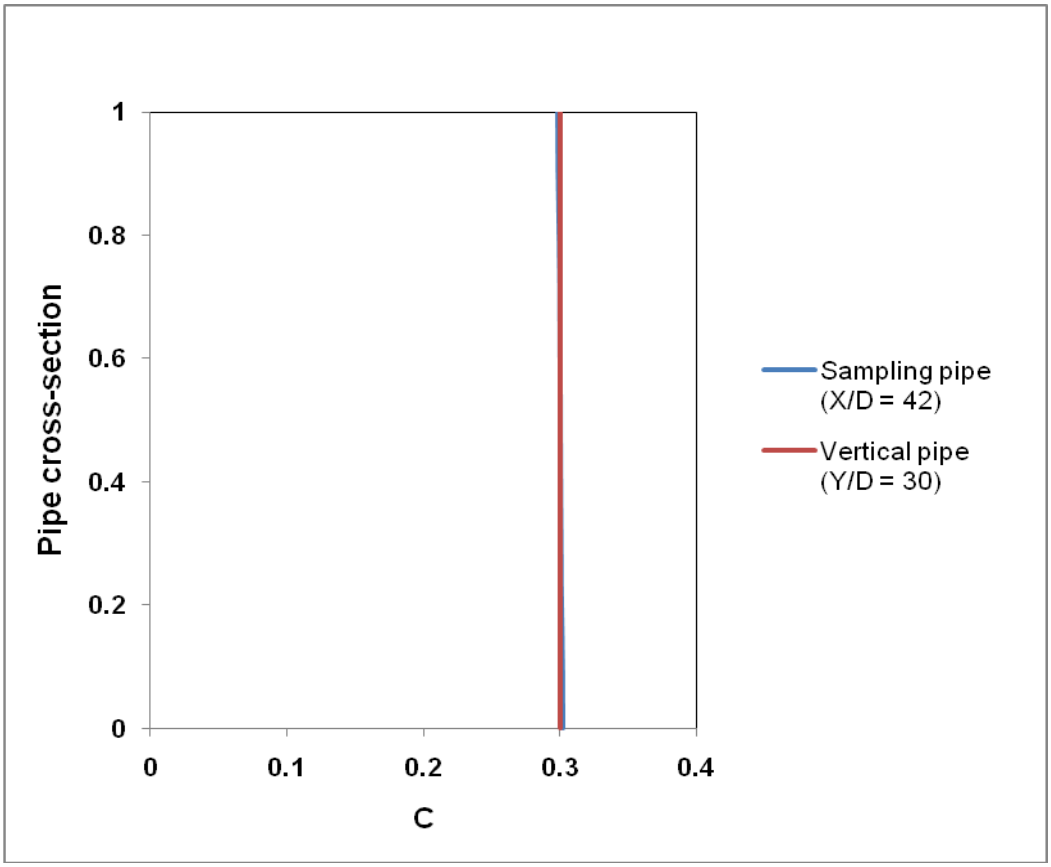

Figure 4.35: Concentration profiles of 30 µm ADP particles at 0.3 initial solids concentration as realized at the vertical pipe and the sampling pipe

After observing the graphs from Figures 4.33 - 4.35, we can say that the concentration profiles registered in the sampling pipe are similar to the concentration profiles at the fully-developed region of vertical pipe for 30 micron particles. The effect of gravity on smaller particles is less. This is in agreement with the deposition velocity calculated from Durand's correlation, smaller particles have low magnitude of deposition velocity(0.47 m/s, shown in Table 4.5) and the velocity in the sampling pipe (1 m/s) is enough for the particle to be uniformly distributed. Therefore, we can observe the uniform concentration profiles in both the regions. In other words, the sample withdrawn represents the sample in the batch reactor for the slurry with 30 µm particles.

The magnitude of deposition velocity for the slurry with different particle sizes at different concentrations is shown in Table 4.6. These values indicate that for all cases, the sampling pipe flow velocity of 1m/s should be high enough to preclude deposition.

Particle Size (μm) (d_p)	**5% Initial solid volume fraction (C)**	**15% Initial solid volume fraction (C)**	**30% Initial solid volume fraction (C)**
	Deposition velocity (V_D) (m/s)	**Deposition velocity (V_D) (m/s)**	**Deposition velocity (V_D) (m/s)**
30	0.33	0.417	0.47
100	0.408	0.509	0.57
300	0.4917	0.6126	0.7

Table 4.6: Variation of deposition velocity in the sampling pipe

The concentration profiles registered at the fully-developed region and the sampling pipe for 100 micron particle size are shown below. Figures 4.36, 4.37, and 4.38 present the concentration profiles at 5%, 15%, and 30% intial solid concentrations respectively.

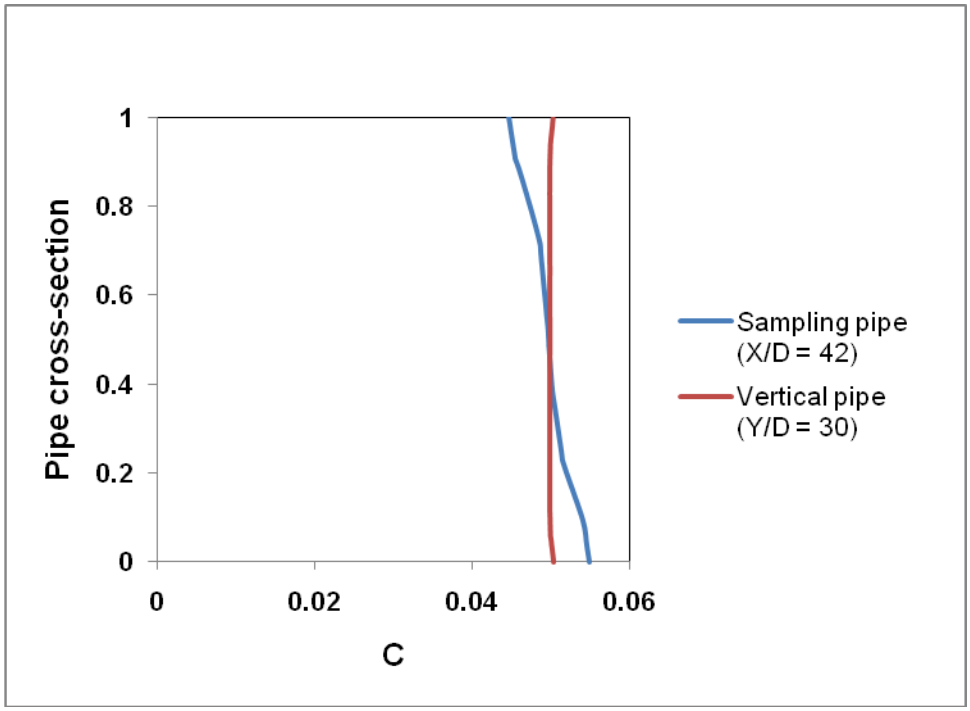

Figure 4.36: Concentration profiles of 100 µm ADP particles at 0.05 initial solids concentration as realized at the vertical pipe and the sampling pipe

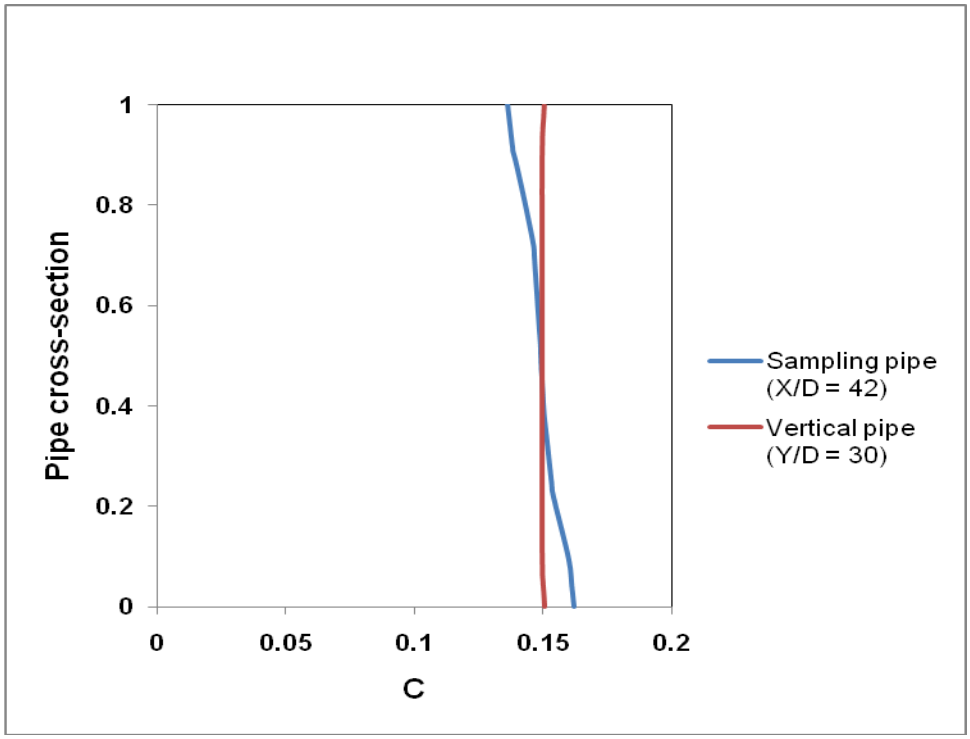

Figure 4.37: Concentration profiles of 100 µm ADP particles at 0.15 initial solids concentration as realized at the vertical pipe and the sampling pipe

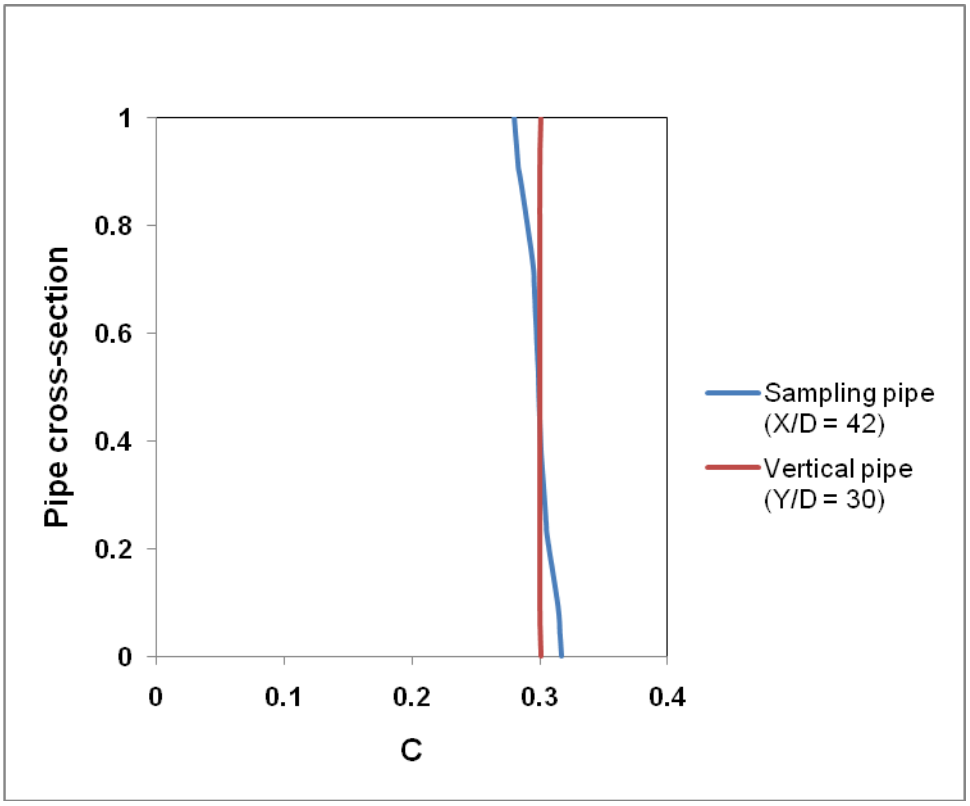

Figure 4.38: Concentration profiles of 100 µm ADP particles at 0.3 initial solids concentration as realized at the vertical pipe and the sampling pipe

One can observe a variation in the concentration profile at the sampling pipe when compared to the concentration profile at the fully-developed of the recirculation loop. This is because the effect of gravity is more for 100 micron particles when compared to smaller particles (30 microns). The 100 micron particles have higher magnitude of deposition velocity. As the magnitude of velocity in the sampling pipe is maintained at the same value for all the particle sizes, the velocity is not sufficient to keep all the 100 micron particles uniformly suspended in the flow. Therefore, we observe a slightly higher concentration of particles at the bottom wall of the sampling pipe when compared to the top wall.

The other interesting observation is the slope of the concentration profiles. When compared to the concentration profile of the slurry with 0.3 initial solids concentration, the concentration profile of the slurry with 0.05 initial solids concentration has reduced spatial

variation. In other words, the concentration profile is more uniform for the slurry with lower percent of initial solids concentration. With the increase in initial solids concentration, the magnitude of deposition velocity increases because the deposition velocity is a function of initial solids concentration. This effect is more clearly seen when all the profiles are plotted on the same graph as shown in Figure 4.39.

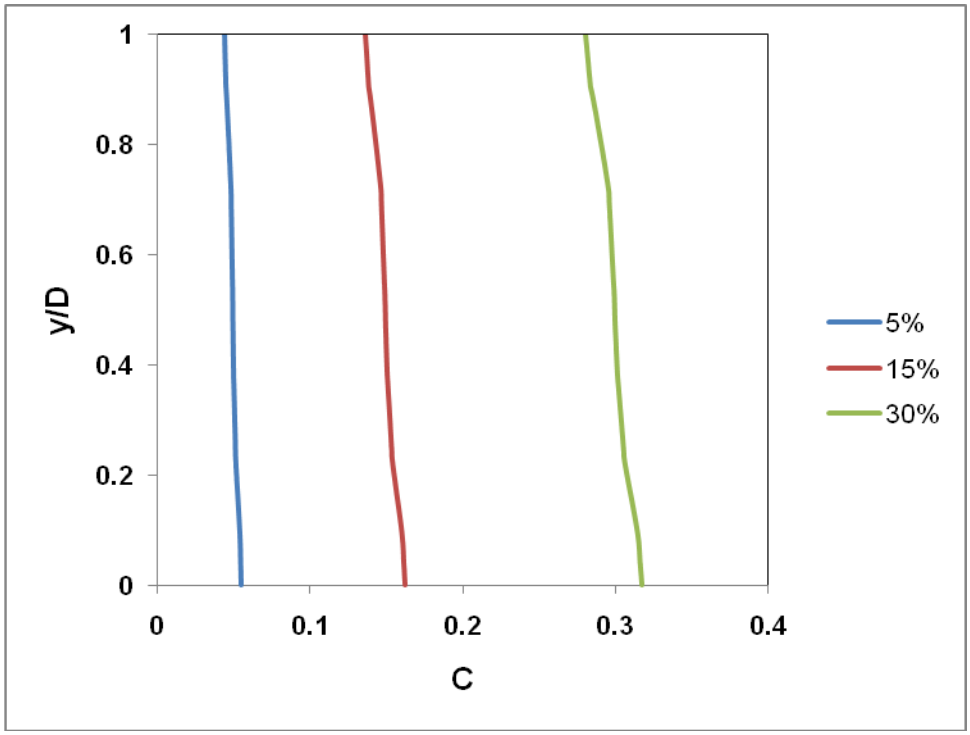

Figure 4.39: Comparison of the concentration profiles of 100 µm ADP particles registered at the sampling pipe at different intial solids concentration

One more observation is the average concentration. Even though the profiles have a slope when compared to the uniform profiles at the fully-developed region of the recirculation loop pipe, the average concentration is almost the same. This shows that the sample withdrawn still represents the slurry in the recirculation loop. The concentration profiles registered at the fully-developed region of the recirculation loop and the sampling pipe for 300 micron particle size are shown below. Figures 4.40 and 4.41 presents the concentration profiles at 5% and 15% intial solid concentrations respectively.

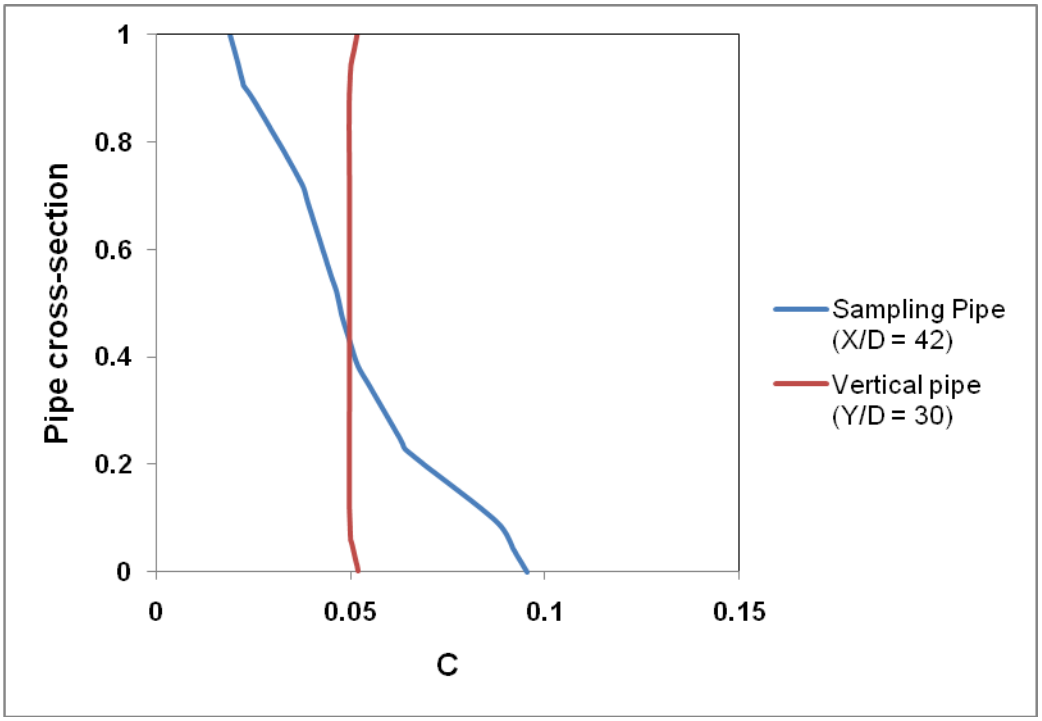

Figure 4.40: Concentration profiles of 300 µm ADP particles at 0.05 initial solids concentration as realized at the vertical pipe and the sampling pipe

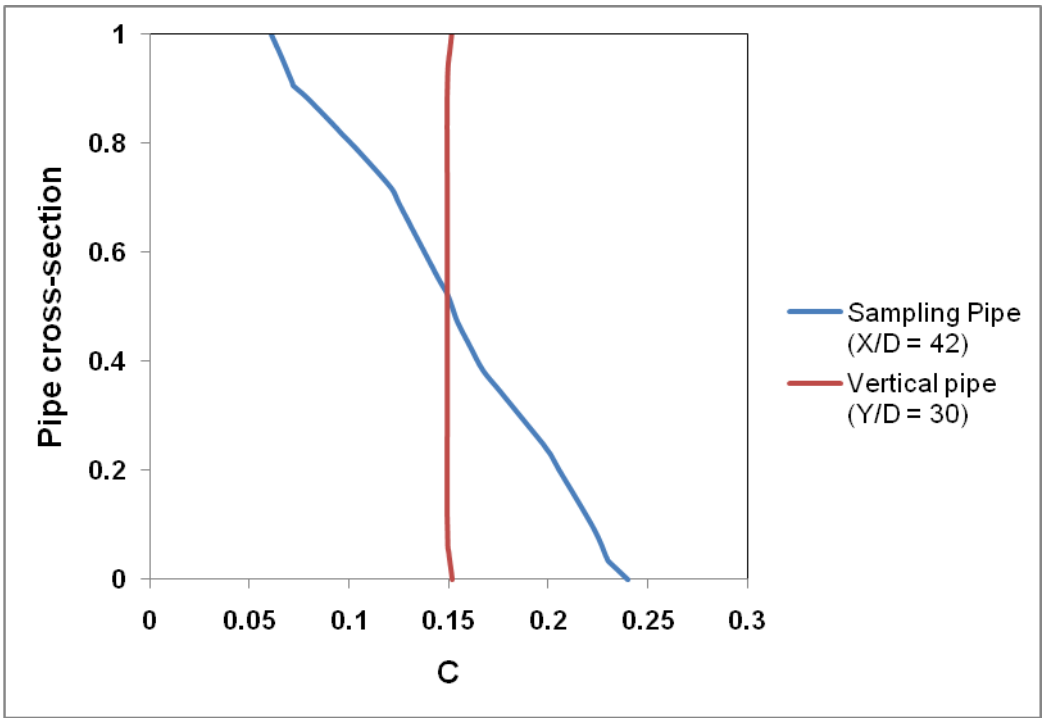

Figure 4.41: Concentration profiles of 300 µm ADP particles at 0.15 initial solids concentration as realized at the vertical pipe and the sampling pipe

A large variation in the concentration profile at the sampling pipe is observed when compared to the concentration profile at the fully-developed region of the vertical pipe. Owing to the size, the effect of gravity is more for 300 micron particles. This is in agreement with the magnitude of deposition velocity which is higher for 300 micron particles when compared to smaller diameter particles (30 and 150 microns). 1 m/s velocity is not enough to keep all the 300 micron particles uniformly distributed. Majority of particles are observed at the bottom wall of the sampling pipe. Therefore, sample withdrawn with 300 micron particles may not represent a good sample because of the flow with high concentration of particles at the bottom wall of the sampling pipe.

Compared to 150 micron particles, we can observe the effect of initial solids concentration on the spatial variation of the profiles more clearly for 300 micron particles in Figure 4.42.

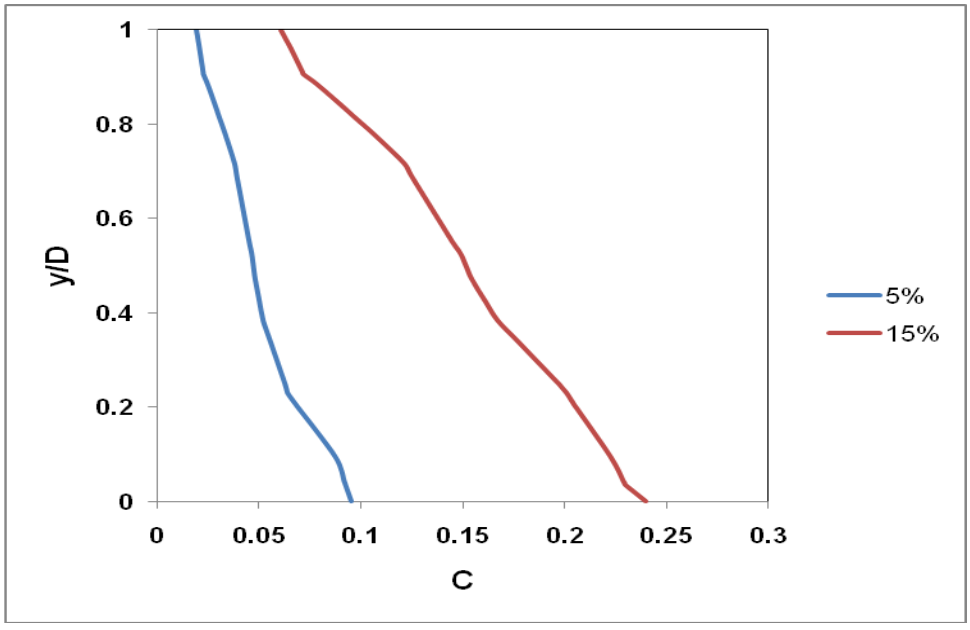

Figure 4.42: Comparison of the concentration profiles of 300 µm ADP particles registered at the sampling pipe at different intial solids concentration

4.8: Contours of volume fraction:

This section presents the contours of volume fraction of the secondary phase (ADP particles). Cross-section contours at the sampling pipe and the contours at the T-junction are presented for all the particle sizes at 15% initial solid concentration. Cross-sectional contours at the sampling (X/D = 42) are presented first followed by the contours at the T-junction.

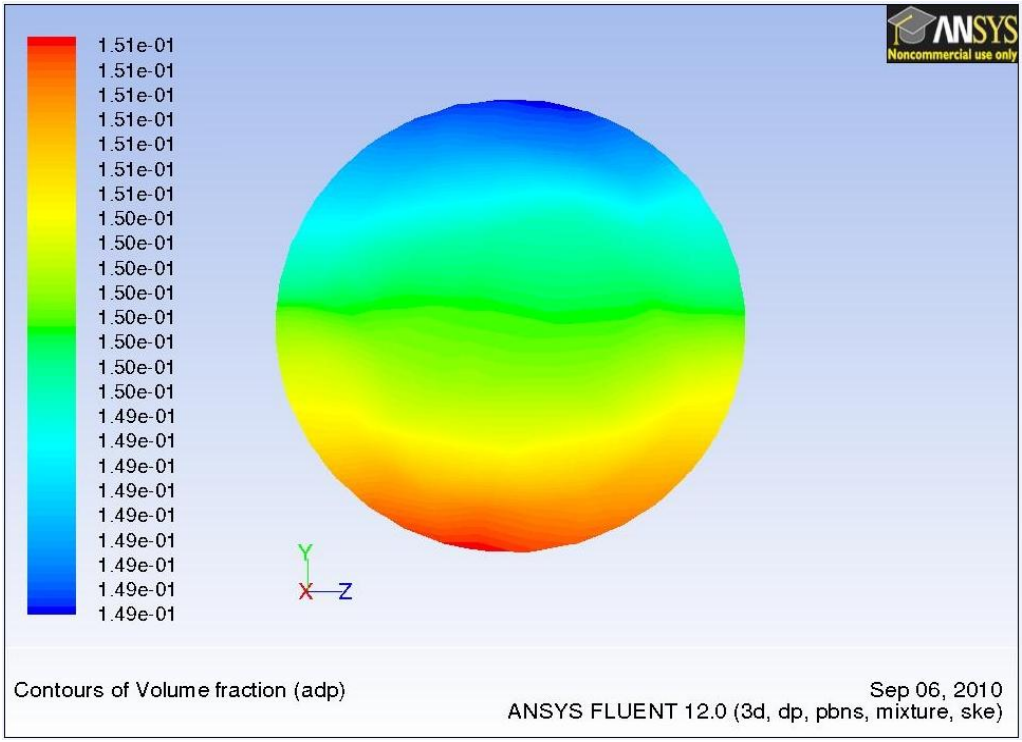

Figure 4.43: Cross-section contours of volume fraction at the sampling pipe for a slurry containing 30 µm ADP particles at 15% initial solids volume fraction

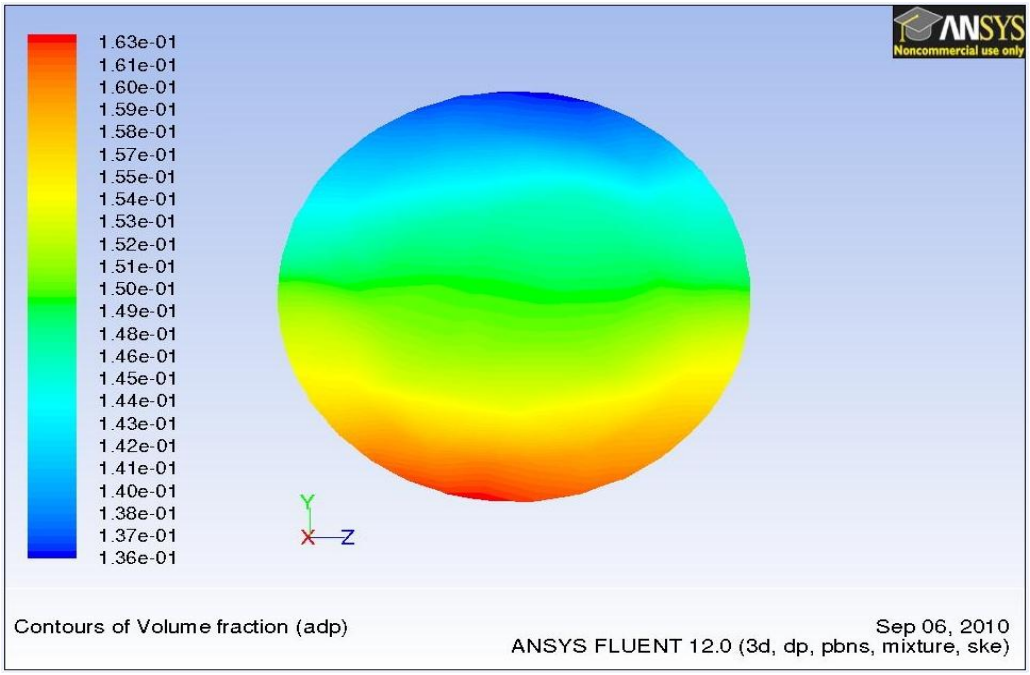

Figure 4.44: Cross-section contours of volume fraction at the sampling pipe for a slurry containing 100 µm ADP particles at 15% initial solids volume fraction

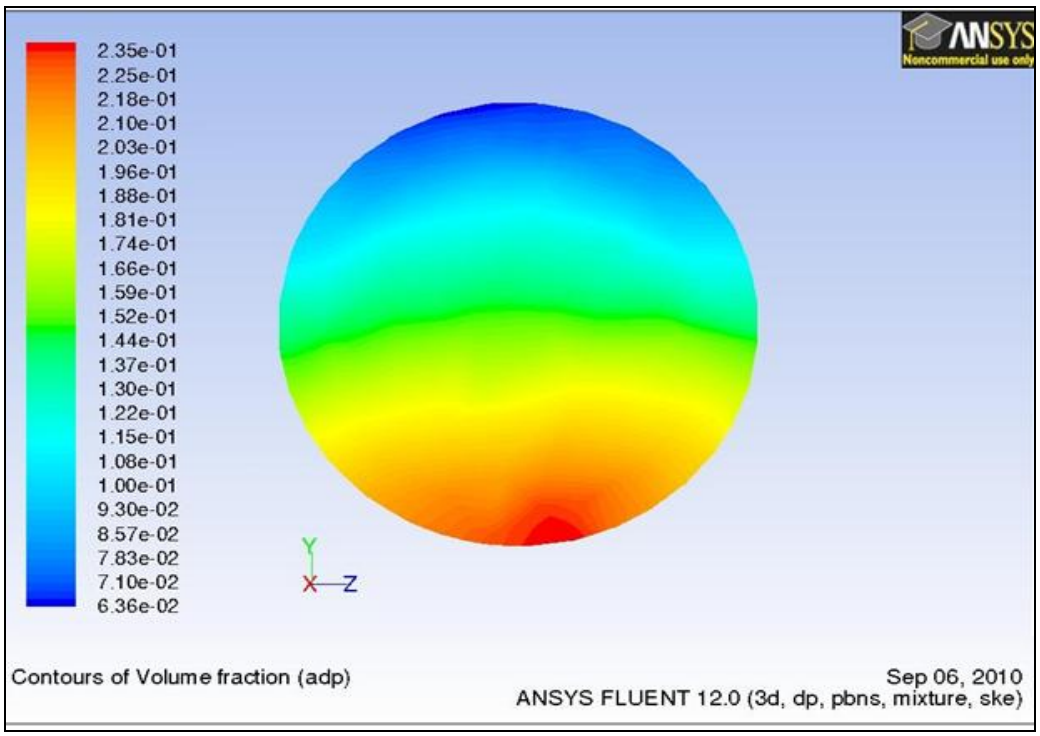

Figure 4.45: Cross-section contours of volume fraction at the sampling pipe for a slurry containing 300 µm ADP particles at 15% initial solids volume fraction

Increase in the color gradient across the cross section of the sampling is observed with the increase in particle diameter. The scale on the left hand side of the each contour plot also represents the greater spatial variation with the increase in particle size. For 30 µm particles the values in the scale are identical, which shows that the particles are distributed uniformly across the pipe cross-section. For 300 µm particles the scale represents a wide range of values. This explains that the particles are not uniformly distributed and the percentage of particles at the bottom wall of the sampling pipe is higher. This may also cause the particles to settle and form a stationary bed. As the model does not account for settling, only high concentrations of particles is shown. As the magnitude of deposition velocity is higher for bigger particles (0.7 m/s), the 1m/s velocity in the sampling pipe is less than the minimum operating velocity which is usually kept as 0.5 m/s more than the deposition velocity (Kaushal 2002). Therefore, a greater number of particles move to the bottom wall of the pipe. Performing sampling under these conditions can give erroneous results. Figures 4.46 - 4.48 present the contours of 30, 100, and 300 micron particles at 15% initial solids concentration.

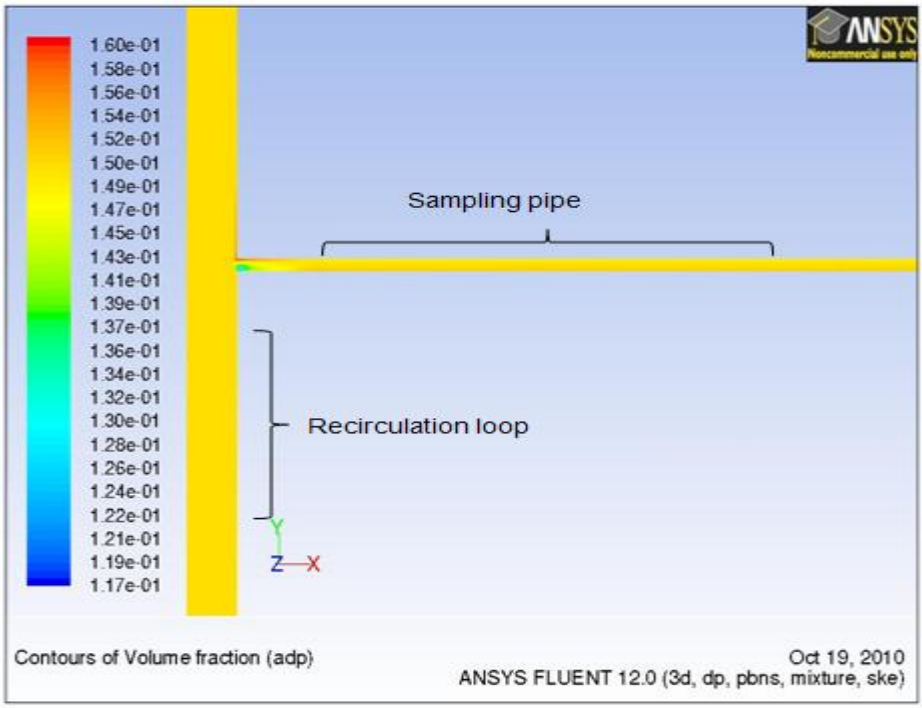

Figure 4.46: Contours of volume fraction for a slurry containing 30 µm ADP particles at 15% initial solids concentration

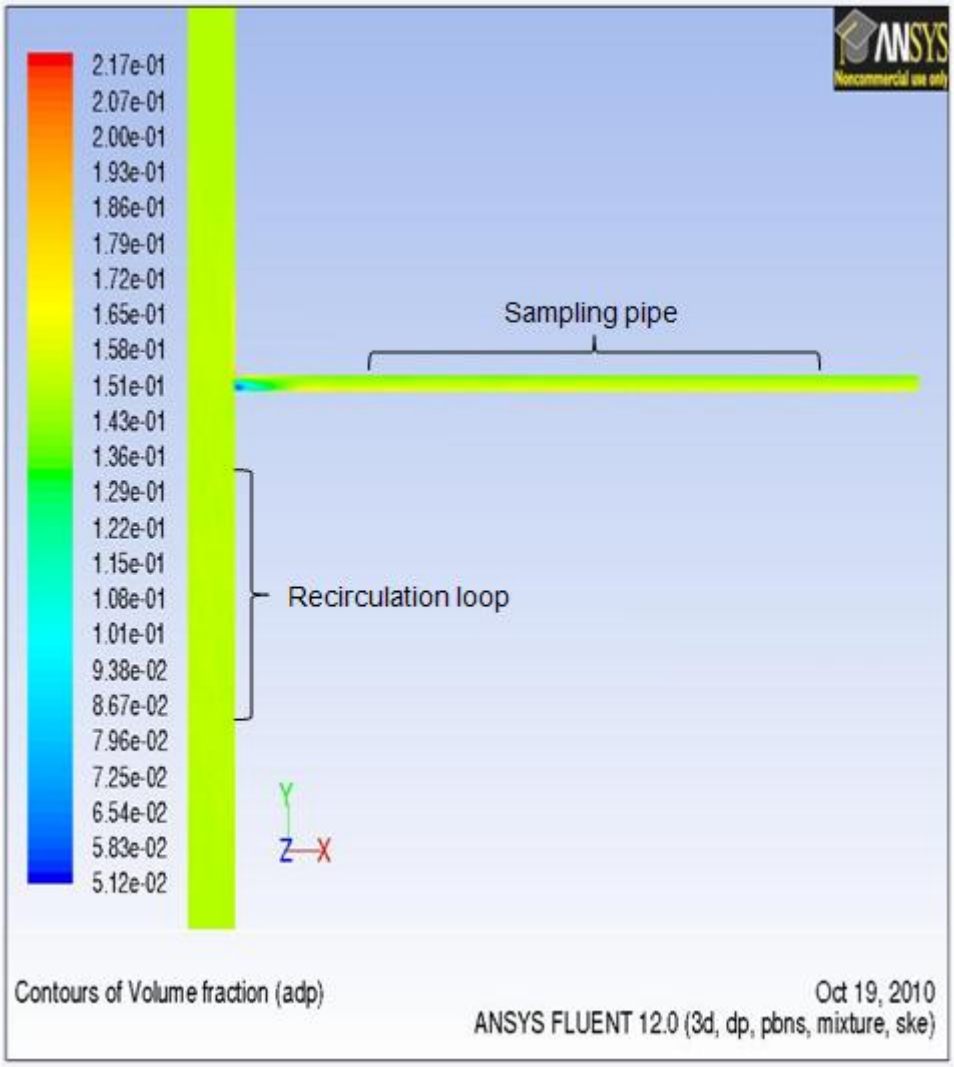

Figure 4.47: Contours of volume fraction for a slurry containing 100 µm ADP particles at 15% initial solids concentration

The contours of volume fraction of the slurry containing 30 µm presents a uniform color gradient at both the recirculation loop and the sampling pipe locations. This explains that the particles are uniformly distributed at both the locations. This validates the results presented for 30 µm particles. Even the slurry containing 100 µm particles shows a uniform color gradient at both the locations. This shows that the particles are almost uniformly distributed and performing off-line sampling for a slurry with 30 and 100 µm particles will give a sample that is a good representative of the slurry in the batch reactor.

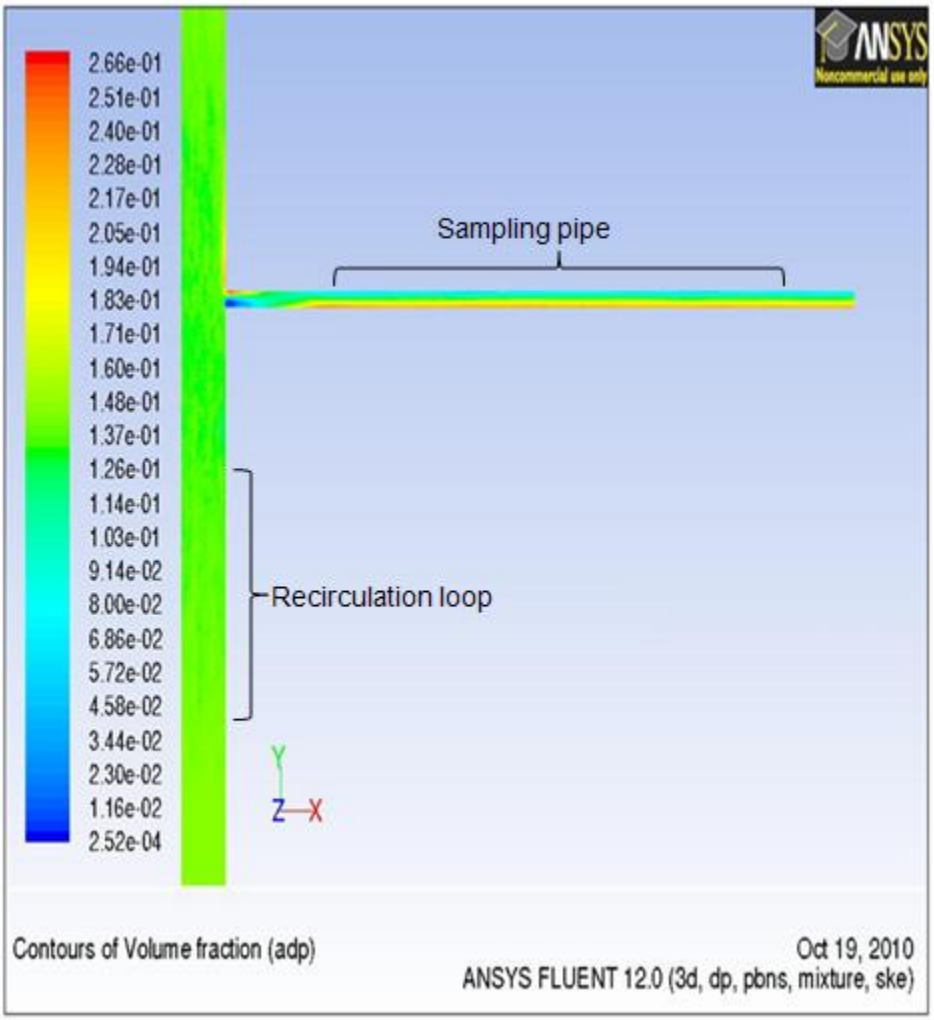

Figure 4.48: Contours of volume fraction for a slurry containing 300 µm ADP particles at 15% initial solids concentration

On the other hand contours of volume fraction for the slurry with 300 µm ADP particles show different colors in the sampling pipe. A red color gradient is observed near the bottom wall of the sampling pipe. This explains that the particle concentration near the bottom is very high. This validates the results presented for 300 µm particles. Therefore, performing off-line sampling analysis for a slurry containing 300 µm particles can give erroneous results because of the greater number of particles at the bottom wall of the sampling pipe. Figures 4.49 – 4.51 present closer views of the contours at the T junction.

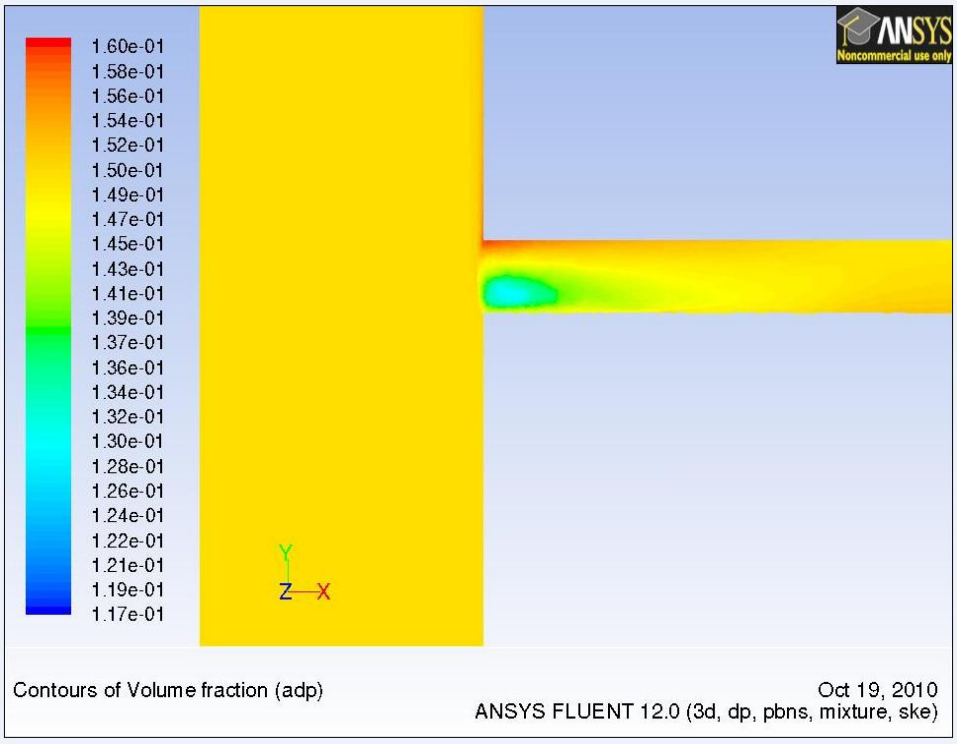

Figure 4.49: Contours of volume fraction of 30 µm particles at 15% concentration

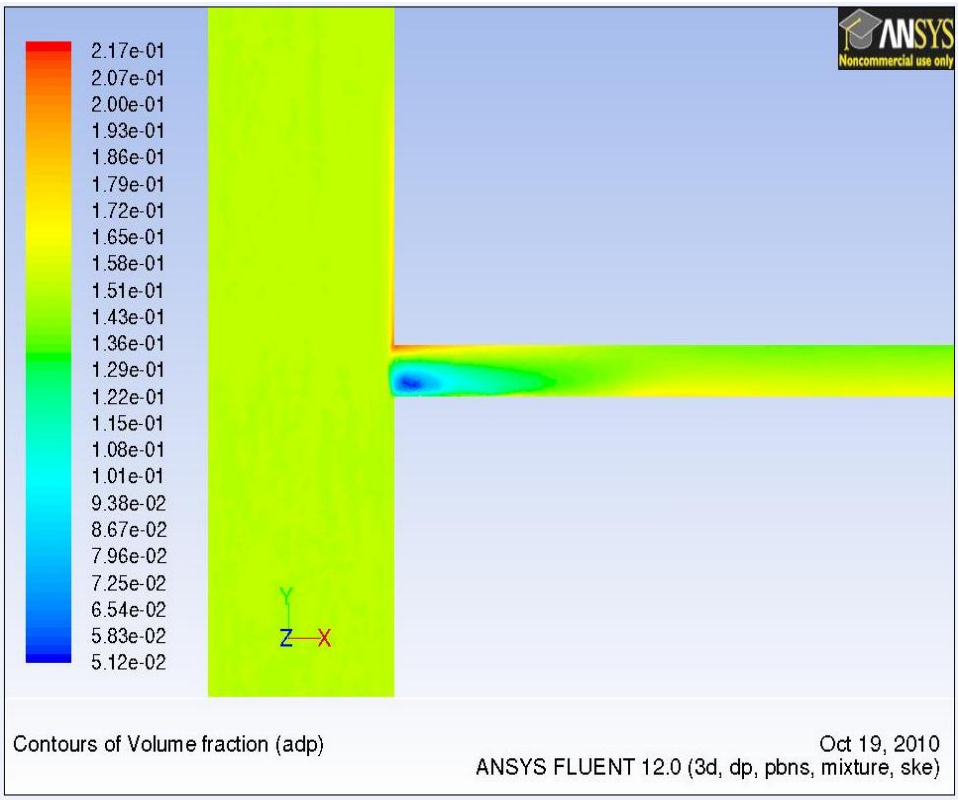

Figure 4.50: Contours of volume fraction of 100 µm particles at 15% concentration

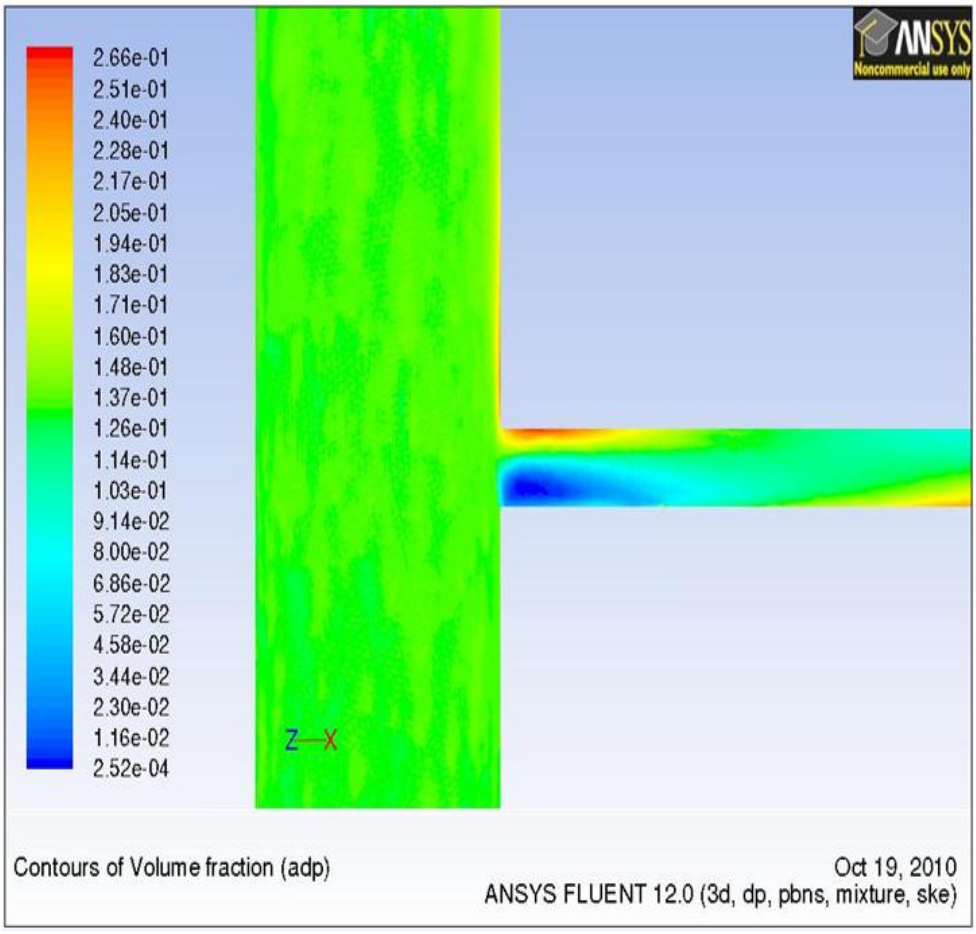

Figure 4.51: Contours of volume fraction of 300 µm particles at 15% concentration

One more important aspect to be considered while performing off-line sampling is possible blockage or plugging. The possible location of the deposition of particles is detected by observing the contours of volume fraction of the particles at the T-junction as shown in Figure 4.52.

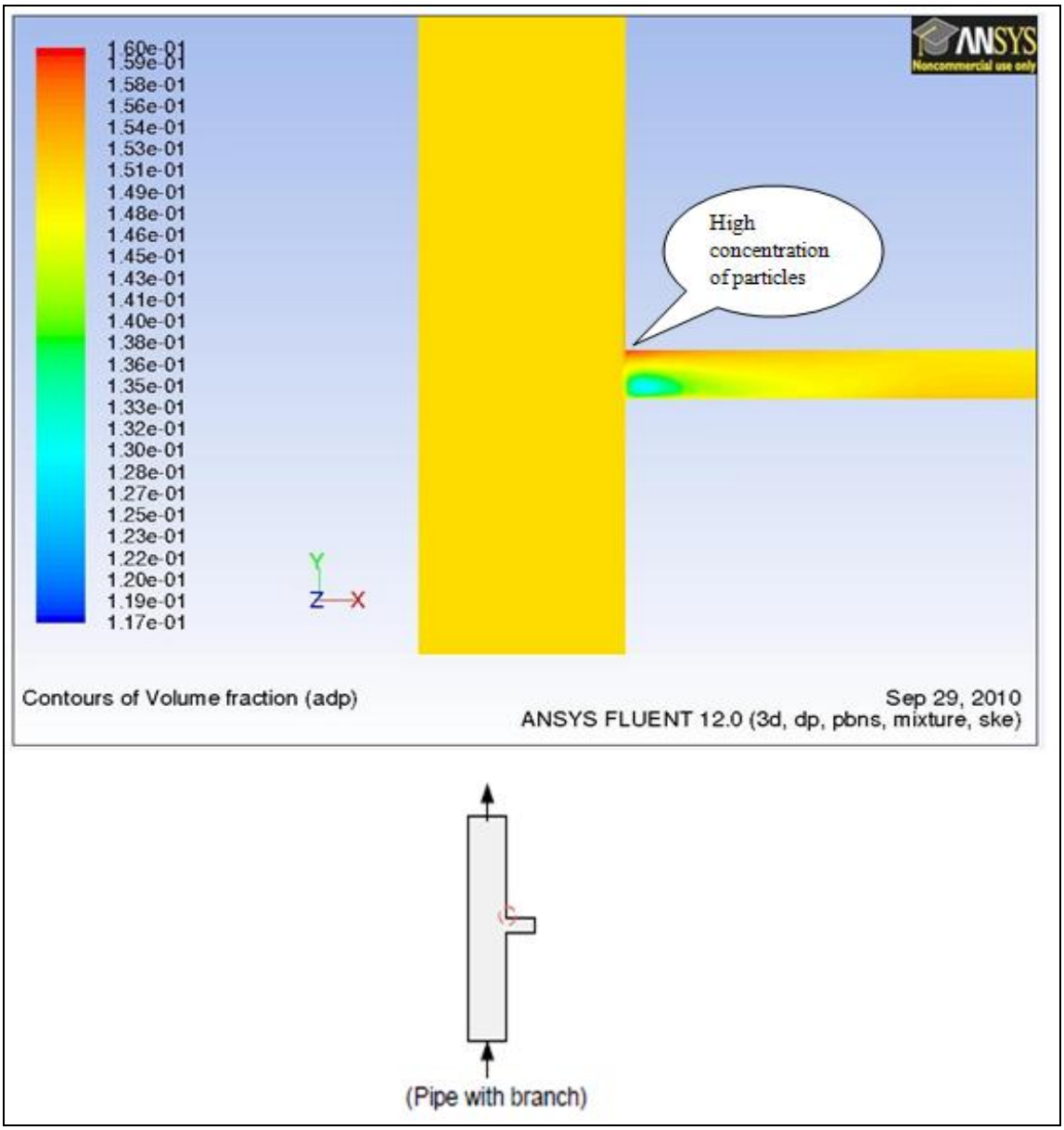

Figure 4.52: Location of high concentration of particles predicted by the present model (top) and by Lee et al. (2001)

The above contour shows a higher concentration of particles at the entrance to the sampling pipe. This may cause erosion of the pipe junction, leading to erroneous results and damage to the whole system. Therefore, it is a good idea to consider alternative geometries to avoid this problem. The model does not account for settling, due to this only high concentration regions are presented without taking in account the settling of particles.

In conclusion, the concentration profiles of the slurry with smaller particles are uniform (reduced spatial variation) at the fully-developed region of horizontal pipe. With the increase in particle size, there is a greater variation in the profiles. The concentration near the bottom wall is more when compared to the top wall because of the effect of gravity and the magnitude of deposition velocity. On the other hand, the concentration profiles of the slurry flowing in a vertical pipe display almost uniform distribution of particles for all the particle sizes. The profiles are unaffected by the changes in concentration, particle size, and density within the parameter range studied. Withdrawing a sample or measuring with NIR probe from the edge of the horizontal pipe will give erroneous results because of the non-uniform distribution of particles. While in vertical pipes, because of the uniform distribution of particles, withdrawing a sample will give a sample that is a good representative of the sample in the batch reactor. Therefore, the fully-developed region of the vertical pipe is recognized as a good location to perform off-line sampling and NIR Spectroscopic analysis.

The concentration profiles of the slurry in the sampling pipe are dependent on the particle size and initial solid concentration. The concentration profiles of the slurry with 30 micron particles are similar to the profiles in the fully-developed region of the recirculation loop. Therefore, the slurry sample withdrawn from the full-developed region of the vertical pipe with 30 micron particles is a good representative of the sample in the batch reactor. The concentration profiles of 100 micron particles in the sampling pipe shows a small variation when compared to profiles in the fully-developed region of the recirculation loop, but the average concentration is the same in both the regions. Therefore, the sample with 100 micron particles is still a representative of the sample in the batch reactor. For the slurry with 300 micron particles, the profiles in the sampling pipe display high spatial variation with more concentration near the bottom wall. The volume fraction contours also displayed greater concentration of particles near

the bottom wall of the sampling pipe. Therefore, sampling a slurry with 300 μm particles may give erroneous results and the sample is not a good representative.

CHAPTER V

CONCLUSIONS AND RECOMMENDATIONS

5.1 Conclusions:

The sample withdrawn from the recirculation loop for Mass-Spectroscopic analysis must be a good representative of the total slurry volume in the batch reactor. Off-line sampling is one of the techniques for sample withdrawal. To perform off-line sampling and NIR Spectroscopy, it is best that the concentration profiles of a particle-laden slurry be as uniform as possible. Therefore, the concentration profiles in horizontal and vertical pipes are predicted by computational fluid dynamics to find a good location to perform off-line sampling and NIR Spectroscopy. The effect of particle size and initial solid concentration on the concentration profiles in the sampling pipe located at the fully-developed region of the recirculation loop is also investigated. This gave rise to the following conclusions:

1. The present computational model was validated for velocity and concentration profiles with the experimental data available in the literature. The validations proved that the present computational model is working well and the results presented are substantially accurate.

2. The concentration profiles of the slurry in the horizontal pipe displayed greater spatial variation than the profiles in the vertical pipe, with the increase in particle size (100micron and 150 micron), because of the effect of gravity.

3. The concentration profiles of the slurry flowing in vertical pipe displayed nearly uniform distribution of particles (30, 100, and 150 microns) for volume fractions up to 30%.

4. Therefore, the fully-developed region in the vertical pipe is recognized as a good location for performing off-line sampling and NIR Spectroscopic analysis.

5. The concentration profiles of the slurry with 30 and 100 µm particles are similar at both the regions (sampling pipe and recirculation loop) and 300 µm particles displayed much greater spatial variation in the sampling pipe.

6. Therefore, slurries with less than 100 µm particles can be sampled through off-line sampling technique with good accuracy using the modeled parameters, avoiding effects of strongly non-uniform concentration profiles.

5.2 Recommendations:

1. The effect of diameter of the sampling pipe and the velocity in the sampling pipe on the concentration profiles of the slurry can be studied to get better understanding of the off-line sampling technique.

2. The Euler multi-phase model can be used to predict the concentration profiles as it a more advanced model, but computationally more intensive

3. Determine the effect of different elbow designs at the junction of the sampling pipe on the concentration profiles. A suitable junction must be designed to reduce erosion or deposition of particles and also improve performance for bigger particles.

4. An obvious recommendation would be to perform experiments and investigate the performance of off-line sampling technique.

REFERENCES

Brown, G. J. (2002) Erosion prediction in slurry pipeline tee-junctions. *Applied Mathematical Modelling,* 26**,** 155-170.

Cho, D. S. (2010) private communication, University of Tennessee, Knoxville, TN.

Cody, R. B., J. A. Laramee & H. D. Durst (2005) Versatile new ion source for the analysis of materials in open air under ambient conditions. *Analytical Chemistry,* 77**,** 2297-2302.

Crowe, C. T., Sommerfeld, M., and Tsuji, Y. (1998) *Multiphase flows with droplets and particles*, CRC Press LLC, Boca Raton, FL.

Dole, M., L. L. Mack & R. L. Hines (1968) Molecular beams of macro ions. *Journal of Chemical Physics,* 49**,** 2240-2249.

Durand, R. & E. Condolios. 1963. *The hydraulic transport of coal and solid materials in pipes: [paper 4]*. London: National Coal Board.

Ekambara, K., R. S. Sanders, K. Nandakumar & J. H. Masliyah (2009) Hydrodynamic simulation of horizontal slurry pipeline flow using ANSYS-CFX. *Industrial & Engineering Chemistry Research,* 48**,** 8159-8171.

Fadel F. E., J.F. Daniel., Michael I. K & R. P. Walter (2001) Measurement of the critical deposition velocity in slurry transport through a horizontal pipe. *Conference: 9th International Topical Meeting on Robotic and Remote Systems*, Seattle, Washington, 11 pages

Gillies, R. G., Shook, C. A., and Xu, J. (2004) Modeling heterogeneous slurry flows at high velocities, *The Canadian Journal of Chemical Engineering*, 82, 1060-1065.

Horning, E. C., M. G. Horning, D. I. Carroll, I. Dzidic & Stillwel.Rn (1973) New picogram detection system based on a mass-spectrometer with an external ionization source at atmospheric-pressure. *Analytical Chemistry,* 45**,** 936-943.

Kaushal, D. R. & Y. Tomita (2002) Solids concentration profiles and pressure drop in pipeline flow of multisized particulate slurries. *International Journal of Multiphase Flow,* 28**,** 1697-1717.

Kaushal, D. R., Y. Tomita & R. R. Dighade (2002) Concentration at the pipe bottom at deposition velocity for transportation of commercial slurries through pipeline. *Powder Technology,* 125**,** 89-101.

Kumar, A., D. R. Kaushal & U. Kumar (2008) Bend pressure drop experiments compared with Fluent. *Engineering and Computational mechanics*, 6, 35-42.

Lahiri, S. K. & K. C. Ghanta (2009) Computational fluid dynamics simulation of solid-liquid slurry flow. *Hydrocarbon Processing,* 88**,** 99-104.

Lu Yi-yu., Liu Yong., and Kang Yong (2009) Numerical simulation on turbulent flow field in convergent divergent nozzle. *Journal of Coal Science & Engineering*, 15, 434-439.

Pope, S. B. (2000) *Turbulent Flows*, Cambridge University Press, New York, NY.

Roco, M. C. & C. A. Shook (1983) Modeling of slurry flow - the effect of particle-size. *Canadian Journal of Chemical Engineering,* 61**,** 494-503.

Schlichting, H. (1979) *Boundary layer theory*, 3 ed., McGraw-Hill, New York.

Sumner, R. J., M. McKibben & C. A. Shook (1990) Concentration and velocity distributions in turbulent vertical slurry flows. *Ecoulements Solide Liquide,* 2, 2**,** 33-42.

Tu, J. Y. & C. A. J. Fletcher (1995) Numerical computation of turbulent gas-solid particle flow in a 90^0 bend. *AICHE Journal,* 41**,** 2187-2197.

Wasp, E. J. (1970) Technical and economic review of slurry pipelines. *Canadian mining and metallurgical bulletin*, 63**,** 283-290.

Wasp, E. J., J. P. Kenny & R. L. Gandhi. 1977. *Solid-liquid flow: Slurry pipeline transportation*. Rockport Mass: Trans. Tech Publications.

White, F. M. (2006) *Viscous fluid flow*, 3 ed., McGraw -Hill, New York, NY.

Wilcox, D. C. (2006) *Turbulence modeling for CFD*, 3 ed., DCW Industries, La Canada, CA.

Wildman, D. J., Ekmann, J. M., Kadambi, J. R., and Chen, R. C. (1992) Study of the flow properties of slurries using the refractive index matching technique and LDV, *Powder Technology*, 73, 211-218.

APPPENDIX

EXPERIMENTAL SETUP

Figure A1 shows the model designed in SolidWorks and Figure A2 presents the developed experimental setup in the laboratory that have the capability to analyze a particle-laden slurry.

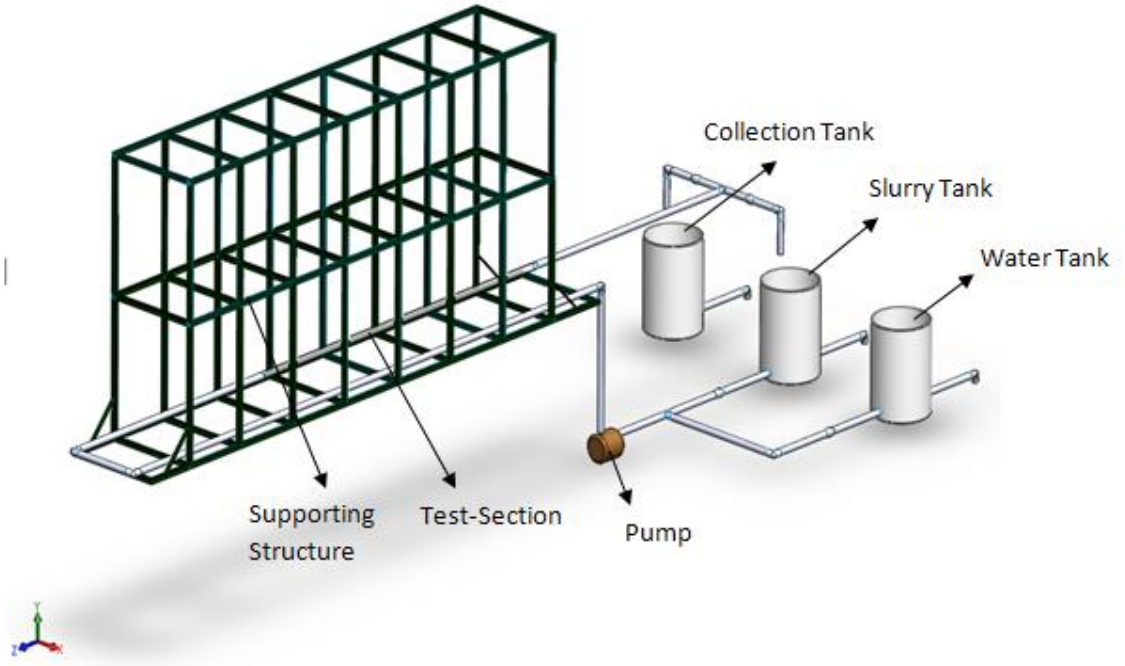

Figure A1: Experimental layout designed in SolidWorks

Figure A2: Experimental setup

VITA

Karthik Ramisetty

Candidate for the Degree of

Master of Science

Thesis: PREDICTION OF CONCENTRATION PROFILES OF A PARTICLE - LADEN SLURRY FLOW IN HORIZONTAL AND VERTICAL PIPES

Major Field: Mechanical Engineering

Biographical:

Education:
Completed the requirements for the Master of Science in Mechanical Engineering at Oklahoma State University, Stillwater, Oklahoma in December, 2010.

Completed the requirements for the Bachelor of Technology in Mechanical Engineering at Jawaharlal Nehru Technological University, Hyderabad, Andhra Pradesh, India, June 2008.

Experience:
Design Intern: December 2007-April 2008
Bharath Dynamics Limited, Hyderabad, Andhra Pradesh, India

Teaching Assistant: January 2008-December 2010
Department of Mechanical and Aerospace Engineering
Oklahoma State University

Research Assistant: August 2009-December 2010
Department of Mechanical and Aerospace Engineering
Oklahoma State University

Professional Memberships:
Member of American Society of Mechanical Engineers (ASME)
Member of Golden Key International Honor Society
Member of The Honor Society of Phi Kappa Phi

Name: Karthik Ramisetty Date of Degree: December 2010*

Institution: Oklahoma State University Location: Stillwater, Oklahoma

Title of Study: PREDICTION OF CONCENTRATION PROFILES OF A PARTICLE - LADEN SLURRY FLOW IN HORIZONTAL AND VERTICAL PIPES

Pages in Study: 113 Candidate for the Degree of Master of Science

Major Field: Mechanical Engineering

Scope and Method of Study: The effect of particle diameter and initial solids concentration on the concentration profiles of a Xylene - 2 amino, 4, 6 dimethyl pyrimidine (ADP) slurry flowing in horizontal pipe, vertical pipe, and vertical pipe with a branch (sampling pipe) was simulated using computational fluid dynamics. ANSYS FLUENT 12.0 was used as the computational fluid dynamic software. The k-epsilon turbulence model with standard wall functions coupled with the mixture multi-phase model was used to simulate all the test cases. A grid independence study was performed and fully-developed flow regions are predicted for horizontal and vertical pipes. The model was validated with experimental data sets available in the literature. The concentration profiles at the fully-developed region of the horizontal and vertical pipes are compared. The concentration profiles in the sampling pipe are compared with those registered at the fully-developed region of the vertical pipe.

Findings and Conclusions: The present computational model predicts the velocity and the concentration profiles of a slurry flowing in horizontal and vertical pipes with an acceptable degree of accuracy. It was found that the concentration profiles in the horizontal pipe displayed greater spatial variation, whereas the concentration profiles in the vertical pipe displayed reduced spatial variation; they are almost uniform. Owing to this, the fully-developed region of the vertical pipe will serve as a good location for performing off-line sampling and near infra-red spectroscopic analysis of a particle-laden slurry.

It was found that the concentration profiles in the sampling pipe and the fully-developed region of the vertical pipe are almost uniform and similar for 30 and 100 µm ADP particles. For bigger particles (300 µm ADP particles), the concentration profiles in the sampling pipe displayed greater spatial variation with higher concentration of particles observed at the bottom wall of the sampling pipe because of the effect of gravity. Owing to this, the off-line sampling method is suitable for sampling slurries with less than 100 µm particles using the modeled parameters, avoiding effects of strongly non-uniform concentration profiles.

ADVISER'S APPROVAL: Dr. Frank W. Chambers